Design and synthesis of APE1 inhibitors as putative anticancer agents

A Thesis submitted to the Central University of Punjab

For the Award of

Master of Pharmacy

In

Medicinal Chemistry

by

Gagandeep Kaur

Supervisor : Dr. Raj Kumar

Co-supervisor : Dr. Anil K. Mantha

Centre for Chemical & Pharmaceutical Sciences

School of Basic & Applied Sciences

Central University of Punjab

Bathinda

October, 2014

CERTIFICATE

I declare that the dissertation entitled "**Design and synthesis of APE1 inhibitors as putative anticancer agents**" has been prepared by me under the guidance of Dr. Raj Kumar, Assistant Professor, Centre for Chemical and Pharmaceutical Sciences and Dr. Anil K. Mantha, Assistant Professor, Centre for Biosciences, School of Basic and Applied Sciences, Central University of Punjab. No part of this dissertation has formed the basis for the award of any degree or fellowship previously.

Gagandeep Kaur

Centre for Chemical and Pharmaceutical Sciences
School of Basic and Applied Sciences,
Central University of Punjab,
Bathinda, India - 151001

Date:

CERTIFICATE

We certify that Gagandeep Kaur has prepared her dissertation entitled "**Design and synthesis of APE1 inhibitors as putative anticancer agents**", for the award of M. Pharm. degree in Medicinal Chemistry under our guidance. She has carried out this work at the Centre for Chemical and Pharmaceutical Sciences, School of Basic and Applied Sciences, Central University of Punjab.

Dr. Raj Kumar

(Supervisor)

Assistant Professor

Centre for Chemical & Pharmaceutical Sciences,

Central University of Punjab,

Bathinda-151001

Dr. Anil K. Mantha

(Co Supervisor)

Assistant Professor

Centre for Biosciences

Central University of Punjab

Bathinda-151001

Date:

ABSTRACT

Design and synthesis of APE1 inhibitors as putative anticancer agents

Name of student	:	Gagandeep Kaur
Registration Number	:	CUPB/MPHARM-MC/SBAS/CPS/2012-13/04
Degree for which submitted	:	M.Pharm. (Medicinal Chemistry)
Name of supervisor	:	Dr. Raj Kumar
Name of co-supervisor	:	Dr. Anil K. Mantha
Centre	:	Chemical and Pharmaceutical Sciences and Centre for Biosciences
School of Studies	:	School of Basic and Applied Science

Key words: APE1, BER Pathway, DNA Repair, Anticancer, AP-sites

Success in chemotherapy has not been attained completely yet and has remained a worried issue from years. Various reasons drive this failure, but the much talked about is failure due to emergence of resistance to chemotherapeutic drugs due to various factors. One of the major reasons here we have targeted is the resistance developed against DNA damaging chemotherapy due to over activation of APE1 enzyme evolved in BER pathway, which is the major repair pathway responsible for 95% of the DNA repair. Design and synthesis of APE1 inhibitors using rational approach fulfilling the pharmacophoric requirements has been carried out in this research work. Molecular modelling studies were performed to confirm that designed compounds fit well into the repair active cavity. 14 compounds have been designed and synthesized having pyrazolo-quinazolines core structure. The anticancer potential of the 8 representative compounds was evaluated against rat C-6 glial cell line at different concentrations. All synthesized compounds showed good anticancer activity against rat C-6 glial cell lines. The inhibitory potential of the compounds obtained from the MTT assay results helped us to formulate the SAR studies. Further ROS measurement was also carried out using DCFDA assay. Compounds showing good MTT results were also found to be potential antioxidants which conclude their mechanism of anticancer activity through APE1 inhibition. The active compounds may be taken further for lead optimisation and mechanistic interventions for their in vitro binding studies on APE1 in future.

Gagandeep Kaur Dr. Raj Kumar Dr. Anil Mantha

ACKNOWLEDGEMENTS

First and the foremost I thank my God Almighty for His grace and mercy towards me and helping me at every stage of my work, giving me the strength, the wisdom and the fill for successfully completing my work diligently.

With immense pleasure and sincere sense of gratitude, I would foremost like to express my heartfelt indebtness to my supervisor **Dr. Raj Kumar**, Assistant Professor, Centre for Chemical and Pharmaceutical Sciences for his patient guidance, encouragement, valuable advices and continous moral support throughout my research and thesis writing. I heartily thank him for being a person of high vision and creating a very comfortable research environment to work within. His motivational group meetings really build a new energy to carry forward the work with more thrill and recollect yourself even in low phases of research. I am grateful to him for the liberty and freedom he gave us to do our work own way, do mistakes, manipulate, learn, approach with new ideas and then come out with something new on our own basis instead of being spoon feeder. Sincere thanks for his detailed review, constructive criticism and continous monitoring and care about the progress of the work since the inception of the hypothesis till research and preparation of the thesis. I am extremely indebted to him for the scientific attitude he has installed in me which will definitely stand in all my future endeavors. I could not have imagined having a better advisor and mentor for my M.Pharm.

I gratefully acknowledge My Co-Supervisor **Dr. Anil Mantha**, Assistant Professor, Centre for Biosciences for his advice, supervision, and crucial contribution in biological activity of compounds and encouragement and support throughout my research and writing thesis. His broad knowledge, understanding and personal guidance have been the guiding light for my thesis work. A sincere thanks to him for giving his precious time for checking my thesis and everready helping attitude.

I wish to express my warm and sincere thanks to **Prof. (Dr.) P. Ramarao**, **Acting Vice Chancellor and DAA, Central University of Punjab, Bathinda** for his cooperation, loving support and allowing me to avail the essential infrastructure and library facilities and providing me the opportunity and all the necessary facilities for carrying out the research work.

I wish to express my warm and sincere thanks to **Prof. (Dr.) Jairup Singh**, **Ex. Vice Chancellor, Central University of Punjab, Bathinda** for providing me the opportunity and all the necessary facilities for carrying out the research work.

I would like to express my deepest gratitude to **Prof. (Dr.) R.C. Sharma**, Professor in-charge, Examinations for his valuable guidance and generous advice.

I am very grateful to all the faculty members **Dr. Vikas Jaitak, Dr. Vinod Kumar,** and **Dr. Harish Holla** of Centre for Chemical and Pharmaceutical Sciences for being very supportive and caring for us at every step.

I would love to thank my friends **Barinder Singh** and **Raman** for helping me in statistical part of my thesis, forwarding me the required articles and helping, encouraging and supporting me throughout my M.Pharm. Thanks to my friends **Shephali**, **Guramrit**, **Haspreet**, **Preeti** and **Bhawna Di**, for being with me always. I thank **Mr. R.P. Cholia** for carrying out my biological screening part.

I love to thank **Monika Di** and **Akanksha** for being my helping hands always, for the continous love and support. Without you I can't imagine my M.Pharm. Thank you **Sheetal** for being such a lovely roommate. Your wonderful personality inspires me to find happiness whatever the circumstances are.

I thank my friends and fellow labmates **Anil, Ashish, Gaurav, Mayank** and **Vijayinder** for being so helping and caring whenever and wherever i needed them. Cheers to the cup of teas and the fun we had together. A sincere thanks and respect to all my **seniors** for guiding me and helping me wherever needed. Thanks to all my lovely **juniors** for being a cheerful part of our CPS family. Thanks **Archana** and **Anuradha** for helping me completing my last minute works.

I would like to acknowledge **Mr. Rajesh Tiwari**, **Mr. Roshan** and **Mr. Vishal** for providing me the necessary labwares required in my synthetic work.

I also extend my thanks for the co-operation offered by the non-teaching staff members for their generous help.

At the outset I bow down my head to my family, without them my university education would not have been possible at all. I thank **Mom**, **Dad**, bro **Babal** for all their love, cooperation, understanding, motivation and supporting me spiritually

throughout my life. My loving thanks are due to all my relatives who complete my family.

The good wishes of all my well-wishers are gratefully acknowledged and sincere thanks to all the fellows who have helped me directly or indirectly.

Gagandeep Kaur

TABLE OF CONTENTS

LIST OF TABLES

LIST OF FIGURES

LIST OF SCHEMES

LIST OF APPENDICES

LIST OF ABBREVIATIONS

Sr.No	Full Form	Abbreviation
1.	Single Strand Breaks	SSBs
2.	Base Excision Repair Pathway	BER
3.	Nucleotide Excision Repair	NER
4.	Mismatch Repair	MMR
5.	O6-methylguanine DNA Alkyltransferase	MGMT
6.	Double Strand Breaks	DSBs
7.	Homologous Recombination	HR
8.	Non-homologous End Joining	NHEJ
9.	Human APE1	HAPE
10.	Apurinic/apyrimidinic	AP
11.	Apurinic/apyrimidinic Endonuclease 1	APE1
12.	Transcription Factor	TF
13.	Cysteine	Cys
14.	Redox EffectorFactor1	Ref-1
15.	Protein Data Bank	PDB
16.	Hydrogen Peroxide	H_2O_2
17.	Hypochlorous Acid	HOCl
18.	Thioredoxin	TRX
19.	Helicobactor Pylori	H.Pylori
20.	Gastric Epithelial Cell	GEC
21.	Early Growth Response Protein 1	EGR-1
22.	Nuclear Factor Kappa B	NF-kB
23.	Activator Protein 1	AP-1
24.	Paired Box Protein	Pax-6
25.	Activating Transcription Factor	ATF
26.	cAMP Response Element-binding Protein	CREB
27.	Hepatic Leukemia Factor	HLF

28.	Phosphatase and Tensin Homolog	PTEN
29.	Central Nervous System	CNS
30.	Mitochondrial DNA	mtDNA
31.	Electron Transport Chain	ETC
32.	Reactive Oxygen Species	ROS
33.	Ionising Radiations	IR
34.	Polymerase β	Pol β
35.	Short Patch	SP
36.	Long Patch	LP
37.	Zebrafish APE1	Zape1
38.	Library of Pharmacologically Active Compounds	LOPAC
39.	7 nitro-indole-2 carboxylic acid	CRT0044876
40.	Aurintricarboxylic Acid	ATA
41.	(2E)-3-[5-(2,3-Dimethoxy-6-methyl-1,4-benzoquinoyl)]-2-nonyl-2- propenoic acid	E3330
42.	Blood Brain Barrier	BBB
43.	Fourier Transform Infrared	FT-IR
44.	Ultra Violet	UV
45.	Time-of-flight Mass Spectrometry	TOF-MS
46.	Electrospray Ionisation Mass Spectrometry	ESI
47.	Electron Ionisation	EI
48.	Round Bottomed Flask	RBF
49.	Room Temperature	RT
50.	Thin Layer Chromatography	TLC
51.	Dulbecco's Modified Eagle's Medium	DMEM
52.	Phosphate Buffer Saline	PBS
53.	3-(4, 5-dimethylthiazol-2-yl)-2, 5-diphenyl tetrazolium bromide	MTT
54.	Dimethyl Sulfoxide	DMSO
55.	Nuclear magnetic resonance	NMR
56.	Meltind Point	MP

57.	Fetal Bovine Serum	FBS
58.	Micromolar	µM
59.	Standard Deviation	S.D
60.	Structure Activity Realtionship	SAR
61.	3-Dimensional	3-D
62.	2-Dimensional	2-D
63.	Doublet	d
64.	Singlet	s
65.	Multiplet	m
66.	Triplet	t
67.	Doublet of Doublet	dd
68.	Coupling constant	J
69.	Parts Per Million	ppm
70.	Hertz	Hz

CHAPTER 1

INTRODUCTION

1. Introduction

The present scenario of cancer chemotherapy depicts that various factors lead to failure of chemotherapy via several mechanisms such as altered drug target, decrease cellular uptake of drug due to enhanced drug efflux by efflux transporters, drug detoxification by overexpressed drug metabolising enzymes, blocked apoptosis, enhanced DNA repair, altered cell cycle check points, resistance due to enhanced cellular stress responses, and activation of microenvironment induced drug resistance pathways (Saraswathy & Gong, 2013; Tomida & Tsuruo, 2002). However, especially the acquired resistance towards the DNA damaging agents is possibly because of the activation of DNA repair system which causes decreased cell mortality responsive to the DNA damaging chemotherapy (Rodrigues et al., 2013).

DNA damaging factors can be endogenous, exogenous or environmental. Various endogenous DNA repair pathways naturally respond to DNA lesions and repair the damaged DNA (Sancar et al., 2004). These are repair of damaged bases and single strand breaks (SSBs) by base excision repair pathway (BER) (Dianov & Parsons, 2007; Fung & Demple, 2011; Gredilla, 2010; Hitomi et al., 2007; Vascotto et al., 2012), repair of large adducts and bulky lesions by nucleotide excision repair (NER), recognition and repair of mismatches or misalignments of short nucleotide segments by mismatch repair (MMR), direct repair of alkyl adducts by O6-methylguanine DNA alkyltransferase (MGMT), repair of double strand breaks (DSBs) by homologous recombination (HR) and non-homologous end joining (NHEJ) (Kelley & Fishel, 2008; Luo et al., 2010; Rodrigues et al., 2013). Each one of these pathways employ various specialised set of enzymes and proteins (Almeida & Sobol, 2007; Caldecott, 2007; Hung et al., 2005; Klungland & Lindahl, 1997; Kubota et al., 1996).

It has been reported by Lindahl in 1993 that 2,000-10,000 apurinic/apyrimidinic (AP) sites are created every day in each human cell by normal metabolic processes and environmental factors which are subsequently repaired by BER-

pathway (Hegde et al., 2008; Hegde et al., 2012; Lindahl, 1993; Mantha et al., 2013). Certain cancers are deficient in one of the pathways to repair their DNA (e.g. HR) but have alternate pathways for repair i.e. BER-pathway. It has also been found that repair proteins are overexpressed in various cancers. So, BER-pathway can be targeted selectively and innovative anticancer therapy can be developed by design of repair enzyme inhibitors (Rodrigues et al., 2013). Apurinic/apyrimidinic endonuclease 1 (APE1) is selectively targeted which is a key enzyme of BER pathway and is responsible for 95% of the repair activity. APE1 acts on AP sites of damaged DNA and repairs it by various consequent steps. Two types of APE1 repair inhibitors have been developed, specific and nonspecific. Specific ones bind to APE1 and inhibit its binding to endogenous ligand AP DNA and nonspecific repair inhibitors bind (abasic) AP DNA and inhibit APE1 to act on its ligand and thus inhibits repair of damaged DNA. Various inhibitors (Lucanthone, 6-hydroxy-DL-DOPA, Arylstibonic acids etc.) have emerged through random screening of library of compounds and they show various side effects and off target effects (Madhusudan et al., 2005; Simeonov et al., 2009). Now a days rational designing of APE1 repair inhibitors have been carried out on the basis of interactions of co-crystal structure of AP DNA with APE1 (Zawahir et al., 2008). Compounds designed on this basis have shown good IC_{50} values. In the present work we have designed and synthesized some novel APE1 inhibitors based on pharmacophoric requirements as well as resembling the shape of the repair active cavity of APE1 and evaluated them for in vitro anticancer activity.

CHAPTER 2

REVIEW OF LITERATURE

2. Review of literature

2.1 APE1

APE1 was first recognised as Human APE1 (HAPE1) by Demple and co-workers in 1991 (Demple et al., 1991). APE1's C-terminal was found to actively participate in DNA repair BER-pathway. One year later Xanthoudakis and Curran reported that APE1 stimulates DNA binding activity of transcription factor (TF) AP-1 through conserved cysteine (Cys) residue in c-Fos and c-Jun (Xanthoudakis, S & Curran, 1992). It was further explored that N-terminal plays a major role in redox regulation of various TFs (e.g., AP-1, NF-κB, CREB, p53, HIF-1α, STAT3, Pax-6 etc.) which contributes in cell growth and progression, angiogenesis, inflammation, downregulation of apoptosis etc. in malignant melanomas (Abbotts, R. & Madhusudan, 2010; Ando et al., 2008). APE1 converts the inactive TFs to their reduced active form, enhances their binding with DNA and increases expression of various genes responsible for progression and promotion of tumor (Luo et al., 2010; Xanthoudakis, S & Curran, 1992). Thus it was named redox effector factor 1 (Ref-1). Both these functions are independent of each other (Izumi et al., 2005). Any mutation in one's active residue does not alter others' activity (Jayaraman et al., 1997; Luo et al., 2008; Ordway et al., 2003).

APEs play a critical role in repairing of oxidized base damages by BER-pathway. There exist two classes of AP endonucleases, Class I and Class II (Figure 2.1). The Class-II can be further classified into two families which differ in structure but undergo the same mechanism for their function. These families are classified on the basis of their structural similarity with the two endonucleases in E. coli i.e. exoIII and endoIV. APE1 is human homologue of exoIII with 26% sequence identity. APE2 is also an Exonuclease III homologue and is not fully explored yet (Abbotts et al., 2011)

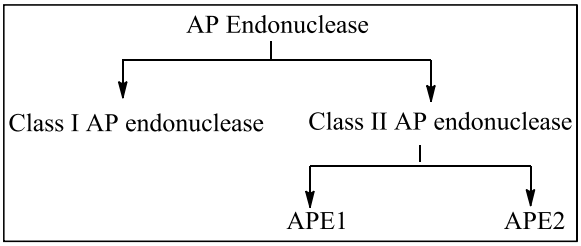

Figure 2.1: Classification of APEs

APE1 is a 318 amino acid long, 35,000 Da globular protein. It consists of two distinct domains N-terminal and C-terminal. Each domain is composed of six stranded β sheets surrounded by α helices. Both collectively forms four layered α/β sandwich fold. Interior comprises of antiparallel β strands, while α helices line the exterior (Gorman et al., 1997; Khaliullin et al., 2012). The first crystal structure of APE1 was reported in 1997 (PDB ID 1BIX) as shown in figure 2.2 (Gorman et al., 1997).

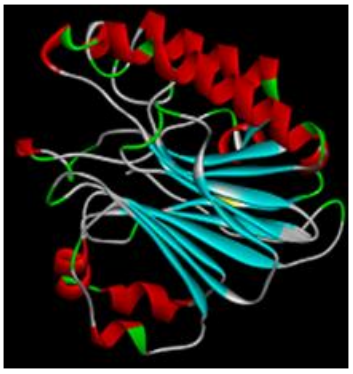

Figure 2.2: Crystal structure of APE1 extracted from PDB 1BIX using autodock

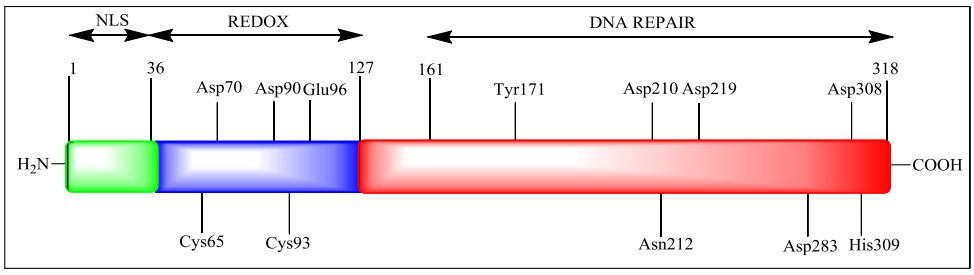

Figure 2.3: Representation of amino acid residues involved in endonuclease and redox activity of APE1. Reproduced from Abbotts et al., 2011

The first 33-35 amino acids in the N-terminal are involved in protein-protein interaction(s) and its RNA binding activity (Mantha et al., 2012). It plays an essential role in transfer of cytoplasmic APE1 to the nucleus during oxidative stress conditions (Jackson, E. B. et al., 2005). The region between 35 and 127 amino acids, is responsible for the redox activity and from 161 to 318, the C-terminal region is responsible for DNA repair activity (Figure 2.3) (Bhakat et al., 2009; Tell et al., 2010).

2.2 EXPRESSION AND REGULATION

The APE1 protein is encoded by the APE1 gene located at the chromosome number 14 which is of 2.6 kb containing four introns and five exons, the first one is non coding (Evans et al., 2000). Gene expression is regulated at transcriptional and post-transcriptional level. It has been seen that hydrogen peroxide (H_2O_2) and hypochlorous acid (HOCl) induces APE1 gene.(Bhakat et al., 2009; Grosch et al., 1998) Oxidative stress i.e. formation of ROS also acts as an inducer of APE1 gene (Hsieh et al., 2001; Pines et al., 2005; Ramana et al., 1998; Tell et al., 2009; Zaky et al., 2008). The ultimate outcome and activation is illustrated in figure 2.4. Further oxidative stress also enhances nuclear translocation of thioredoxin (TRX) which is an important factor for activation of Cys residues of APE1 responsible for redox function. External stimuli like cytokines and hormones are also responsible for regulation of APE1 expression (Bhakat et al., 2009). It is found in an inverse relationship with p53 (Chu et al., 2012; Zaky et al., 2008). APE1 also found to activate p53 and stimulates its DNA binding (Gaiddon et al., 1999). APE1 activates only wild-type p53 for enhanced DNA binding whereas it does not affects mutated p53 (Jayaraman et al., 1997; Kelley et al., 2012). APE1 plays an essential role in p53 mediated apoptosis. It has been found that anti-apoptotic protein Bcl2 directly interact with APE1 and inhibits BER-pathway by downregulation of APE1 gene (Bhakat et al., 2009; Zhao et al., 2008).

Helicobactor pylori (H. pylori) infection is also found to be an inducer of APE1 (Crowe et al., 1995). Further activation of APE1 inhibits gastric epithelial cell (GEC) apoptosis by inducing cell proliferation and causing DNA repair of damaged cells (Chattopadhyay et al., 2010). Various stimulus and their effects have been described in figure 2.5.

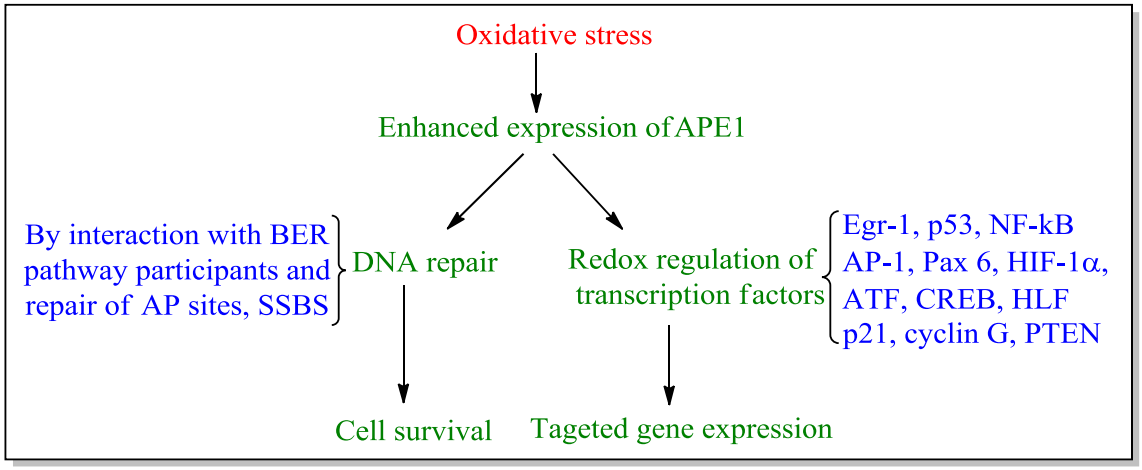

Figure 2.4: Multifunctional role of APE1 in response to oxidative stress (Tell et al., 2009). Early growth response protein 1 (EGR-1), nuclear factor kappa-B cells (NF-kB), activator protein 1 (AP-1), paired box protein (Pax 6), activating transcription factor (ATF), cAMP response element-binding protein (CREB), hepatic leukemia factor (HLF), phosphatase and tensin homolog (PTEN)

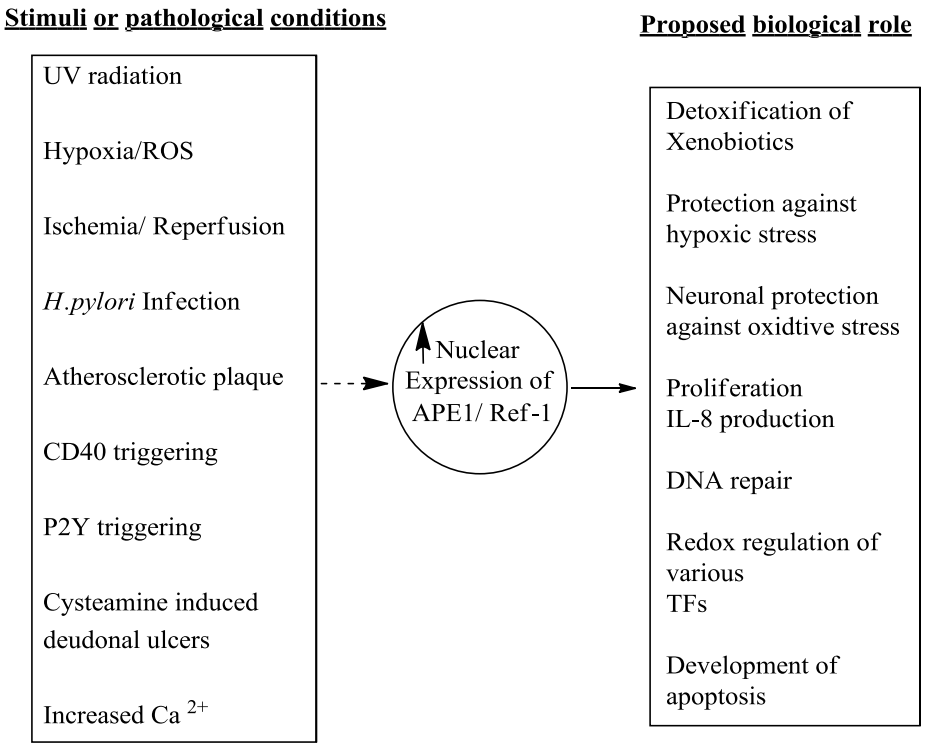

Figure 2.5: Various stimuli activating APE1 expression and function. Reproduced from (Tell et al., 2009)

2.3 LOCATION OF APE1

APE1 is abundantly expressed in many cell extracts i.e. 10^5-10^6 molecules per cell and has a relatively long half life of 8 hr (Zhao et al., 2008). Nuclear expression of APE1 is seen in ovarian, stromal and epithelial cells, adrenal medullary cells, cervical basal cells, and parathyroid glandular epithelial cells, possibly to perform the DNA repair function (Bapat et al., 2009; Kakolyris et al., 1998). APE1 also highly expressed in many selected regions of central nervous system (CNS) (Ono et al., 1995). It is found predominantly in the dentate gyrus and CA3 and CA4 regions of hippocampus (Duguid et al., 1995).

APE1 is highly expressed in cytoplasm of many cell types like macrophages, spermatocytes, hippocampal cells, hepatocytes, hypoglossal motor neurons, and breast cells (Duguid et al., 1995; Kakolyris et al., 1998; Rivkees & Kelley, 1994). APE1 expression in cytoplasm is to keep the newly synthesised TFs in a

reduced state which is their active form. It has been seen that APE1 localized to nucleus on response to oxidative stress (Jackson et al., 2005). In some cells both cytoplasmic and nuclear localisation of APE1 has been seen especially including adreno cortical cells, cerebellar purkinje cells, some cervical cells, pneumocyes, and parietal and mucosal cells of the stomach (Evans et al., 2000; Tell et al., 2005). Higher levels of APE1 are found in cytoplasm as compared to nucleus (Mitra et al., 2007). Expression of APE1 has also found in human and ascidian gametes and embryos (El-Mouatassim et al., 2007).

APE1 is found in scarce quantity in mitochondria, so targeting mitochondrial DNA (mtDNA) repair is an important therapeutic target such as in maintaining neuronal cell genome integrity (Mantha, Anil K. et al., 2013). mtDNA is 10-15 times more susceptible for oxidative damage due to absence of histones and other proteins bound to it which are capable of reducing oxidative damage. Also mtDNA is located in close proximity of electron transport chain (ETC) and more exposure to high levels of ROS. Further in mitochondria NER is absent, so BER-pathway is the major pathway for mtDNA repair which involves APE1 (Hegde et al., 2012; Mantha et al., 2013; Zhao et al., 2008).

2.4 DNA REPAIR ACTIVITY

DNA repair activity is localized to the C-terminal region of APE1. DNA damaging instincts can be endogenous i.e. reactive oxygen species (ROS), hydrolytic damage, non-enzymatic alkylation by S-adenosylmethionine, adduct formation during lipid peroxidation, deamination and depurination [abasic, AP sites] (Lindahl, 1993). Various environmental insults such as hydrocarbons environmental xenobiotics are also responsible for DNA damage (Bernstein et al., 2013; Fishel et al., 2013). Exogenous agents are mainly ionising radiations (IR), radiomimetic drugs, DNA damaging chemotherapeutic agents etc (Jackson, 2001). The major pathway involved for repair of oxidized base damage, AP sites, and strand breaks as discussed above is BER-pathway. BER pathway was discovered by Thomas Lindahl in 1974 (Krokan et al., 2000; Seeberg et al., 1995)(Mitra et al., 2007). BER-pathway is the major target, as

knockout studies of various proteins of this pathway leads to embryonic lethality of the mice models (Wilson & Thompson, 1997; Xanthoudakis, Steven et al., 1996). APE1 and polymerase β (Polβ) are found to be the key players in BER-pathway. No effective backup of APE1 has been seen in mammalian cells (Luo et al., 2010). It alone is responsible for the 95% endonuclease activity in DNA BER-pathway (Demple et al., 1991). BER involves two sub pathways for repair i.e. short patch (SP) and long patch (LP) which differ in involvement of different proteins and also the size of the damaged DNA involved in repair. Mechanism as shown in figure 2.6 involves removal of damaged base by hydrolysing the N-glycosidic bond by enzyme DNA glycosylase in the first step. In SP-BER only one defected base is removed whereas in LP-BER 3-8 damaged bases surrounding the AP site are removed by glycolases. This leaves the DNA backbone intact with the AP site i.e. absence of base. APE1 act on AP site and hydrolyse the phosphodiester bond which is immediately 5' to the AP site. This leaves a free 3' OH group and a deoxyribose-5-phosphate on an AP site. Subsequently other enzymes act to repair the cleaved site. Polymerase β replaces the damaged nucleotide by a new nucleotide and DNA ligase seals the nicks (Hegde et al., 2008; Hegde et al., 2012; Mantha et al., 2013; Mohan & Madhusudan, 2013; Wilson III & Bohr, 2007).

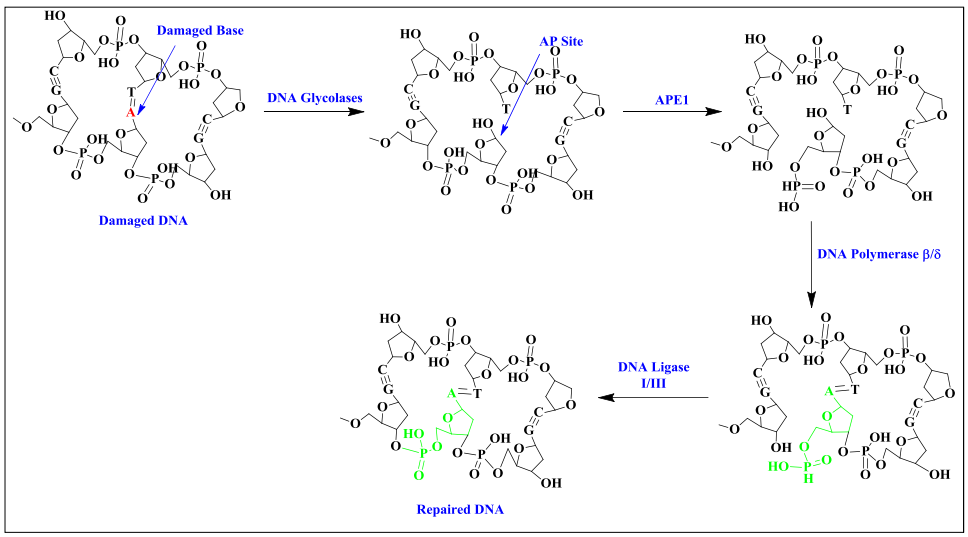

Figure 2.6: Steps and key enzymes involved with BER pathway. Adapted from (Luo et al., 2008)

2.5 MECHANISM OF ENDONUCLEASE ACTIVITY OF C-TERMINAL

2.5.1 Key amino acids involved in APE1's endonuclease activity

The active site in APE1 for endonuclease activity is in the form of a V shaped pocket and lie at the top of the α/β sandwich (Figure 2.7), having two sites for metal ion binding site-A and B (Abbotts et al., 2011; Mol et al., 2000; Oezguen et al., 2011). It is comprised of several amino acid residues (His309, Glu96, Asp283, Thr265, Tyr171, Asn68, Asp210, Asp70, Asp90 and Asn212) which are essential for the endonuclease activity (Mol et al., 2000).

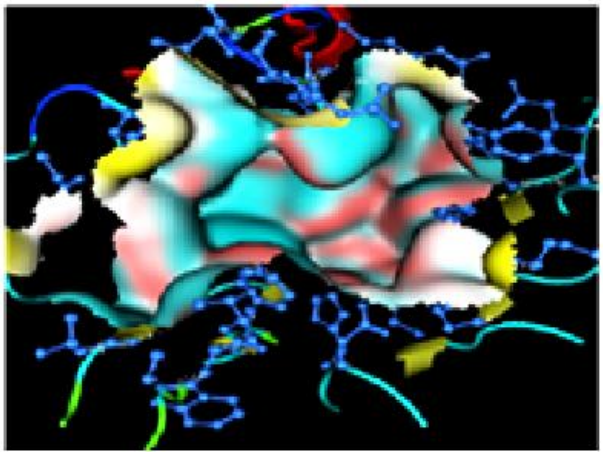

Figure 2.7: Ribbon structure of APE1 showing V shaped endonuclease active site (PDB ID 1DE9)

His309 and Asp283 are believed to play a key role in catalytic activity of APE1 (Figure 2.8 a). Uncharged His309 act as a base and abstracts a proton from water molecule. Asp283 stabilises His309 key residue for endonuclease activity. Resultant hydroxide ion acts as a nucleophile and cleaves the DNA strand at 5' end. Metal ion polarises the transition state and stabilises the negatively charged oxygen atom as shown in figure 2.8 a (Barzilay et al., 1995; Erzberger & Wilson III, 1999). In another proposed mechanism Asp210 activates the attacking water by abstracting the proton from water molecule and form

hydroxide ion nucleophile. Whereas the positively charged His309 facilitated by Asp283 participates in catalytic process by polarising the negatively charged oxygen which was polarised by Mg^{2+} ion (Figure 2.8 b). Mg^{2+} ion here coordinates the phosphate group and stabilises the transition state. Here Asn212 also plays a major role in stabilisation of intermediates and the cleaved phosphodiester deoxyribose (Mol et al., 2000). Yet another mechanism with two metal ions has been proposed with the advent of discovery of two metal ions in the active site of APE1 (Figure 2.8 c) (Beernink et al., 2001; Oezguen et al., 2011; Sanderson et al., 1989).

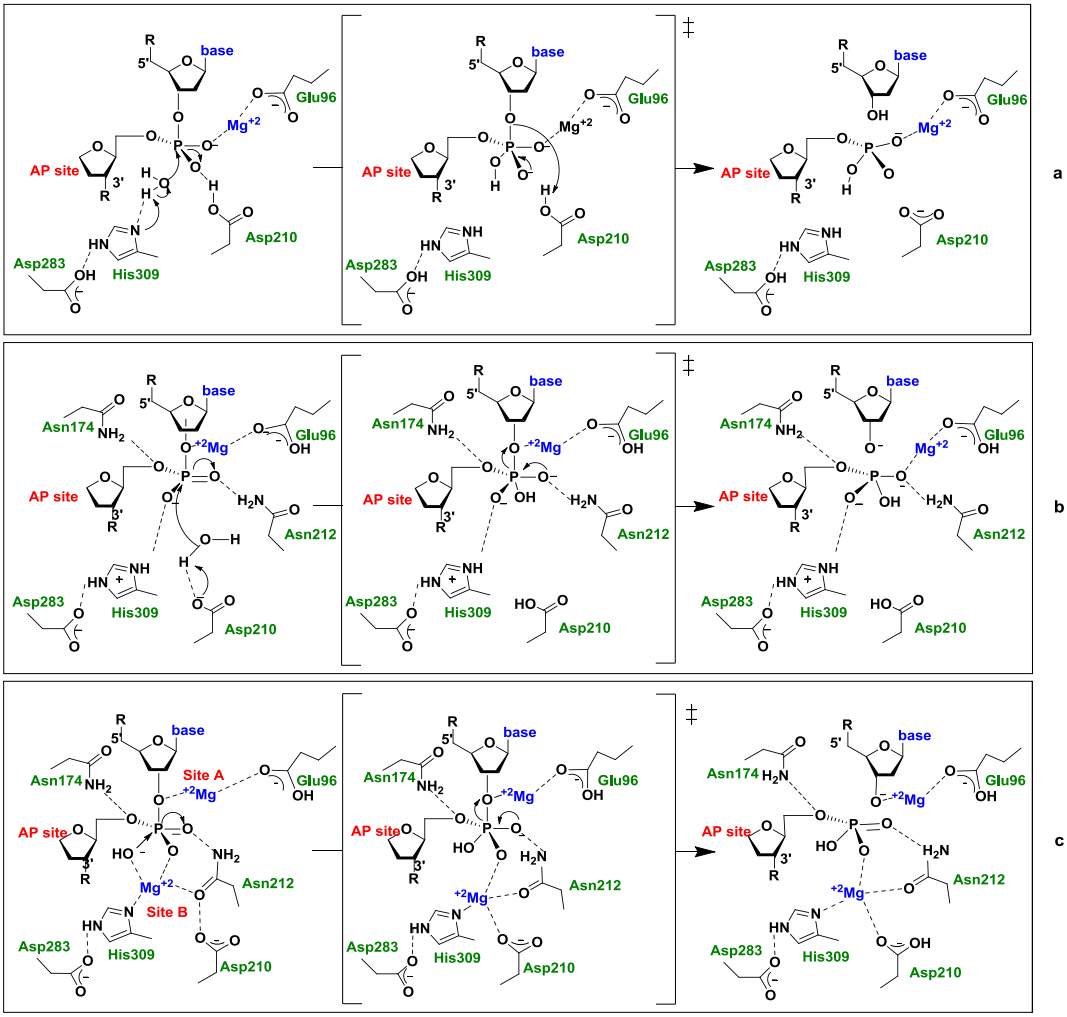

Figure 2.8: Catalytic mechanism(s) of endonuclease activity of active site of APE1. Reproduced from (Khaliullin et al., 2012)

2.6 REDOX ACTIVITY OF N-TERMINAL

APE1/Ref-1 converts the inactive oxidised form of various stress or hypoxia induced TFs including AP-1, NF-κB, ATF/CREB, p53, Pax5, Pax8, c-Myb, HIF-1α and Egr-1 (Bhakat et al., 2009; Cao et al., 2002; Gaiddon et al., 1999; Huang & Adamson, 1993; Lando et al., 2000; Luo et al., 2010; Nishi et al., 2002; Tell et al., 1998; Tell et al., 2009; Tell et al., 2000; Xanthoudakis, S & Curran, 1992) to their reduced active form and thus enhances their DNA binding activity. Various genes are expressed which mediate genomic stability and are involved in cancer enhancement and progression by participating in cell proliferation, angiogenesis and downregulation of apoptosis (Figure 2.9).

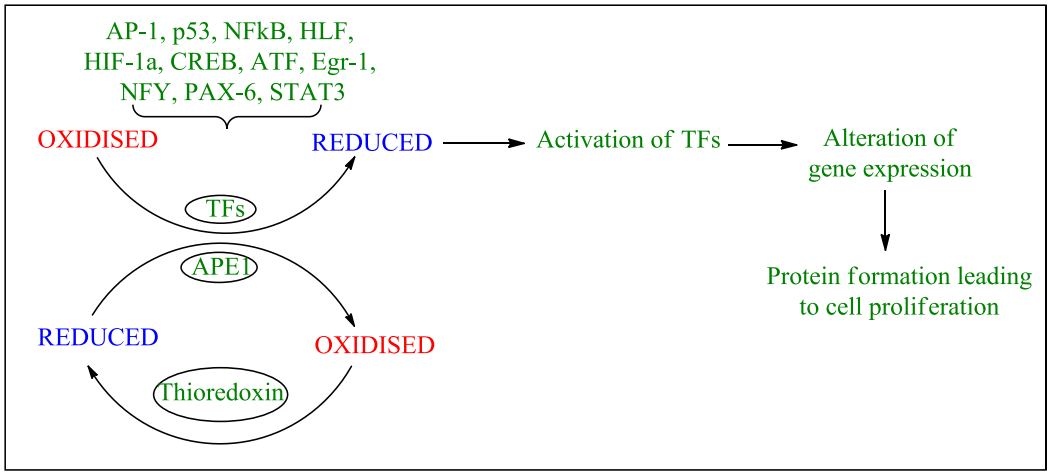

Figure 2.9: The Mechanism of redox regulation of various TFs by APE1/Ref-1. Reproduced from (Luo et al., 2008)

2.6.1 Keys amino acids involved in redox function of APE1/Ref-1

N-terminal's 35 to 127 amino acids are involved in redox function of APE1/Ref-1. This region lies as an extended loop across with β strands. Seven conserved Cys residues are found in human APE1: Cys65, Cys93, Cys99, Cys138, Cys208, Cys296 and Cys310. It is reported that redox function of APE1 is shown only by mammalian APE1 whereas its homologues Zebrafish (zAPE1) lacks it as it contains only five Cys residues compared to seven Cys residue present in mammalian APE1. Cys65 and Cys138 are not conserved in zAPE1

(Georgiadis et al., 2008; Luo et al., 2008). Cys65 was found to be responsible for full redox function of APE1 (Fantini et al., 2010; Georgiadis et al., 2008; Vascotto, Carlo et al., 2011; Walker et al., 1993). Any mutation in Cys65 residue pester APE1 towards redox inactive (Tell et al., 2009).

2.6.2 Redox mechanism

APE1 reduces the Cys residues of TFs, making them (TFs) active for further gene activation processes (Bhakat et al., 2009). Cys65 residue is found on the first β strand which is in the core of the protein, with its side chain pointing towards the hydrophobic pocket away from central β strands sheet. Cys65 is buried in the protein and is not directly water accessible. So, direct involvement of Cys65 in reduction process is yet an unresolved issue.

It is hypothesized that Cys65 forms a disulfide bond with the Cys93 residue (Luo et al., 2012). But both are at large distance from each other i.e. 9 Å, whereas distance of 2.2 Å is required for disulfide bond formation. Also both these residues are present on opposite sides of β sheets. Other residues such as Cys99 and Cys138 are solvent accessible but not close enough to form disulfide bond. Further their mutation with Ala does not cause loss of redox activity implicating that they don't play key role in redox function (Luo et al., 2010). Although mutation of Cys99 with Ser has shown altered activity of enzyme to bind AP site (Mantha et al., 2008). A conformational change may be taking place so that Cys65 may come in vicinity of Cys93 and forms a disulfide bond which is the oxidized form. Thioredoxin (TRX) a redox protein reduces this disulfide bond and makes the Cys65 redox active as illustrated in figure 2.10 (Hirota et al., 1997; Qin et al., 1996). Cys65 further reduces the disulfide bond of TFs and itself again retain the form of disulfide (Luo et al., 2010).

Cys32 of TRX mediates a nucleophilic attack on oxidized disulfide linkage. The mixed disulfide is formed which is resolved by Cys35 resulting in formation of disulfide bond in TRX, thus reducing Cys65 and Cys93 in APE1/Ref-1 and oxidizing itself as shown in figure 2.10. The reduced form of APE1 being the

active form. This activated reduced Cys65 then reduces the disulfide bond of various TFs and converts them to their reduced active form to further perform the functions e.g. activation of target genes expression, cell growth and proliferation.

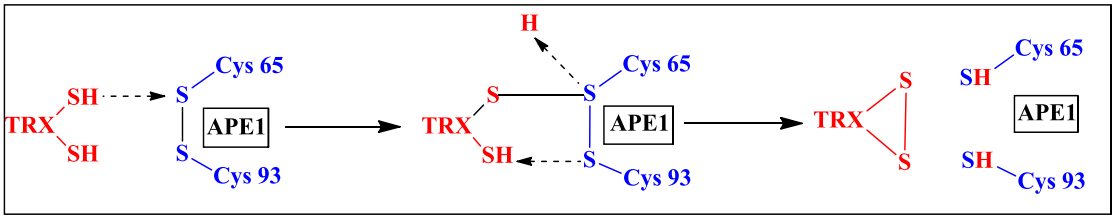

Figure 2.10: Reduction and activation of oxidized Cys residues in APE1/Ref-1 by TRX. Reproduced from (Luo et al., 2012)

2.7 APE1 and CANCER

Relation between cancer cell and APE1 level is of great importance as the role played by APE1 in proliferation of various cancer types and secondly also for developing diagnostic markers for early cancer detection. In case of cervical, prostate, ovarian, colon, rhabdomyosarcomas and germ cell tumors APE1 expression is dramatically elevated as compared to normal tissues. It is in inverse relationship with p53 expression. In other types of cancers APE1 levels are unchanged but their distribution between normal and cancer cells is altered. In case of ovarian and colonic cancer there is also altered expression of APE1 but levels are also elevated at the same time (Evans et al., 2000). In cancer elevated levels of APE1 are linked to both C terminal and N terminal functions i.e. increased DNA repair hence increased resistance to therapeutic agents, decreased therapeutic response, aggressive proliferation, more angiogenesis, short time progression, poor prognosis and hence poor survival rates (Kelley et al., 2012). APE1 levels get upregulated in response of radiation and chemotherapy involving DNA damage. This contributes to treatment resistance and its failure. Apoptosis and APE1 are also closely linked. Decline of APE1 expression is linked with apoptosis. It has also been found that antiapoptotic protein bcl-2 directly interacts with APE1. It inhibits BER by downregulation of

APE1 gene. It can be conferred that when bcl-2 is there it makes the cell cancerous by inhibiting apoptosis, giving the synergistic action with APE1 so there is downregulation of APE1, as bcl-2 is also there for action (Zhao et al., 2008).

Several studies have shown that depletion of APE1 leads to sensitisation of tumour cells to DNA base damage and ultimately death of DNA. Antisense depletion of APE1 is found to hypersensitize HeLa cells to alkylating agents methyl methanesulphonate (MMS), H_2O_2, menadione and paraquet. Antisense APE1 downregulation also hypersensitize lung cancer cells to radiotherapy, pancreatic cancer cells to gemcitabine, and glioma cells to MMS, temozolomide and nitrosoureas. SiRNA mediated APE1 depletion in osteosarcoma also enhances cytotoxicity to alkylating agents and H_2O_2 (Abbotts et al., 2011).

2.8 APE1 INHIBITORS

As endonuclease activity pertaining to C-terminal and redox activity pertaining to N-terminal of APE1 are independent of each other, different inhibitors are reported for their active sites.

2.8.1 Inhibitors of Endonuclease Activity

Any compound that can halt BER-pathway thus results in accumulation of AP sites which are more susceptible to DNA damaging anticancer agents and further damages cancer cell and causes cell death. Thus damage of DNA due to various agents/drugs in cancer cells is much better assured (Wilson & Simeonov, 2010). Many compounds have been successfully screened out as repair inhibitors from random screening of library of compounds. In silico screening of inhibitors have led to identification of several DNA repair inhibitors based on pharmacophore models developed on the basis of interaction of AP DNA with the residues of the active site (Zawahir et al., 2008). The most potent inhibitors are known to have this pharmacophoric scaffold and similarity to 3′ and 5′- deoxyribosephosphate scaffold of AP DNA (Abbotts et al., 2011; Kelley & Fishel, 2008; Mohammed et al., 2011; Naidu et al., 2011). List of APE1

inhibitors synthesized and studied so far are illustrated in figure 2.11 along with their IC_{50} values. These inhibitors act via two mechanisms and are tabulated in Table 2.1.

1) **Specific (direct) Inhibitors:** They interact with APE1 and inhibit it for binding to the abasic DNA i.e. AP site (Liu & Gerson, 2004).

2) **Nonspecific (indirect) Inhibitors:** They bind to AP site on DNA and form a stable adduct. They inhibit APE1 to bind to AP site and display endonuclease activity (Mohammed et al., 2011; Sultana et al., 2012).

Table 2.1: Specific and Non-specific DNA repair inhibitions

Specific DNA repair inhibitors:	**Non specific repair inhibitors:**
CRT0044876	Methoxyamine
6-hydroxy-DL-DOPA	
Myricetine	
Lucanthone	
Arylstibonic Acids	
Aurintricarboxylic acid/(ATA)	

From screening of 5000 compounds Madhusudan et al., reported the first biological and biochemical endonuclease inhibitor for APE1. The compound-1 i.e. CRT0044876 (7 nitro-indole-2 carboxylic acid) was found to be potent and selective inhibitor of APE1 and enhanced cytotoxicity of MMS in vitro but was not developed further as lead compound due to its poor drug like properties and toxicity issues due to the nitro aromatic feature. In another study, Simenov et al., proposed novel inhibitors 6- hydroxy-DL-DOPA, aurintricarboxylic acid (ATA), myricetin and reactive blue 2 (Figure 2.11) from screening of library of pharmacologically active compounds (LOPAC). ATA was found to be the most potent, and enhanced cell killing effect of alkylating agents such as methoxyamine, 6-hydroxy-DL-DOPA, myricetine, reactive blue 2 and methoxymethane sulfonate. But they showed additional off target effects

andsuffer from being unstable in the presence of oxygen (Madhusudan et al., 2005).

Seiple et al., by high-throughput screening of 2000 compounds suggested that arylstibonic acids can be employed as useful scaffolds for designing endonuclease inhibitors (Figure 2.11). The compound 2-nitro-4-stibonobenzoic acid was reported to be the most potent repair inhibitor of APE1 (Seiple et al., 2008) among the tested ones. These compounds were found to have potential towards whole organ toxicity, due to heavy metal antimony (Wilson & Simeonov, 2010).

Zawahir et al., in 2009 designed a set of pharmacophoric models based on interaction of abasic DNA with APE1. A total of 365000 molecules were screened on the basis of these models. Best hits (Figure 2.11) were found on the basis of models H1NI2, H1A1NI2, and A1NI2A3NI (H denoting hydrophobic moiety, NI-negatively ionisable group, A-hydrogen bond acceptor). These were the first molecules designed on the basis of rational drug designing towards AP endonuclease inhibitors (Zawahir et al., 2008).

Methoxyamine was reported to be used in assay for detection of AP sites in vitro in BER-pathway (Liuzzi & Talpaert-Borle, 1985). Later, Taverna et al., and Fischel et al., in their independent studies reported that methoxyamine is an indirect inhibitor of APE1 and further it enhances the cytotoxic effect of TMZ in colon and ovarian cancers respectively (Fishel et al., 2007; Liuzzi & Talpaert-Borle, 1985; Taverna et al., 2001).

Thus Development of small molecule inhibitors of APE1 may lead to inhibition of APE1 activity at C-terminal and may prove as potential therapeutic target in treatment of resistant cancers.

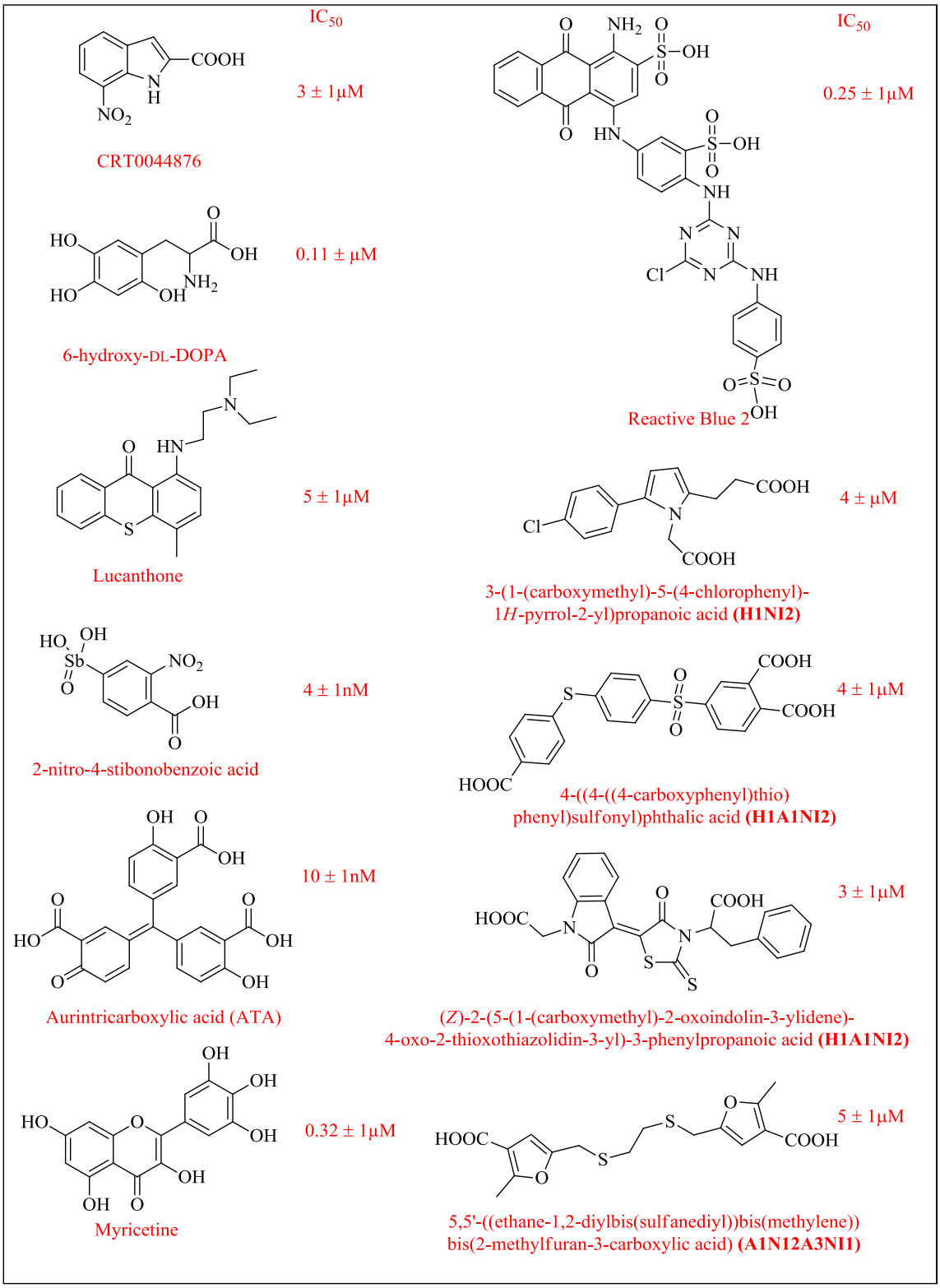

Figure 2.11: Various scaffolds of endonuclease inhibitors of APE1

Pharmacophore guided small molecule APE1 inhibitors:

Various 3D pharmacophore models were designed based on interaction of residues of APE1 with the AP DNA in co crystal structure as shown in figure 2.12 (Zawahir et al., 2008).

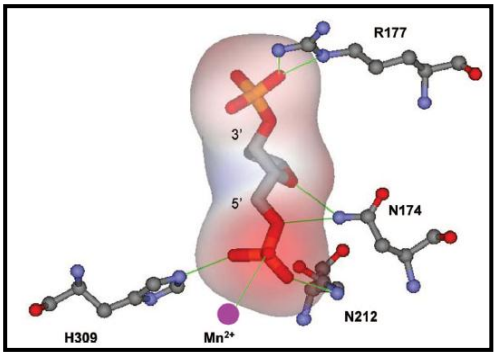

Figure 2.12: Co-crystal structure of APE1 with substrate abasic DNA (Zawahir et al., 2008)

Various interactions were observed which play a key role in determining the pharmacophoric requirements of APE1 inhibitors shown in figure 2.13. Arg177 was found to interact with the negatively charged 3'phosphate of abasic fragment. A hydrophobic pocket containing amino acids Phe253, Trp280 and Ile282 was found to bind the abasic deoxyribose sugar moiety. H-bonding interactions of 5' phosphate were seen with amino acids residues Asn174, Asn212, His309 and Mn^{+2} metal.

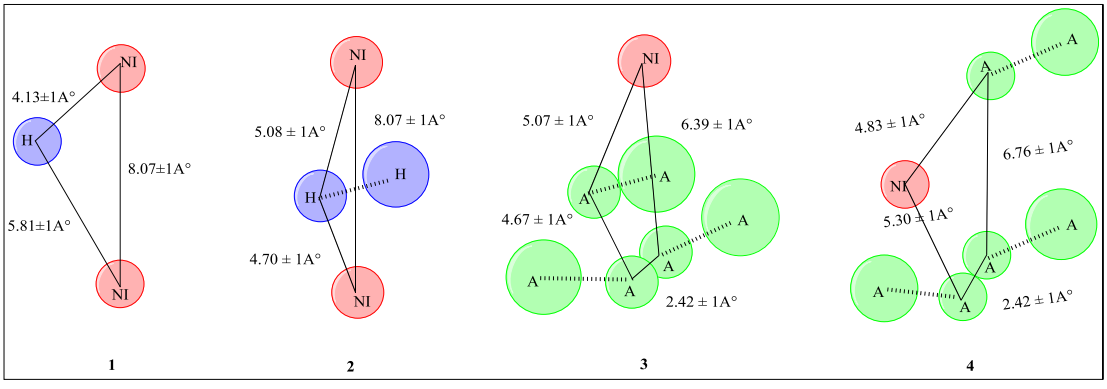

Figure 2.13: Pharmacophoric 3-D models designed on the basis of interaction of AP site DNA with APE1 repair active residues, NI- negatively ionisable

groups (red), H-hydrophobic moiety (blue), and A-hydrogen bond acceptor (green) (Zawahir et al., 2008)

Various 3D pharmacophore models designed based on APE1 interactions with the abasic deoxyribose 3′ and 5′ phosphate backbone in co-crystal structure of APE1 with substrate AP DNA. Various compounds were designed on basis of these models which showed good APE1 endonuclease inhibitory activity.

2.8.2 Redox Inhibitors:

Inhibiting APE1's redox activity appears as a beneficial target in inhibition of cancer cell growth and promoting cancer cell death. Various TFs like HIF-1α, p53, NF-κB, CREB, and AP-1 have been explored as important aspects of cancer including angiogenesis and progression and promotion of tumor cell growth (Khan et al., 2013; Li et al., 2009; Milicevic et al., 2014; Ryu et al., 2014; Shen et al., 2008). By inhibiting APE1's redox activity, these TFs cannot bind to their consenses DNA to display further gene expression and tumor cell signaling of uncontrolled growth and signaling. Various small molecule redox inhibitors, capable of attenuating one or more functions, offer potential for reversal of drug resistance (Dorjsuren et al., 2012; Kelley & Fishel, 2008). List of various redox inhibitors of APE1 are given in figure 2.14.

Lou et al., reported (2E)-3-[5-(2,3-Dimethoxy-6-methyl-1,4-benzoquinoyl)]-2-nonyl-2- propenoic acid (E3330) as inhibitor of redox activity of APE1. E3330 checks growth of cancer cells by inhibiting cell proliferation and angiogenesis (Luo et al., 2008). Manvilla et al., proposed a mechanism for redox inhibition in which E3330 binds specifically to the repair active site of APE1 for stabilization of the enzyme for redox activity and preventing it from undergoing conformational change. Inhibition of endonuclease activity of APE1 was also observed at high concentrations of E3330 (Manvilla et al., 2011). Amidation of E3330 was done by Zhang et al., to confirm whether carboxylate of E3330 is essential for redox function. They found that E3330-amide (IC_{50} - 8.5μM) was more effective redox inhibitor than E3330 (IC_{50} - 20μM) in inhibiting AP1-DNA binding assisted by APE1. In addition E3330-amide did not show any binding to

repair active site which proves that carboxylate is essential for binding to the repair active site and quinone moiety is essential for redox inhibition (Zhang et al., 2013). Nyland et al., synthesized various benzoquinone and napthaquinone derivatives of E3330. Various quinone analogues were analyzed by Kelley et al., such as RN8-51, RN10-52 and RN7-60 as shown in figure 2.14 were found to be the best hits with lowest IC_{50} values (Nyland et al., 2010).

Another study by Raffoul et al., reported that soy isoflavones can cause downregulation of redox activity as well as APE1 enzyme in prostate cancer cells both in in vitro and in vivo (Messina et al., 2006; Raffoul et al., 2007). Earlier study by Yang et al., disclosed that resveratol is involved in inhibition of redox function of APE1 by exhibiting reduced DNA binding of AP1 and NF-κB TFs which play major role in cancer progression (Yang et al., 2005). At high concentrations it was also found to inhibit APE1 endonuclease activity. But neither it has been supported by others nor it is shown to be effective at physiological levels (Luo et al., 2010).

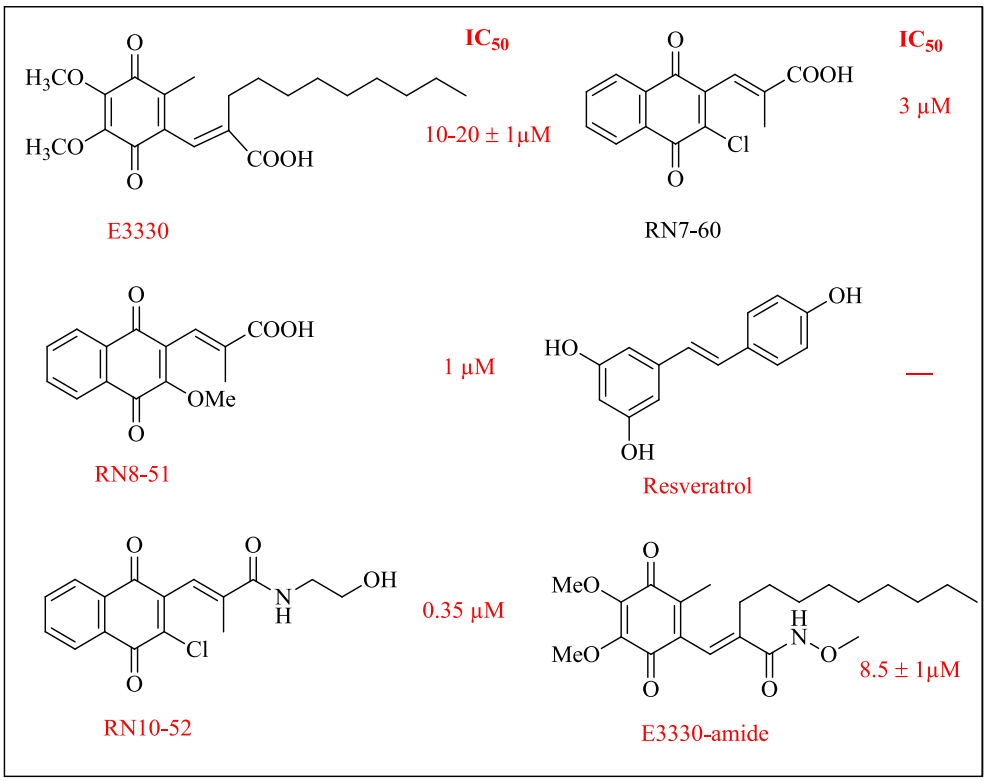

Figure 2.14: Various scaffolds of redox inhibitors of APE1

2.9 CLINICAL STATUS

Till now only two APE1 inhibitors are in clinical trials approved by FDA, USA.

1) **Lucanthone:** Due to its high lipophilicity it can easily cross blood brain barrier (BBB). It is in Phase II clinical trials for treatment of brain Metastases from non-small cell lung adjuvant to radiotherapy. It is required in much lower doses clinically as compared to in vitro studies (Naidu et al., 2011; Wilson & Simeonov, 2010).

2) **Methoxyamine:** It is currently in phase I clinical trials being pursued by TRACON pharmaceuticals. It is studied with temozolomide (TMZ) for treatment of advanced or metastatic solid tumors, primary brain tumors, lung cancer and various other malignancies. A significant preclinical data from Gerson laboratory reveals that methoxyamine increases the cytotoxicity of various alkylating agents as TMZ and carmustine significantly (Wilson & Simeonov, 2010).

CHAPTER 3

RATIONALE FOR THE PROPOSAL

3. Rationale for the proposal

It has been seen from the literature review that one of the general pharmacophores for endonuclease activity is the compounds having central hydrophobic moiety and two negatively ionisable groups at the ends (Figure 3.1). These pharmacophoric models were designed on the basis of interactions of APE1 with the abasic deoxyribose 3' and 5' phosphate backbone in co crystal structure of APE1 with abasic DNA substrate as shown in figure 3.2 (Zawahir et al., 2008). Some of the synthesized compounds were found to have very good IC_{50} values as shown in figure 2.11.

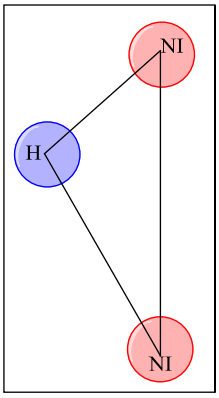

Figure 3.1 Pharmacophoric model with central hydrophobic group linked with two negatively ionisable groups. H; Hydrophobic group, NI; Negatively ionisable group

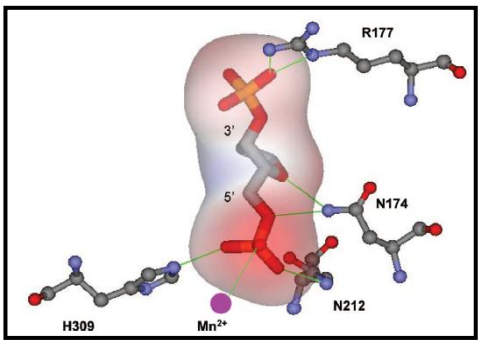

Figure 3.2 Co crystal structure of APE1 with substrate abasic DNA.

Further, it has been observed that the endonuclease cavity of APE1 is V shaped, and increase in resemblance of the structure of the repair inhibitors with the shape of the cavity leads to increase in activity (Figure 3.3).

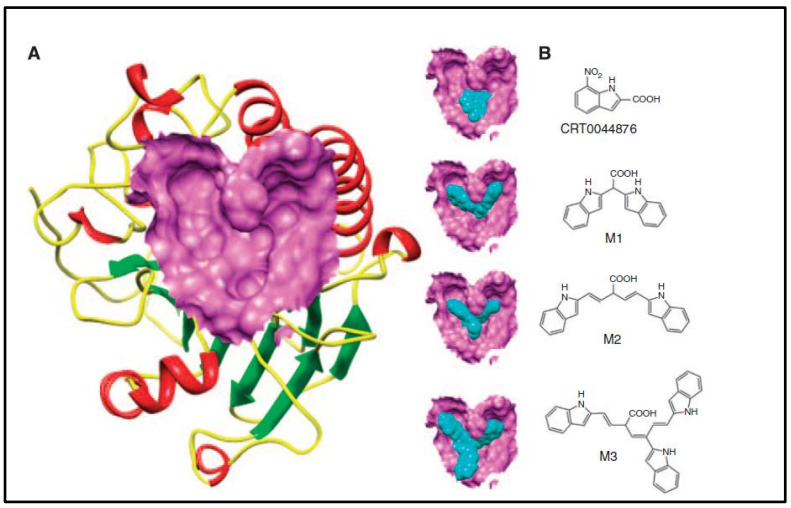

Figure 3.3: (A) V shaped repair active site containing 10 critical amino acid residues essential for endonuclease activity of APE1. (B) Three prototypical scaffolds M1, M2 and M3 based on CRT0044876 and their docked poses into APE1 active site. They showed increase in activity with increase in shape based similarity with APE1 active site (Mohammed et al., 2011)

So we have designed our compounds fulfilling the pharmacophoric requirements of endonuclease activity resembling the shape of the cavity. The designed compounds have one or two negatively ionisable groups at the ends and its shape consists of three arms which may fit into the V shaped endonuclease cavity APE1.

For further ensuring that our compounds fit well to the endonuclease active site molecular modeling studies of the designed compounds were performed. It raises the speculation that designed compounds may exhibit anticancer activity by APE1 inhibition. As there is one chiral centre in the compound both the isomers of each compound were docked.

Molecular docking studies were carried out using the selected ligand molecules using Maestro 9.3 molecular docking suite (Glide). Ligand molecules were designed on the basis of pharmacophore discussed and V shaped cavity of the enzyme. 3D structure of the enzyme was extracted from the PDB ID 1DE9. The docking poses of both isomers were compared with the pose of the standard inhibitor **6-Hydroxy-DL-DOPA.** Ligand molecules were prepared using respective wizard applications, where functions such as addition of hydrogen atoms, fixing of charges and orientation of groups, 2D to 3D conversion, corrected bond lengths and bond angles, states, tautomers, stereochemistry's, ring conformation, etc. was incorporated into ligand molecules followed by minimization and optimization in Optimized Potential for Liquid Simulations (OPLS_2005) force field (Friesner et al., 2004; Friesner et al., 2006). Finally, one conformation for each ligand was generated, and ready for docking. Consequently, input protein molecule was prepared using respective wizard applications, where changes such as addition of hydrogen atoms, assigning bond orders, create zero order bonds to metal, fixing of the charges and orientation of groups were incorporated into the raw PDB structure. After the completion of ligand and protein preparations, a receptor-grid file was generated. For running the grid generation module, we have scaled Van der Waals radii of receptor atoms by 1.00 Á with a partial atomic charge of 0.25. The active site of the receptor provides an accurate scoring function with thermodynamic optimal energy and is calculated on a grid by various sets of fields. After the formation of receptor-grid file, flexible ligands with rigid receptor molecular docking were performed. The final energy evaluation is done on the basis of G-score.

Table 3.1 Docking pose and interactions of designed ligands

Structure (Name)	Docking pose	Dock Score Kcal/ mole	Interactions
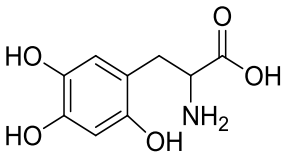 **Hydroxy-DL-DOPA (Standard)**	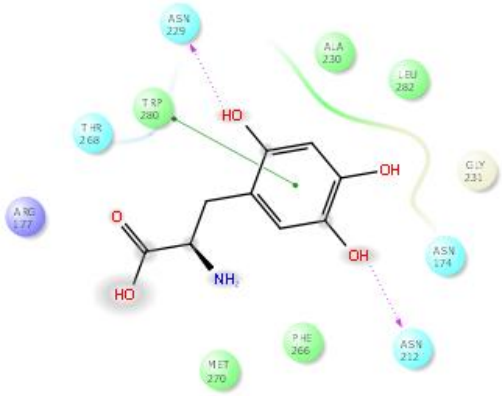	-3.58	π-π TRP 280, H-bonding ASN212 and ASN 229
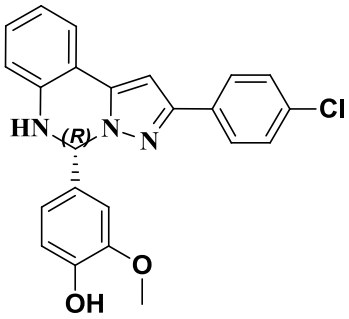 **GR5G-c *R***	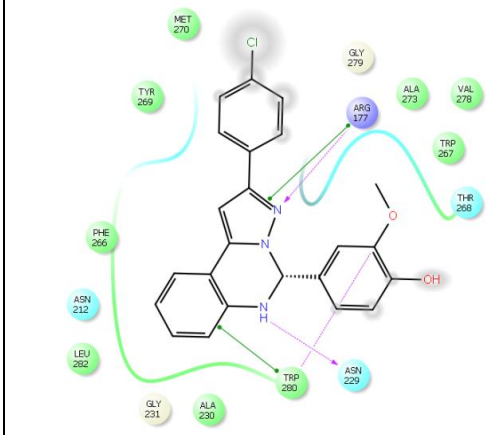	-4.64	π-π TRP 280 and ARG 177 H- bonding ARG 177, TRP 280 and ASN 229
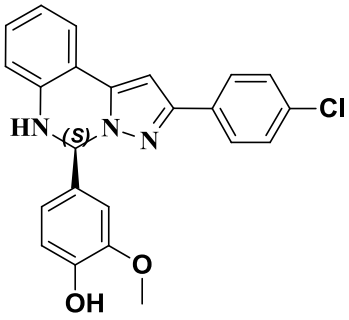 **GR5G-c *S***	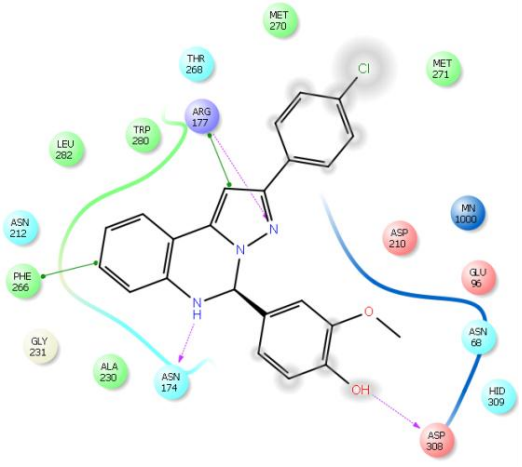	-5.05	π-π ARG 177 and PHE 266 H-Bonding ARG 177, ASN 174 and ASP 308

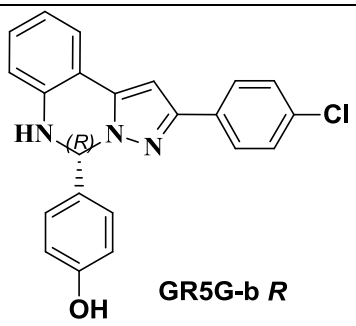 GR5G-b *R*	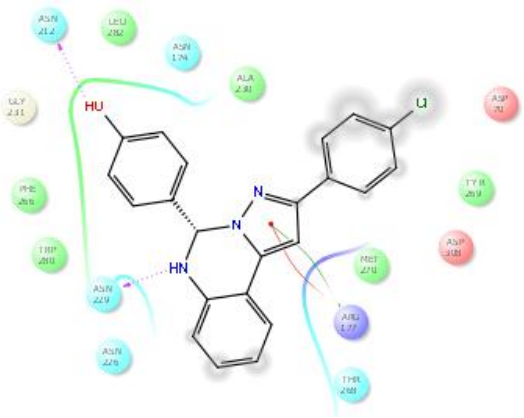	-5.68	π-π ARG 177 H-Bonding ASN 212 and ASN 229 π-cation ARG 177
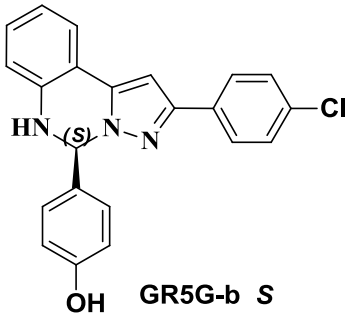 GR5G-b *S*	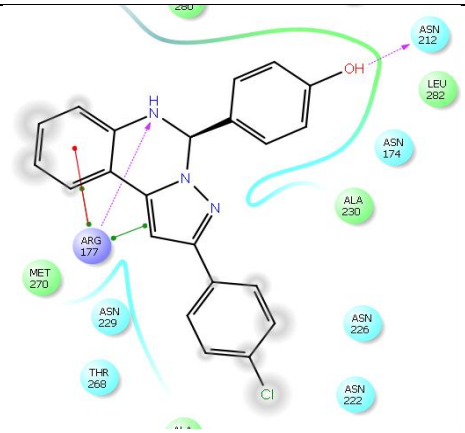	-5.78	π-π - ARG 177 H-bonding- ARG 177, ASN 212 π cation- ARG 177
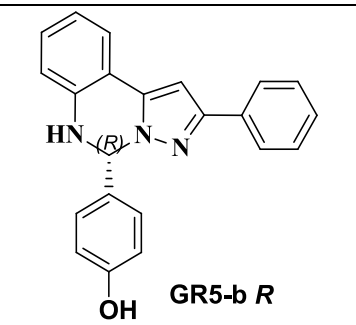 GR5-b *R*	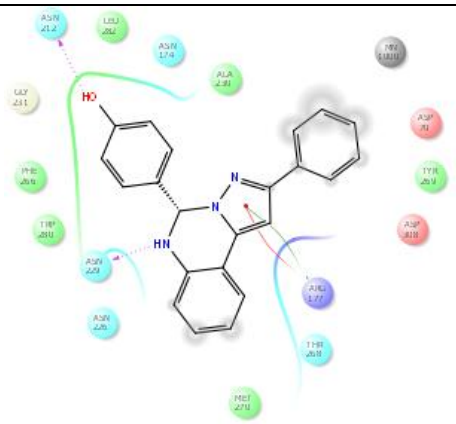	-5.61	π-π -ARG 177 H Bonding- ASN 229, ASN 212 π cation– ARG 177
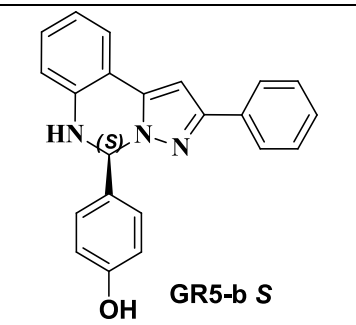 GR5-b *S*	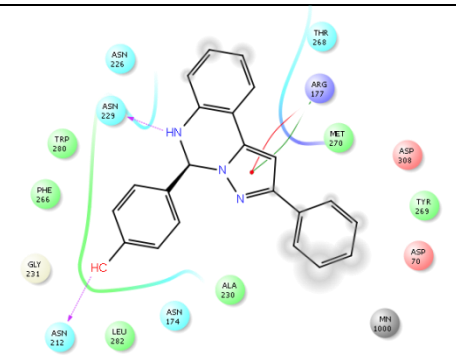	-4.04	π-π – ARG 177 H- Bonding ASN 212, ASN 229 π cation-ARG 177

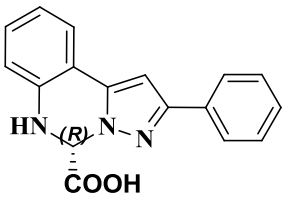 GR5 *R*	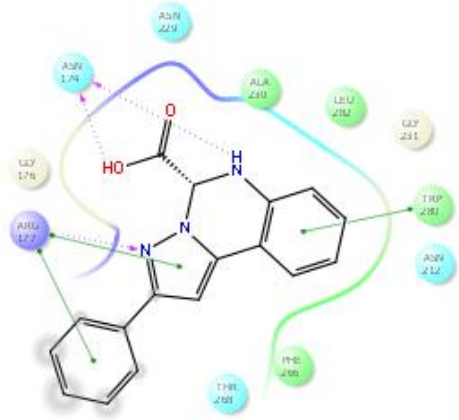	-5.55	π-π TRP 280, ARG 177 H-Bonding- ASN 174, ARG 177
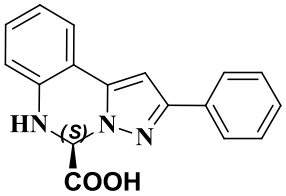 GR5 *S*	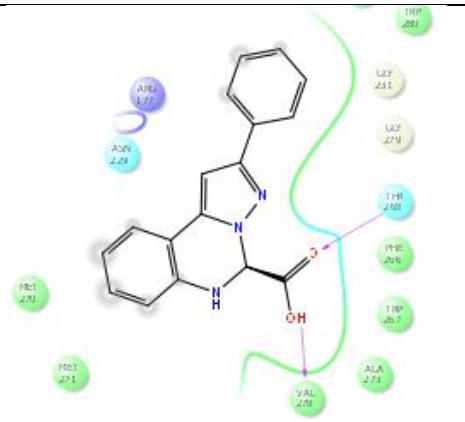	-5.62	H- Bond THR 268, VAL 278
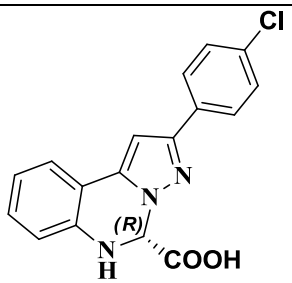 GR5G *R*	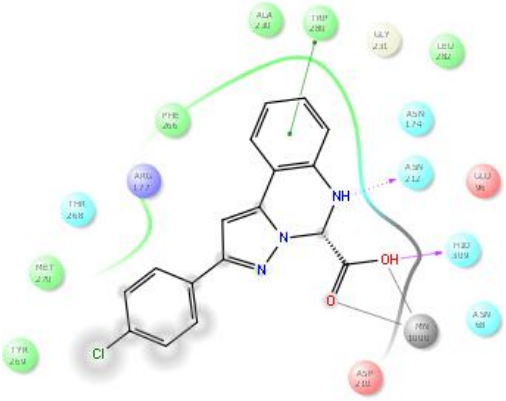	-5.46	π-π TRP 280 Mn^{+2} Coordination H-Bonding (Side Chain)- ASN 212 H-Bond (Backbone) HIS 309
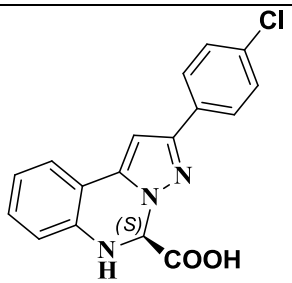 GR5G *S*	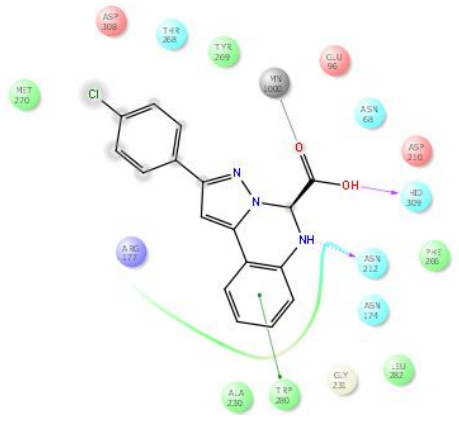	-5.48	π-π-TRP 280 Metal Coordination- Mn^{+2} H Bond- His 309 H Bonding- ASN 212

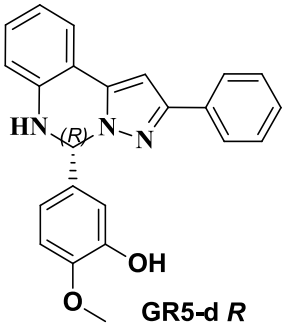 GR5-d *R*	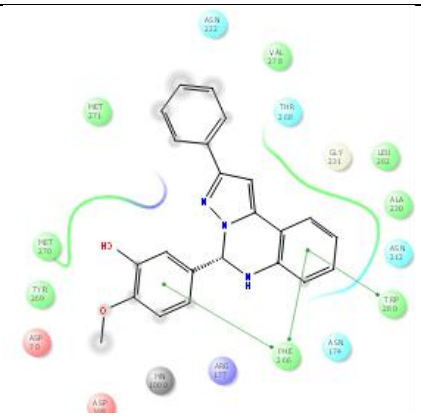	-4.63	π-π PHE 266 and TRP 280
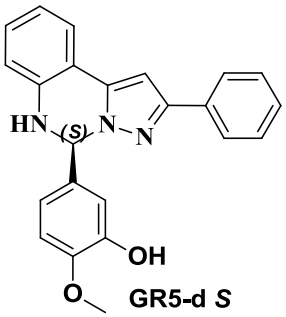 GR5-d *S*	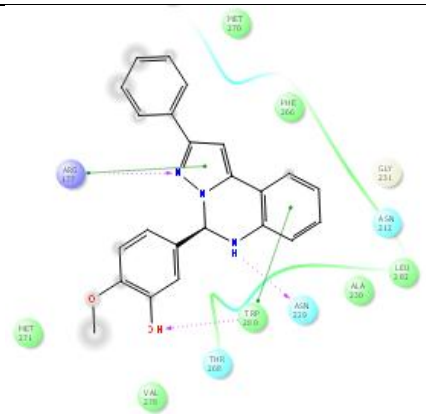	-4.62	π-π ARG 177, TRP 280 H-Bonding- TRP 280, ASN 229 and ARG 177
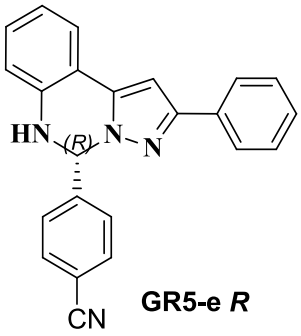 GR5-e *R*	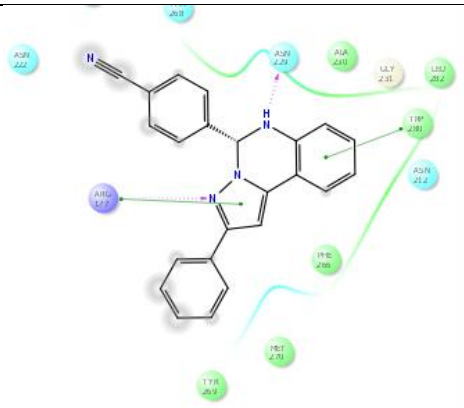	-3.89	π-π TRP 280, ARG 177 H Bonding- ARG 177, ASN 229
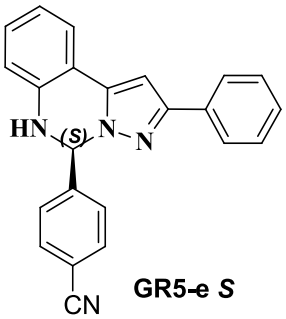 GR5-e *S*	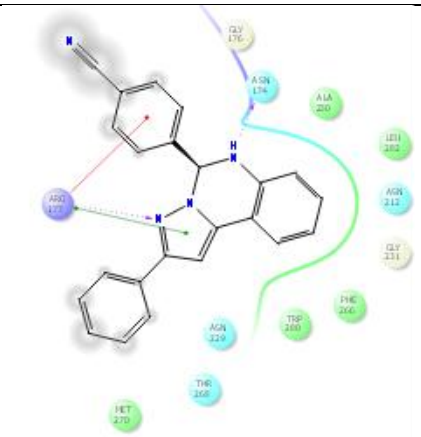	-4.33	π-π ARG 177 H-Bonding- ARG 177, ASN 174 π cation- ARG 177

As we hypothesized that our compounds may exert their anticancer effect via inhibiting APE1 enzyme, we investigated the binding interactions of the compounds by docking designed compounds into the APE1 endonuclease cavity using Maestro 9.6 molecular docking suite. The 3D structure of the target protein was obtained from protein data bank (PDB ID-1DE9). All the compounds have one chiral center, so both ***R*** and ***S*** isomers of each designed compound was docked in the repair active site of APE1. The results obtained were compared with **6-Hydroxy-DL-DOPA** which is an established APE1 repair inhibitor. Both ***R*** and ***S*** isomers of the designed compounds were found to occupy the same cavity as that of standard inhibitor **6-Hydroxy-DL-DOPA** having interactions with common amino acids Arg 177, Asn 212, Asn 229, Trp 280, Phe 266 conserved. Arg 177 was found to be majorly involved in hydrogen bond interactions, π-π interactions and cation interactions through its guanidino group with pyrazolo quinazoline moiety. Standard inhibitor was found to have interactions with Trp 280, Asn 212, Asn 229 and a metal ion Mn^{+2}, the established interactions of endonuclease active residues (Simeonov et al., 2009). The interaction energies of designed compounds were calculated by dock score as given in table 3.1. ***S*** isomer was found to have extra interactions with repair active residues as compared to ***R***. Also dock score of all the designed compounds was found to be lower than standard **6-Hydroxy-DL-DOPA.** ***S*** isomer was found to have even lower interaction energies than ***R***. This overall endorsed that the compounds fit well in the endonuclease activity and are good candidates for APE1 inhibition. **GR5G-c**, **GR5-b** and **GR5G-b** (Figure 3.5) were found to be the best compounds with least interaction energies of less than -5.50 kcal/mole as compared to -3.58 kcal/mole of **6-Hydroxy-DL-DOPA** -. These compounds contain negatively ionisable group OH and electron withdrawing Cl group at other end fulfilling our pharmacophoric requirements.

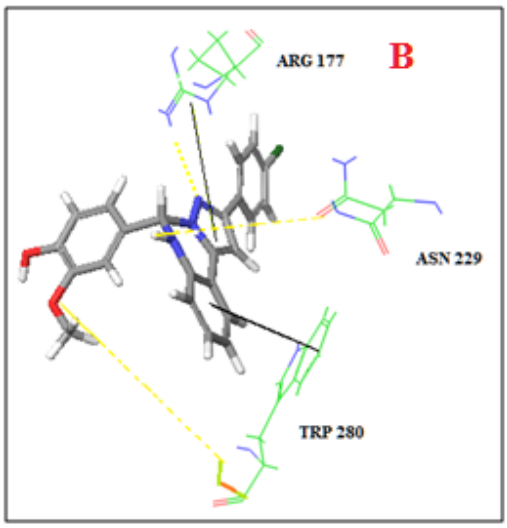

Figure 3.4: Docking pose of standard APE1 repair inhibitor **6-Hyroxy-DL-DOPA** showing interactions with the active residues of endonuclease cavity of APE1

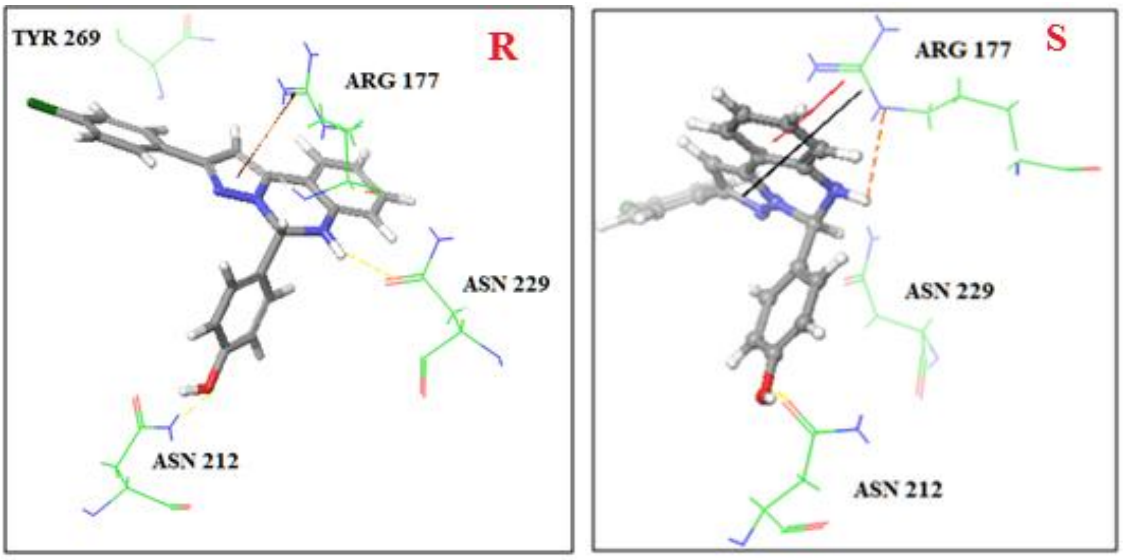

Figure 3.5: Docking pose of ***R*** and ***S*** of **GR5G-b** in showing standard interactions with the active residues of endonuclease cavity of APE1

CHAPTER 4

OBJECTIVES

4. Objectives

With the available literature background, the following objectives were set:

1. Synthesis of the designed compounds pertaining to formula 1.

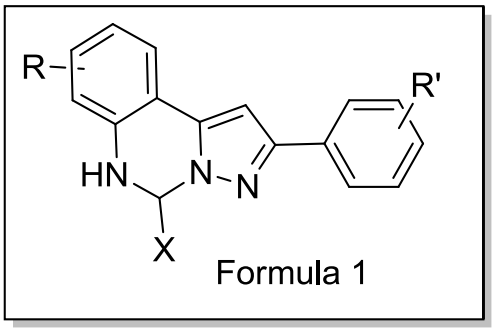

Formula 1

Where R, R' can be any electron donating or withdrawing groups

X = H, COOH, $COOCH_3$, aryl group with or without substitutions

2. In vitro cell line based evaluation for anticancer potential of the synthesized compounds.

CHAPTER 5

MATERIALS AND METHODS

5 Materials and Methods

5.1 Synthesis

5.1.1 General

1. All the reagents were of AR/GR quality and were purchased from Sigma-Aldrich, Loba-Chemie Pt. Ltd., S.D. Fine Chemicals, Sisco Research Laboratory and Avra Synthesis Ltd. and were used without further purification.
2. Sartorius analytical balance (BSA224S-CW) and Mettler Toledo were used for the weighing purposes. JSGW heating mantle, Tarson spinot digital, ILMVAC RO dist. digital rota vapour, digital hop top and NSW oven/vacuum oven were used during the course of reaction.
3. The progress of the reaction was monitored by TLC, using n-hexane/ethyl acetate and chloroform/methanol as the mobile phase on pre-coated Merck TLC (TLC silica gel 60, F254) plates in JSGW UV/fluorescent analysis cabinet and/or iodine chamber.
4. Melting points were recorded on Stuart melting point apparatus (SMP-30) with open glass capillary tubed and were uncorrected.
5. Infrared (IR) spectra of compounds were recorded with KBr on a Bruker FT-IR spectrophotometer.
6. ^{1}H and ^{13}C Nuclear magnetic resonance (NMR) spectra were recorded at Panjab University, Chandigarh in $CDCl_3$/d_6-DMSO on a Bruker Avance II (400 MHz) NMR spectrometer using TMS (δ = 0) as an internal standard.
7. Mass spectra were recorded on TOF-MS/ESI at Panjab University, Chandigarh and MS/EI at Central University of Punjab, Bathinda.

5.1.2 Synthesis of *(E)-3-(2-nitrophenyl)-1-phenylprop-2-en-1-one* (GR1)

A mixture of 2-nitrobenzaldehyde (100 mg, 0.66 mmol) and aryl ketone (79 mg, 0.66 mmol) in glacial acetic acid (5 mL) was stirred in 100 mL round bottomed flask (RBF). Conc. Sulphuric acid (4-5 drops) was added to the reaction mixture in ice cold condition and further stirred at room temperature (RT) for 24 h. Completion of the reaction was determined by thin layer chromatography (TLC). After the completion, the reaction mixture was poured on ice-cold water and filtered. The solid was washed with water and dried to obtain the crude product. The crude product was recrystallized from methanol to get pure compound (Konieczny et al., 2007).

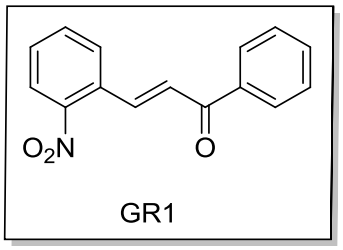

GR1

Yield: 85%, 142.37 mg, Creamy white solid, **MP**: 89-90°C (Alarcon et al., 2013).

IR (KBr, cm^{-1}): 1666 (C=O), 1610 (C=C), 1510 (N=O), 1342 (N=O), 1014 (C-N).

^{1}H NMR ($CDCl_3$, 400 MHz): 8.12 (1H, d, J = 15.9 Hz), 8.02 (3H, bs), 7.69-7.74 (2H, m), 7.50 - 7.57 (4H, m), 7.34 (1H, d, J = 15.9 Hz).

^{13}C NMR ($CDCl_3$, 75 MHz): 190.22, 148.34, 140.03, 137.20, 133.56, 133.09, 131.08, 130.31, 129.13, 128.62, 126.97 and 124.86.

5.1.3 Synthesis of *(E)-1-(4-chlorophenyl)-3-(2-nitrophenyl)prop-2-en-1-one* (GR1G)

A mixture of 2-nitrobenzaldehyde (100 mg, 0.66 mmol) and p-chloro acetophenone (189 mg, 0.66 mmol) in glacial acetic acid (5 mL) was stirred in 100 mL round bottomed flask (RBF). Conc. Sulphuric acid (4-5 drops) was added to the reaction mixture in ice cold condition and further stirred at room temperature (RT) for 24 h. Completion of the reaction was determined by thin

layer chromatography (TLC). After the completion, the reaction mixture was poured on ice cold water and filtered. The solid was washed with water and dried to obtain the crude product. The crude product was recrystallized from methanol to get pure compound (Konieczny et al., 2007).

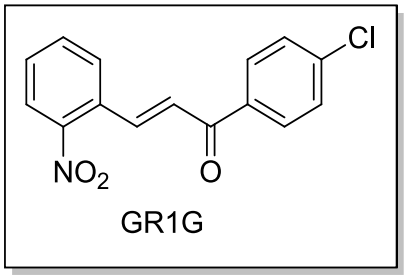

GR1G

Yield : 78%, 145.08 mg, Yellow solid, **MP**: 90 - 93°C (Alarcon et al., 2013).

IR (KBr, cm^{-1}): 1670 (C=O), 1610 (C=C), 1511 (N=O), 1341 (N=O), C-Cl (750), 1090 (C-N).

5.1.4 Synthesis of 5-(2-nitrophenyl)-3-phenyl-4,5-dihydro-1H-pyrazole (GR2)

To a mixture of GR1 (100 mg, 0.37 mmol) in methanol (5 mL) was added hydrazine hydrate (0.053 mL, 1.11 mmol). The reaction mixture was refluxed for 2 h. After completion of the reaction (TLC), methanol was evaporated under reduced pressure using rotary evaporator. Solid product was than extracted with ethyl acetate (10 mL × 3). Organics were washed with brine (10 mL × 3), dried over anhydrous Na_2SO_4 and evaporated under reduced pressure using rotary evaporator to obtain the final product **GR2** (Levai, 2005).

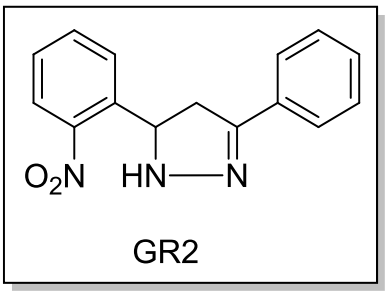

GR2

Yield: 97%, 102.3 mg, Orange crystalline solid, **MP**: 140-142°C (Levai, 2005).

IR (KBr, cm^{-1}): 3310 (N-H stretch), 1575 (N-H bend), 1517 (N=O), 1350 (N=O), 1605 (C=N), 1056 (C-N).

^{1}H NMR ($CDCl_3$, 400 MHz): 7.96 (2H, t, J = 8.4 Hz), 7.65 (3H, m), 7.41 (4H, m), 6.05 (D_2O exchangeable NH, 1H, s), 5.42 (1H, t, J = 13.2 Hz), 3.80, (1H, q, J = 14.2 Hz), 3.01 (1H, q, J = 13.2 Hz).

5.1.5 Synthesis of 3-(4-chlorophenyl)-5-(2-nitrophenyl)-4,5-dihydro-*1H*-pyrazole (GR2G)

To a mixture of GR1 (100 mg, 0.37 mmol) in methanol (5 mL) was added hydrazine hydrate (0.053 mL, 1.11 mmol). The reaction mixture was refluxed for 2 h. After completion of the reaction (TLC), methanol was evaporated under reduced pressure using rotary evaporator. Solid product was than extracted with ethyl acetate (10 mL × 3). Organics were washed with brine (10 mL × 3), dried over anhydrous Na_2SO_4 and evaporated under reduced pressure using rotary evaporator to obtain the final product **GR2G** (Levai, 2005).

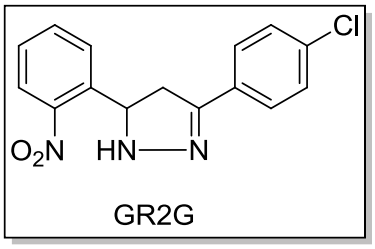

GR2G

Yield: 97%, 101.72 mg, Brownish solid, **MP**: 134-136°C (Lévai, 2005).

IR (KBr, cm^{-1}): 3267 (N-H stretch), 1590 (N-H bend), 1520 (N=O), 1344 (N=O), 1607 (C=N), 1092 (C-N), 747 (C-Cl).

5.1.6 Synthesis of 5-(2-nitrophenyl)-3-phenyl-1H-pyrazole (GR3)

To a solution of GR2 (100 mg, 0.37 mmol) in DMSO was added catalytic amount of molecular iodine and reaction mixture was refluxed at 130-140°C for 4-6 h. After the completion of the reaction (TLC), the reaction mixture was poured in ice cold water; solid product was extracted using ethyl acetate.

Excess iodine was removed adding sodium thiosulfate. Organic layer was washed with brine (10 mL × 3), dried over sodium sulphate and was finally evaporated under reduced pressure using rotary evaporator to obtain the product (Lokhande et al., 2005).

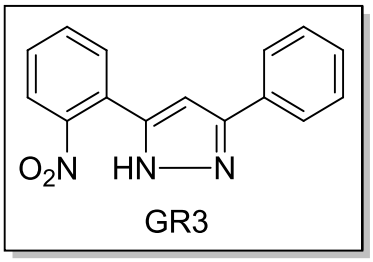

GR3

Yield: 92%, 91.31 mg, Brownish solid, **MP**: 194-196°C (Lokhande et al., 2005).

IR (KBr, cm^{-1}): 3456 (N-H stretch), 1664 (C=C), 1620 (C=N), 1524 & 1348 (N=O), 1144 (C-N).

^{1}H NMR ($CDCl_3$, 400 MHz): 7.67-7.76 (3H, m), 7.56-7.63 (3H, m), 7.33-7.51 (5H, m).

^{13}C NMR ($CDCl_3$, 100 MHz): 149.02, 146.37, 146.16, 132.09, 130.97, 129.04, 128.74, 128.04, 126.47, 125.62, 124.56, 123.82 and 102.59.

5.1.7 Synthesis of 3-(4-chlorophenyl)-5-(2-nitrophenyl)-1H-pyrazole (GR3G)

To a solution of GR2G in methanol (100 mg, 0.33 mmol), was added 8-10 equiv. oxone. Reaction mixture was refluxed for 4-6 h. Reaction was monitored by TLC. Excess oxone was removed by filtration and filtrate was recrystallized in methanol to obtain the pure product (Lokhande et al., 2005).

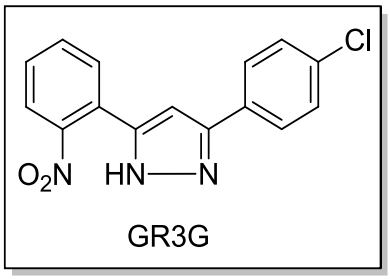

GR3G

Yield: 92%, 91.38 mg, Brown solid, **MP:** 185 – 186 °C (Lokhande et al., 2005).

IR (KBr, cm^{-1}): 3342 (N-H stretch), 1601 (C=N), 1519 & 1343 (N=O), 1186 (C-N), 780 (C-Cl).

5.1.8 Synthesis of 2-(3-phenyl-1H-pyrazol-5-yl) aniline (GR4)

To a mixture of GR3 (10.38 mmol, 2.75 g) in methanol (5 mL) was added $SnCl_2$ (8-10 equivalent). The reaction mixture was refluxed for 24 h. After the completion of the reaction (TLC), methanol was evaporated under reduced pressure using rotary evaporator. Solid product was than extracted with ethyl acetate (10 mL × 3). Excess of $SnCl_2$ was precipitated in water by neutralizing the reaction mixture with 5% NaOH. Organics were washed with brine (10 mL × 3), dried over anhydrous Na_2SO_4 and evaporated under reduced pressure using rotary evaporator to obtain the final product **GR4** (Bellamy & Ou, 1984)**.**

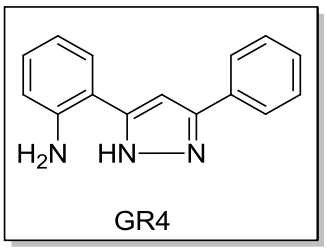

GR4

Yield: 95%, 88.24 mg, Yellow solid, **MP:** 165-166°C (Bellamy & Ou, 1984).

IR (KBr, cm^{-1}): 3360 (N-H), 3285 (N-H), 1613 (C=N), 1579 (C=C), 1248 (C-N).

^{1}H NMR ($CDCl_3$, 400 MHz): 13.23 (D_2O exchangeable NH, 1H, bs), 7.81 (1H, s), 7.79 (1H, s), 7.31 - 7.54 (4H, m), 7.00 (2H, s), 6.75 (1H, d, J =7.91 Hz), 6.61 (1H, t, J = 7.32 Hz), 6.22 (D_2O exchangeable NH, 2H, bs).

5.1.9 Synthesis of 2-(3-(4-chlorophenyl)-1H-pyrazol-5-yl) aniline (GR4G)

To a mixture of GR3G (100 mg, 0.37 mol) in methanol (5 mL) was added $SnCl_2$ (8-10 equivalent). The reaction mixture was refluxed for 24 h. After the completion of the reaction (TLC), methanol was evaporated under reduced pressure using rotary evaporator. Solid product was than extracted with ethyl acetate (10 mL × 3). Excess of $SnCl_2$ was precipitated in water by neutralizing the reaction mixture with 5% NaOH. Organics were washed with brine (10 mL × 3), dried over anhydrous Na_2SO_4 and evaporated under reduced pressure using rotary evaporator to obtain the final product **GR4** (Bellamy & Ou, 1984).

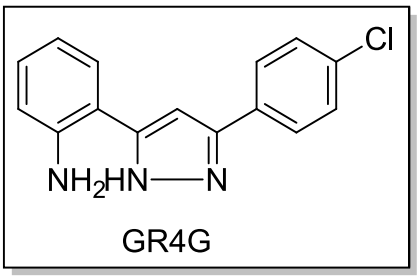

GR4G

Yield: 95%, 85.70 mg, Yellow solid, **MP:** 184-186°C (Bellamy & Ou, 1984).

IR (KBr, cm^{-1}): 1614 (C=N), 1490 (C=C), 1215 (C-N), 748 (C-Cl).

^{1}H NMR ($CDCl_3$, 400 MHz): 13.2 (D_2O exchangeable NH, 1H, bs), 7.82 (2H, d, J = 8.3 Hz), 7.46 (2H, d, J = 8.3 Hz), 7.04 (2H, m), 6.68 - 6.81 (1H, m), 6.53 - 6.67 (2H, m).

5.1.10 Synthesis of 2-phenyl-5,6-dihydropyrazolo[1,5-c]quinazoline-5-carboxylic acid (GR5)

To a solution of GR4 (100 mg, 0.4255 mmol) in acetonitrile was added glyoxylic acid (31.4 mg, 0.4355 mmol) (50% aqueous soln) at 10-15 °C. The reaction

mixture was stirred for 5 min. After the completion of reaction (TLC), reaction mixture was evaporated using rotary evaporator and pure solid product was obtained (Murai et al., 2008).

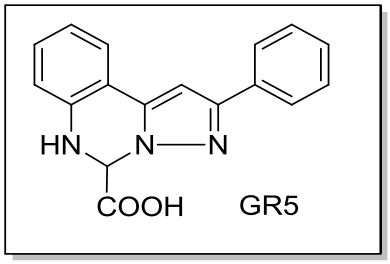

GR5

Yield: 98%, 121.35 mg, Creamy white solid, **MP:** 190-192 °C.

^{1}H NMR ($CDCl_3$, 400 MHz, δ with TMS = 0): 12.4 (1H, s), 7.84 (2H, d, J = 7.29 Hz), 7.51 (1H, d, J = 7.16 Hz), 7.38-7.45 (4H, bs), 7.30 (1H, q, J = 5.56 Hz), 7.11 (1H, m), 7.04 (1H, s), 6.90 (1H, d, J = 8 Hz), 6.80 (1H, m), 6.01 (1H, d).

^{13}C NMR ($CDCl_3$, 100 MHz, δ with TMS=0): 169.75, 151.07, 139.43, 138.34, 132.95, 129.07, 128.09, 127.57, 125.14, 123.65, 118.53, 114.75, 112.84, 96.49 and 68.41.

5.1.11 Synthesis of 2-phenylpyrazolo[1,5-c]quinazoline (GR5-a1)

To a solution of GR4 (100 mg, 0.4255 mmol) in methanol, was added glyoxylic acid (31.4 mg, 0.4355 mmol) (50% aqueous soln) at 10-15 °C. The reaction mixture was stirred for 5 min. After the completion of reaction (TLC), reaction mixture was evaporated using rotary evaporator and solid mixture of products was obtained which was further purified by coloumn chromatography. Two spots on TLC were separated at 5% and 15% EtOAc: Pet Ether. Compound at 5% polarity was separated and characterized to obtain GR5-a1.

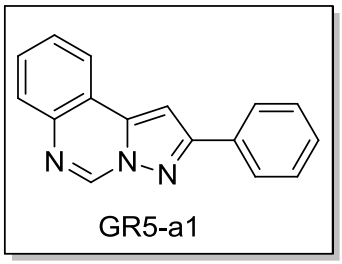

GR5-a1

Yield: 30%, 37.14 mg, Creamy solid, **MP**: 145-150 °C (Kumar & Kumar, 2014).

IR (KBr, cm^{-1}): 3019 (CH), 1620 (C=N), 1539 (C=C), 1215 (C-N).

^{1}H NMR ($CDCl_3$, 400 MHz): 9.11 (1H, s), 8.00-8.06 (3H, m), 7.95 (1H, m), 7.58-7.68 (2H, m), 7.47-7.51 (2H, m), 7.41-7.45 (1H, m), 7.24 (1H, s).

^{13}C NMR ($CDCl_3$, 100 MHz): 155.95, 140.09, 139.72, 139.31, 132.15, 129.85, 129.32, 128.84, 128.75, 128.18, 126.73, 123.32, 119.99 and 95.42.

MS (EI): 245 $[M]^+$.

5.1.12 Synthesis of methyl 2-phenyl-5,6-dihydropyrazolo[1,5-c]quinazoline-5-carboxylate (GR5-a2)

To a solution of GR4 (100 mg, 0.4255 mmol) in methanol, was added glyoxylic acid (0.24 mL, 0.4355 mmol) (50% aqueous soln) at 10-15 °C. The reaction mixture was stirred for 5 min. After the completion of reaction (TLC), reaction mixture was evaporated using rotary evaporator and solid mixture of product obtained was further purified by coloumn chromatography. Two spots on TLC were separated at 5% and 15% EtOAc: Pet Ether. Compound at 15% polarity was separated and characterized to obtain GR5-a2 (Murai et al., 2008).

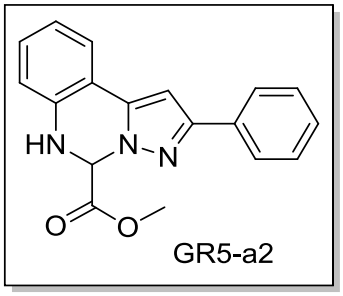

GR5-a2

Yield: 67%, 82 mg, Creamish white solid, **MP**: 210-212°C.

^{1}H NMR ($CDCl_3$, 400 MHz): 7.84 (2H, d, J = 5.88 Hz), 7.51 (1H, d, J = 6.4 Hz), 7.40 (2H, s), 7.32 (1H, d, J = 6.16 Hz), 7.14 (1H, s), 7.04 (1H, s), 6.88 (3H, t, J = 10 Hz), 6.11 (1H, s), 3.67 (3H, s).

^{13}C NMR ($CDCl_3$, 100 MHz): 168.40, 151.56, 138.43, 138.19, 132.51, 128.91, 128.05, 127.38, 125.05, 123.98, 123.36, 118.86, 114.70, 96.17, 68.08 and 52.13.

MS (ESI): 306 $[M+1]^+$, 328 $[M+Na]^+$

5.1.13 Synthesis of 4-(2-phenyl-5,6-dihydropyrazolo[1,5-c]quinazolin-5-yl)phenol (GR5-b)

A mixture of GR4 (100 mg, 0.425 mmol) and 4-hydroxybenzaldehyde (70.64 mg, 0.425 mmol) was dissolved in methanol and refluxed for 1h. After the completion of the reaction (TLC), the reaction mixture was left to cool. Precipitated solid was obtained by decanting extra methanol and recrystallized from methanol (Colotta et al., 1996).

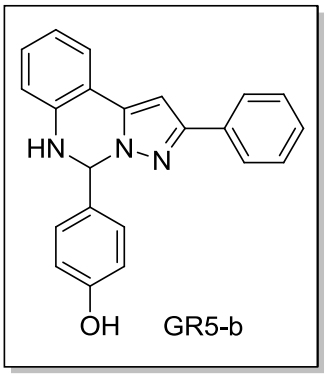

GR5-b

Yield: 86%, 121 mg, Brownish solid, **MP**: 215-218°C.

IR (KBr, cm^{-1}): 3387 (OH), 1612 (C=N), 1591 (C=C), 1233 (C-N), 1279 (C-O).

^{1}H NMR ($CDCl_3$, 400 MHz): 9.34 (D_2O exchangeable NH, 1H, bs), 7.79 (2H, m), 7.51 (1H, dd, J = 8.8 Hz), 7.37 (2H, t, J = 7.36 Hz), 7.27 (1H, t, J =7.32

Hz), 7.18 (D_2O exchangeable OH,1H, s), 7.10 (3H, q, J = 8.6 Hz), 7.01 (1H, s), 6.85 (1H, d, J = 7.8 Hz), 6.76 (1H, m), 6.68 (2H, q, J = 7.32), 6.57 (1H, s).

MS (ESI) m/z = 340 $[M+1]^+$

5.1.14 Synthesis of 2-methoxy-4-(2-phenyl-5,6-dihydropyrazolo[1,5-*c*]quinazolin-5-yl)phenol (GR5-c)

A mixture of GR4 (100 mg, 0.425 mmol) and 4-hydroxy, 3-methoxy benzaldehyde (64.6 mg, 0.425 mmol) was dissolved in methanol and refluxed for 1h. After the completion of the reaction (TLC), the reaction mixture was left to cool. Precipitated solid was obtained by decanting extra methanol and recrystallized from methanol (Colotta et al., 1996).

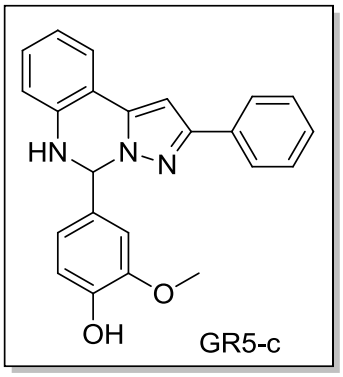

GR5-c

Yield: 90%, 131 mg, Light yellow solid, **MP**: 194-198 °C.

IR (KBr, cm^{-1}): 3401 (OH), 3015 (C-H), 1673 (C=N), 1590 (C=C), 1216 (C-N).

^{1}H NMR ($CDCl_3$, 400 MHz): 8.97 (D_2O exchangeable NH, 1H, bs), 7.80 (2H, d, J = 1.16 Hz), 7.53 (1H, dd, J = 8.68 Hz), 7.37 (2H, m), 7.27 (1H, t, J = 7.4 Hz), 7.22 (D_2O exchangeable OH, 1H, bs), 7.10 (1H, m), 7.03 (1H, s), 6.95 (1H, t, J = 3.32 Hz), 6.87 (1H, d, J = 7.97 Hz), 6.77 (1H, m), 6.68 (1H, d, J = 8.16 Hz), 6. 57 (2H, t, J = 6.24 Hz), 3.70 (3H, s).

^{13}C NMR ($CDCl_3$, 100 MHz, δ with TMS = 0): 150.47, 147.27, 146.73, 140.39, 138.25, 133.18, 131.65, 129.11, 128.37, 127.38, 125.09, 123.55, 118.72, 118.08, 114.92, 114.68, 112.83, 110.49, 96.17, 71.04 and 55.44.

MS (ESI) m/z = 370 $[M+1]^+$

5.1.15 Synthesis of 2-methoxy-5-(2-phenyl-5,6-dihydropyrazolo[1,5-*c*]quinazolin-5-yl)phenol (GR5-d)

A mixture of GR4 (100 mg, 0.425 mmol) and 4-hydroxybenzaldehyde (64.6 mg, 0.425 mmol) was dissolved in methanol and refluxed for 1h. After the completion of the reaction (TLC), the reaction mixture was left to cool. Precipitated solid was obtained by decanting extra methanol and recrystallized from methanol (Colotta et al., 1996).

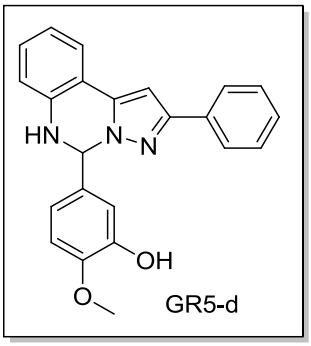

GR5-d

Yield: 86%, 124 mg, Yellow solid, **MP**: 115-118°C.

IR (KBr, cm^{-1}): 3384 (OH), 2929 (CH), 2852 (CH), 1617 (C=N), 1439 (C=C), 1130 (C-O), 1217 (C-N).

^{1}H NMR ($CDCl_3$, 400 MHz, δ with TMS = 0): 7.80 – 7.82 (2H, m), 7.52 (1H, d, J = 7.52 Hz), 7.35 – 7.39 (2H, m), 7.29 (1H, m), 7.12 – 7.16 (1H, m), 6.84 – 6.91 (3H, m), 6.70 – 6.79 (3H, m), 6.58 (1H, s), 3.82 (3H, s).

MS (ESI) m/z = 370 $[M+1]^+$

5.1.16 Synthesis of 4-(2-phenyl-5,6-dihydropyrazolo[1,5-*c*]quinazolin-5-yl)benzonitrile (GR5-e)

A mixture of GR4 (100 mg, 0.425 mmol) and 4-hydroxybenzaldehyde (55.67 mg, 0.425 mmol) was dissolved in methanol and refluxed for 1h. After the completion of the reaction (TLC), the reaction mixture was left to cool.

Precipitated solid was obtained by decanting extra methanol and recrystallized from methanol (Colotta et al., 1996).

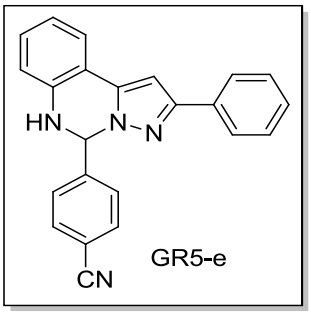

GR5-e

Yield: 75%, 110 mg, Off white solid, **MP**: 178-180 °C.

IR (KBr, cm^{-1}): 3059 (C-H), 2229 (C≡N), 1613 (C=N), 1591 (C=C), 1219 (C-N).

^{1}H NMR ($CDCl_3$, 400 MHz, δ with TMS = 0): 9.34 (D_2O exchangeable NH, 1H, bs), 7.79 (2H, t), 7.51 (1H, q), 7.37 (2H, t), 7.27 (1H, t), 7.18 (1H, s), 7.10 (3H, q), 7.01 (1H, s), 6.85 (1H, d), 6.76 (1H, m), 6.68 (2H, q) and 6.57 (1H, s).

MS (ESI) m/z = 349 $[M+1]^+$

5.1.17 Synthesis of 2-(4-chlorophenyl)-5,6-dihydropyrazolo[1,5 c]quinazoline-5-carboxylic acid (GR5G)

To a solution of GR4G in acetonitrile (100 mg, 0.371 mmol) was added glyoxylic acid (0.042mL, 0.371 mmol) (50% aqueous soln) at 10-15 °C. The reaction mixture was stirred for 5 min. After the completion of reaction (TLC), reaction mixture was evaporated using rotary evaporator and solid product was obtained (Murai et al., 2008).

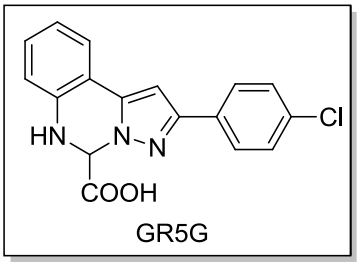

GR5G

Yield: 97%, 115.98 mg, Creamish white solid, **MP:** 210-213 °C.

IR (KBr, cm^{-1}): 2500-3000 broad band (O-H stretch), 1715 (C=0 stretch), 770 (C-Cl stretch)

^{1}H NMR ($CDCl_3$, 400 MHz, δ with TMS = 0): 9.34 (1H, s), 7.9 (2H, d, J = 7.29 Hz), 7.63 (2H, d, J = 8.24 Hz), 7.38-7.53 (4H, bs), 7.26 (2H, d,), 6.69 (1H, s).

5.1.18 Synthesis of 2-(2-chlorophenyl)pyrazolo[1,5-*c*]quinazoline (GR5G-a1)

To a solution of GR4G (100 mg, 0.371 mmol) in methanol, was added glyoxylic acid (0.042mL, 0.371 mmol) (50% aqueous soln) at 10-15 °C. The reaction mixture was stirred for 5 min. After the completion of reaction (TLC), reaction mixture was evaporated using rotary evaporator and solid mixture of products was obtained which was further purified by coloumn chromatography. Two spots on TLC were separated at 5% and 15% EtOAc: Pet Ether. Compound at 5% polarity was separated and characterized to obtain **GR5G-a1**.

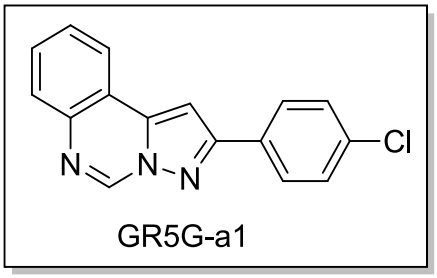

GR5G-a1

Yield: 30%, 36.24 mg, Off white solid, **MP**: 200-202 °C (Kumar & Kumar, 2014).

IR (KBr, cm^{-1}): 3019 (C-H), 1619 (C=N), 1477 (C=C), 1215 (C-N), 773 (C-Cl).

^{1}H NMR ($CDCl_3$, 400 MHz): 9.33 (1H, s), 8.23-8.26 (1H, m), 8.05-8.09 (2H, m), 7.90-7.93 (1H, m), 7.76 (1H, d, J = 0.6 Hz), 7.67-7.74 (2H, m), 7.53-7.57 (2H, m).

^{13}C NMR ($CDCl_3$, 100 MHz): 153.57, 139.50, 139.40, 139.13, 133.89, 130.66, 129.77, 128.82, 128.13, 128.09, 127.83, 123.49, 119.39 and 95.95.

MS (EI) 280 $[M]^+$

5.1.19 Synthesis of methyl 2-(4-chlorophenyl)pyrazolo[1,5-c]quinazoline-5-carboxylate) (GR5G-a2)

To a solution of **GR4G** (100 mg, 0.371 mmol) in methanol, was added glyoxylic acid (0.042mL, 0.371 mmol) (50% aqueous soln) at 10-15 °C. The reaction mixture was stirred for 5 min. After the completion of reaction (TLC), reaction mixture was evaporated using rotary evaporator and solid mixture of products was obtained which was further purified by coloumn chromatography. Two spots on TLC were separated at 5 and 15% EtOAc: Pet Ether. Compound at 15% polarity was separated and characterized to obtain **GR5G-a2** (Murai et al., 2008).

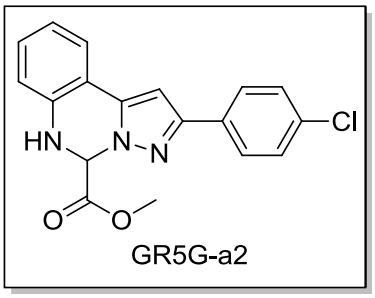

GR5G-a2

Yield: 60%, 72.48 mg, Creamish white, **MP**: 215-217 °C.

^{1}H NMR ($CDCl_3$, 400 MHz): 7.80-7.75 (2H, m), 7.52 (1H, dd, J = 7.72 Hz), 7.38 (2H, dd, J = 6.72 Hz), 7.26 (1H, d, J = 5.52 Hz), 7.00 (1H, s), 6.95 (1H, dt, J = 7.76 Hz), 6.83 (1H, d, J = 7.52 Hz), 6.00 (1H, d, J = 1.92 Hz), 4.98 (D_2O exchangeable NH, 1H, s), 3.68 (3H, s).

^{13}C NMR ($CDCl_3$, 100 MHz): 169.18, 151.71, 138.64, 138.04, 135.95, 133.80, 131.59, 129.69, 128.82, 127.15, 120.93, 115.56, 114.09, 97.29, 68.79 and 53.22.

5.1.20 Synthesis of 4-(2-(2-chlorophenyl)-5,6-dihydropyrazolo[1,5-*c*]quinazolin-5-yl)phenol (GR5G-b)

A mixture of GR4G (100 mg, 0.371 mmol) and 4-hydroxybenzaldehyde (45.35 mg, 0.371 mmol) was dissolved in methanol and refluxed for 1h. After the

completion of the reaction (TLC), the reaction mixture was left to cool. Precipitated solid was obtained by decanting extra methanol and recrystallized from methanol (Colotta et al., 1996).

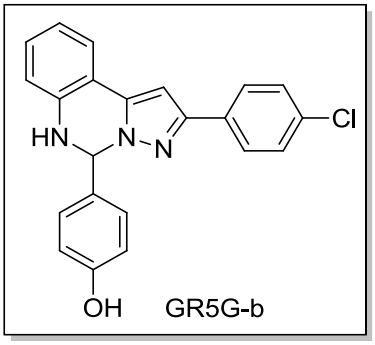

GR5G-b

Yield: 80%, 110 mg, Off white solid, **MP**: 230-232 °C.

IR (KBr, cm^{-1}): 3302 (OH), 1615 (C=N), 1590 (C=C), 1247 (C-N), 748 (C-Cl).

^{1}H NMR ($CDCl_3$, 400 MHz): 9.38 (D_2O exchangeable NH, 1H, bs), 7.78 (2H, t, J = 6.8 Hz), 7.51 (1H, dd, J = 0.84 Hz), 7.41 (2H, m), 7.22 (D_2O exchangeable OH, 1H, bs), 7.08 (4H, m), 6.86 (1H, d, J =7.92 Hz) , 6.77 (1H, t, J = 7.53 Hz), 6.68 (2H, t, J = 6.4 Hz), 6.57 (1H, s).

^{13}C NMR ($CDCl_3$, 100 MHz): 157.60, 149.31, 140.43, 138.35, 132.13, 131.98, 129.21, 128.40, 127.51, 126.63, 123.58, 118.00, 114.91, 114.63, 96.31 and 71.00.

MS (ESI) m/z = 374 $[M+1]^+$

5.1.21 Synthesis of 4-(2-(2-chlorophenyl)-5,6-dihydropyrazolo[1,5-*c*]quinazolin-5-yl)-2-methoxyphenol (GR5G-c)

A mixture of GR4G (100 mg, 0.371 mmol) and 4-hydroxybenzaldehyde (56.39 mg, 0.371 mmol) was dissolved in methanol and refluxed for 1h. After the completion of the reaction (TLC), the reaction mixture was left to cool. Precipitated solid was obtained by decanting extra methanol and recrystallized from methanol (Colotta et al., 1996).

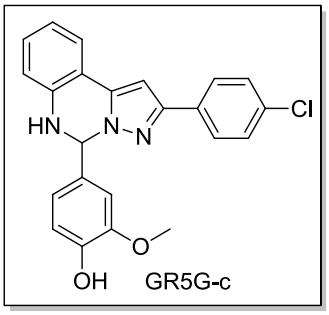

Yield: 88%, 130 mg, Off white solid, **MP**: 195-198 °C.

IR (KBr, cm^{-1}): 3010 (C-H), 1616 (C=N), 1515 (C=C), 1218 (C-N), 744 (C-Cl).

MS (ESI) m/z = 404 $[M+1]^+$

5.2 Biological Studies

5.2.1 Chemicals

1. Dulbecco's Modified Eagle's Medium (DMEM), Penicillin, Streptomycin (PS), antibiotic solution, phosphate buffer saline (PBS) and fetal bovine serum (FBS) media were used for culture of the cancer cell lines and were purchased from HiMedia.
2. 3-[4,5-dimethylthiazol-2-yl]-2,5-diphenyl tetrazolium bromide (MTT) dye was used for cell proliferation assay and was purchased from HiMedia.
3. Dimethyl Sulfoxide (DMSO), extrapure (AR grade) was purchased from Societa a Responsabilita Limitata (SRL), India.

5.2.2 Instruments

Table 5.2.1. List of Instruments Used in Biological Evaluation

S.No.	Instruments	Purpose	Company
1	Automatic Cell Counter	Counting of cells	Invitrogen,
2	Incubator	Cell growth	Eppendorf
3	Centrifuge 5430 R	Centrifugation	Eppendorf
4	Inverted microscope	Visualization of cells	Magnus, Olympus
5	Laminar Air Flow	Aseptic condition	Klen Airflow
6	UV-Vis Spectrophotometer	Absorption studies	Biotek, USA

5.2.3 Cell Line Under Study

Rat C-6 glial cell line was used for evaluating antiproliferative assay and this cell line was generously gifted by Prof. Gursharan Kaur, GNDU, Amritsar.

5.2.4 Routine Assays in Cell Culture Laboratory

A. Culturing of the Cell Lines

C-6 cancer cells were grown in DMEM media containing 10% FBS, 100 units/mL penicillin, and 100 µg/mL streptomycin and were maintained at 37 °C in a 5% CO_2 humidified incubator. When the cells became 70-80% confluent, culture medium was removed and discarded. Then the cells were rinsed with PBS to remove all the traces of serum that contains trypsin inhibitor. After that, trypsin-EDTA 0.25% (w/v) solution was added to the flask. It was then allowed to incubate until cells were detached from the surface (trypsinization). Subsequently, trypsin was inactivated by the addition of media containing serum (1mL). Centrifugation was done on 1200 rpm at 37˚C for 10 min for harvesting the cells. Further, supernatant was disposed and resuspension of the cell pellet was done using 2 mL of the media. The cell number was counted using automated cell counter. The cells were transferred to fresh media every three days.

B. Maintenance and Sub-Culturing of Cell Lines

The maintenance of C-6 cultured cell line was done in 25 cm^2 or 75 cm^2 flasks containing DMEM medium supplemented with 10% FBS, 1x Penicillin and Streptomycin antibiotic solution and afterward incubated at 37˚C in a humidified atmosphere containing 5% CO_2 and 95% humidity (Mantha et al., 2012).

The cells were sub cultured in 25 cm^2 flasks and become important when the cell lines have attained 70-80% growth. The reagents necessary for the procedure were placed in water bath maintained at 37 ˚C for 10-15 min earlier to the sub-culturing. During sub-culturing, trypsin was added. After 5 min, 1 mL of media containing serum was added for ceasing the action of trypsin. Cells were then transferred to 15 mL centrifuge tubes and centrifuged for 10 min at 1200 rpm. The supernatant was cast aside and the pellet was again resuspended in complete media. The cell lines were transferred to fresh media every two days.

5.2.5 Evaluation of Antiproliferative Activity of the Synthesized Compounds (MTT Assay)

The assay was specified by Mosmann in 1983 and is also known as cell viability assay. This in vitro colorimetric assay is based on cleavage of tetrazolium rings of pale yellow MTT by mitochondrial dehydrogenase enzyme from viable cells resulting in formation of dark blue formazon crystals. The formazon crystals get accumulated in healthy cells as they are impermeable to cell membranes. So these are solubilised using DMSO. The number of surviving cells is directly proportional to level of formazon product formed. The results of assay are read using Shimadzu double-beam spectrophotometer at the Central Instrumentation Facility (CIF) of CUPB (Figure 5.2.1). (Mirzayans, 2007; Mosmann, 1983).

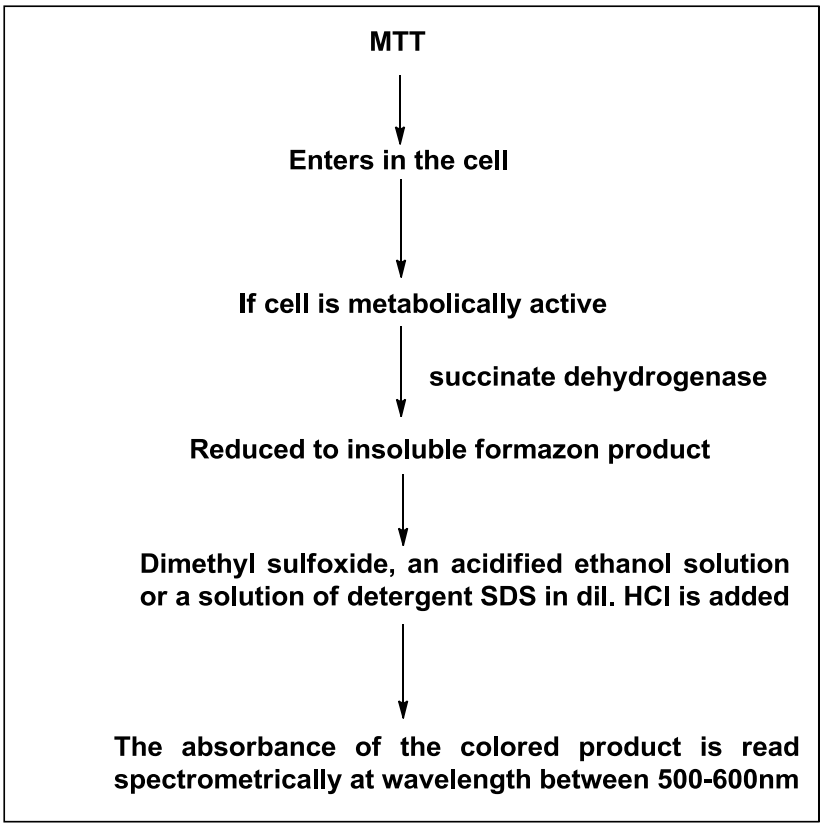

Figure 5.2.1: Rudimentary Principle of MTT Assay

Material: MTT (3-[4,5-dimethylthiazol-2-yl]-2,5-diphenyl tetrazolium bromide), Phosphate buffer solution, DMSO (Dimethylsulfoxide).

Procedure: Rat C-6 glial cells were counted on the automated cell counter. About 8,000-10,000 cells were seeded in each well of the 96 well plate. The plate was incubated at 37 ˚C with 5% CO_2 for 24 h. At the end of the 24 h, treatment was given to the cells in five concentrations of 1 µM, 5 µM, 15 µM, 30 µM and 50 µM. The cells were further incubated for 12 h, 48 h and 72 h. The media was removed from each well and MTT solution (5 mg/10mL) was added. This was incubated in the dark for 4 h. At the end of 4 h, the MTT solution was disposed from each well and the intracellular precipitate was dissolved in DMSO solution and the absorbance of the violet colour formed as consequence of DMSO addition is read spectrometrically at 570 nm. The same procedure was repeated every time after 12 h, 48 h and 72 h.

5.2.6 DCFDA Assay:

The treated and control rat C-6 glial cells (1×10^5), cultured in 96-well plates were equilibrated in PBS and incubated in the dark for 30 min with 100µM of H_2DCF-DA (Invitrogen) [Ex_{478nm}/Em_{518nm}]. After washing twice with PBS, fluorescence was then read at the excitation wavelength of 478 nm and emission wavelength of 518 nm using BioTek Microplate Reader as per the protocol described (Dhiman & Garg, 2011).

5.3 Statistical Analysis:

All the statistical analysis was done using MS Excel 2013 and graphs were plotted using prism 5.0 (Graph Pad Software). IC_{50} values were calculated using scatter plot.

CHAPTER 6

RESULTS AND DISCUSSION

6 Results and Discussion

6.1 Chemistry

For the synthesis of compounds pertaining to formula 1, following scheme was followed.

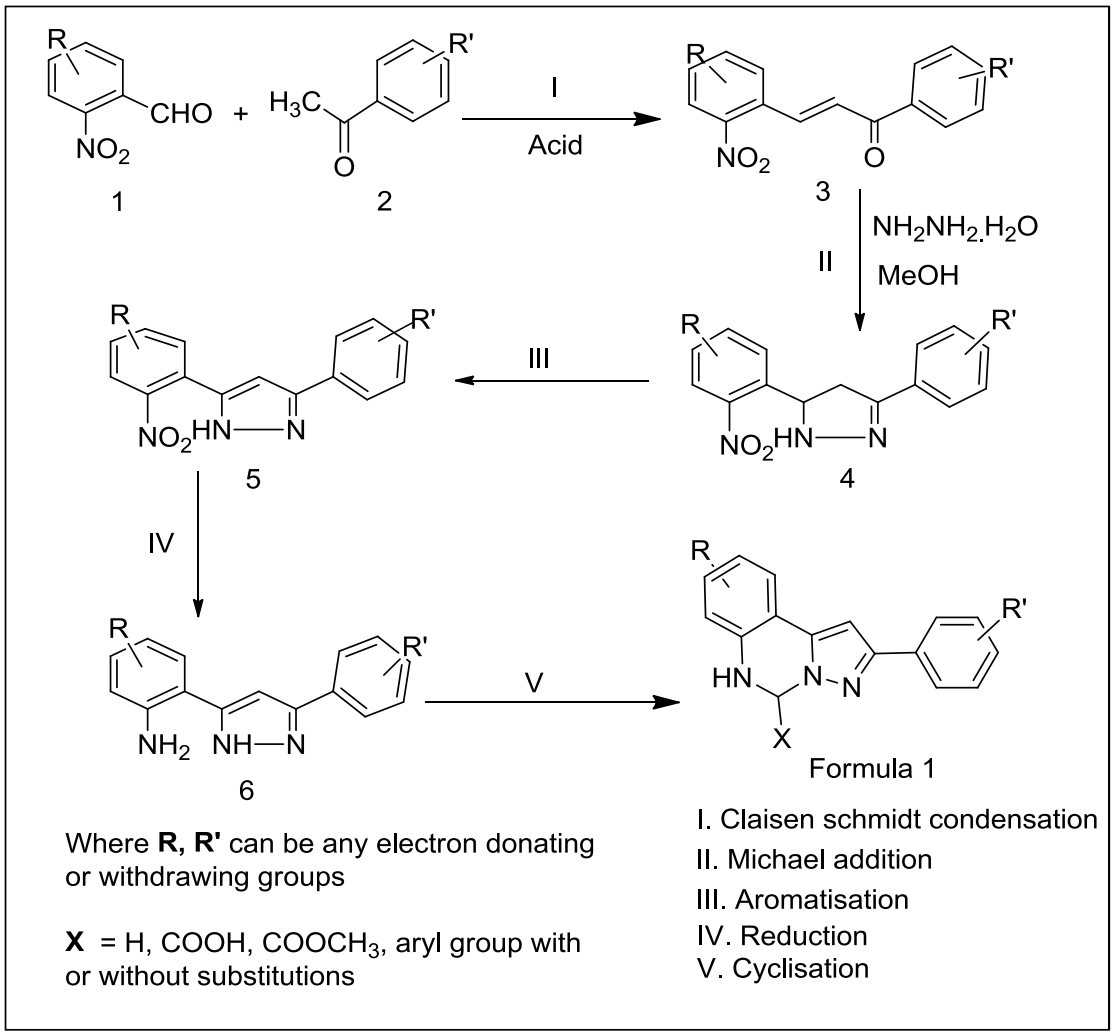

Scheme 6.1.1: Proposed route for synthesis of designed compounds

6.1.1 Synthesis of nitro substituted 1,3-diarylpropenones

The synthesis of nitro substituted 1,3-diaryl propenones was carried out through Claisen-Schmidt condensation of 2-nitrobenzaldehyde with aryl ketones in presence of glacial acetic acid and few drops of concentrated sulphuric acid (Scheme 6.1.2) (Konieczny et al., 2007).

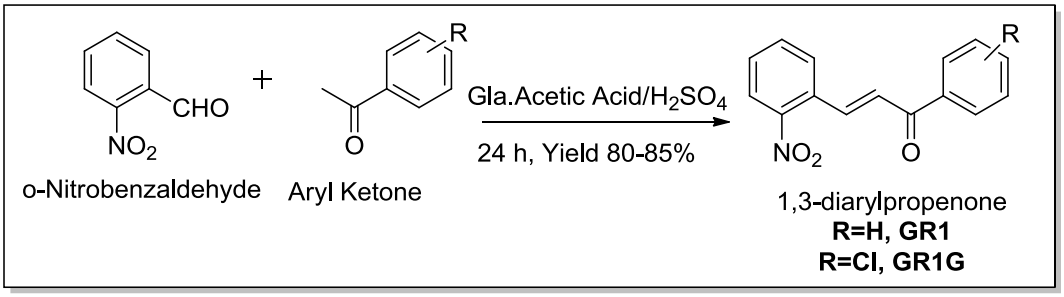

Scheme 6.1.2: Synthesis of 1, 3-diaryl propenones.

Mechanistically, acid catalysed Claisen-Schmidt condensation involves the nucleophile attack of carbanion on the electrophilic carbon of the aldehyde in the process rendering the oxygen electron rich which takes up the proton from reaction solution. The final step of the reaction is dehydration which affords the nitro substituted 1,3-diaryl propenones (Figure 6.1.1)**.**

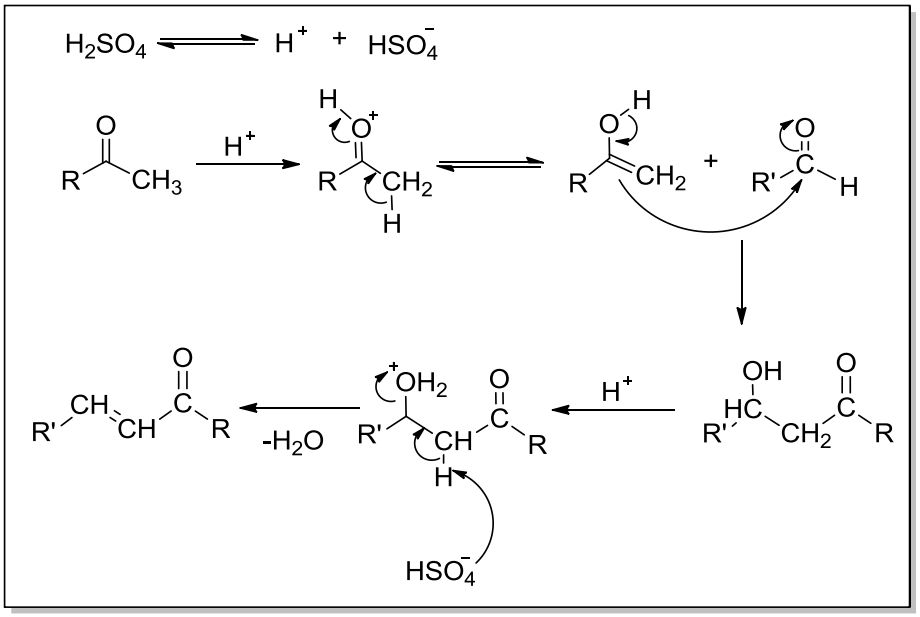

Figure 6.1.1: Mechanism of synthesis of 1,3-diaryl propeonones

The synthesized compounds (Figure 6.1.2) were characterized by melting point (MP), Infrared spectroscopy (IR) and Nuclear Magnetic Resonance (NMR) spectroscopy. For all the synthesized compounds, characteristic IR absorptions frequencies were observed at 1660-1670 cm^{-1} for carbonyl group which was

much lower than the normal value of 1710 cm^{-1}. The reason for this decrease is the conjugation of α, β unsaturation with the carbonyl compound. Conjugation is known to increase the single bond character of the C=O and C=C bonds in the resonance hybrid, lowering their force constants and as a result lowering the frequencies. Other absorption frequencies observed were at 1610 cm^{-1} (C=C stretch), 1510 and 1342 cm^{-1} (N=O stretch) 1284-1281 cm^{-1} (C-O stretch), 1653-1585 cm^{-1} (C=C aromatic). Melting point for these compounds was seen to be in the range of 85-95˚C which are uncorrected.

In ^{1}H NMR spectra we always detected the following typical peaks of 8.12 ppm for CH close to nitro group and 7.34 ppm for CH away from nitro group. J value of the olefenic protons 15.9 justifies the trans nature of the compounds. For all compound the aromatic protons appeared as multiplet at above 7.00 ppm. ^{13}C NMR indicated the characteristic peak at 190 ppm for carbonyl carbon (C=O) and 148.34 ppm for C=N carbon.

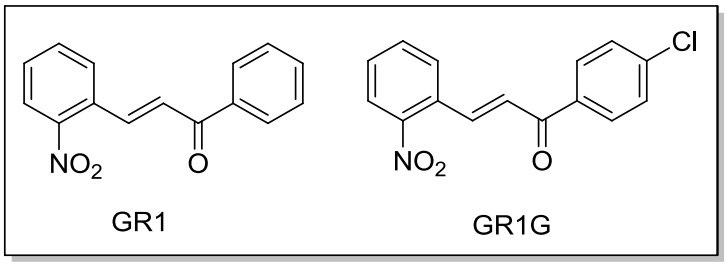

Figure 6.1.2: Structures of synthesized nitro substituted 1,3-diaryl propenones

6.1.2 Synthesis of 3-(2-nitrophenyl)-1-aryl-4,5-dihydro-1*H*-pyrazolines

Synthesis of 3-(2-nitrophenyl)-1-phenyl-4,5-dihydro-1H-pyrazoline (scheme 6.1.3) mainly follows the mechanism for Michael Addition which takes place between the hydrazine hydrate and enone moiety of the 1,3-diaryl propenones. This reaction was carried out in the presence of methanol (Levai, 2005).

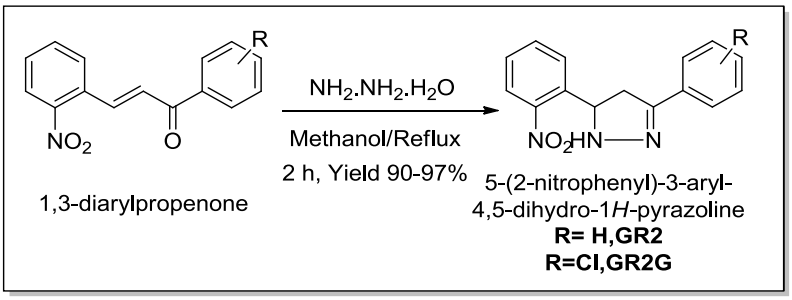

Scheme 6.1.3: Synthesis of 2H-pyrazolines

All the pyrazolines so obtained (Figure 7.1.3) were pure and were characterized by MP, IR and NMR. IR spectrum showed absorptions which fell in between 3250-3350 cm^{-1} (NH stretch), 1632-1590 cm^{-1} (C=N stretch) and 1223-1176 cm^{-1}(C-N stretch).

^{1}H NMR spectra of the pyrazoline derivatives showed the ABX system with three double doublets out of which one double doublet was de-shielded and appeared more downfield than the other two. The three double doublets represent the three protons of the pyrazoline nucleus; confirming its formation. The chemical shift for these protons appeared in the range of 5.55-5.91 ppm with the J values falling in the range of 7.6-12 Hz, 3.15-3.80 ppm with the J values falling in the range of 10-14 Hz, 2.91-3.15 ppm with the J values falling in the range of 7.6-14 Hz. The protons of the benzene ring appeared in the range of 7.24-7.78 ppm, varying according to the substitution on the ring.

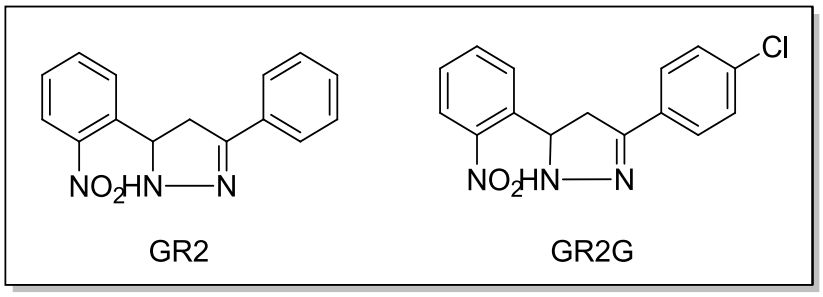

Figure 6.1.3: Structures of synthesised 2H-pyrazolines

6.1.3 Synthesis of 5-(2-nitrophenyl)-3-aryl-1*H*-pyrazoles

Dehydrogenation of 4,5-dihydropyrazoline using I_2/DMSO or oxone resulted in the aromatization of pyrazoline ring [Scheme 6.1.4] (Lokhande et al., 2005).

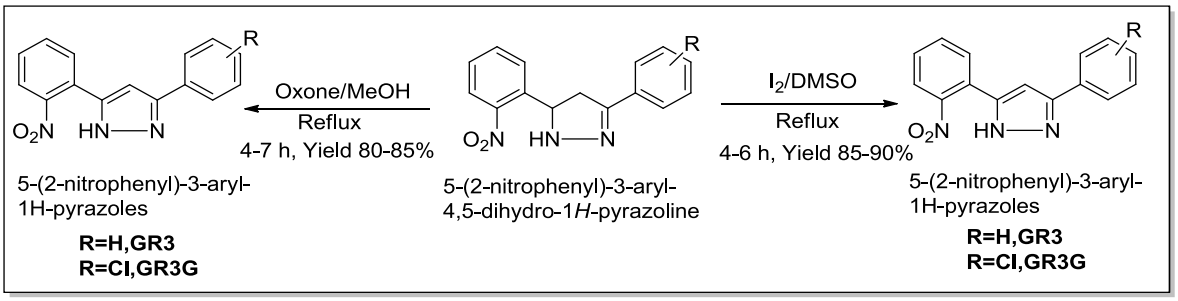

Scheme 6.1.4: Synthesis of 5-(2-nitrophenyl)-3-aryl-1H-pyrazoles

All the pyrazoles so obtained were pure (Figure 6.1.4) and characterized by MP, IR and NMR.

IR spectra showed absorptions which fell in range of 1605-1615 cm^{-1} (C=C) owing to aromatization in addition to other IR peaks.

^{1}H NMR showed the disappearance of ABX pattern due to aromatisation. Appearance of peak at 6.69 ppm further confirmed the formation of pyrazole.

^{13}C NMR showed three most characteristic peaks at 149.02, 146.37 and 146.16 ppm for de-shielded carbon attached to NO_2, NH and N respectively. Peak corresponding to 102.59 ppm appeared due to pyrazole carbon.

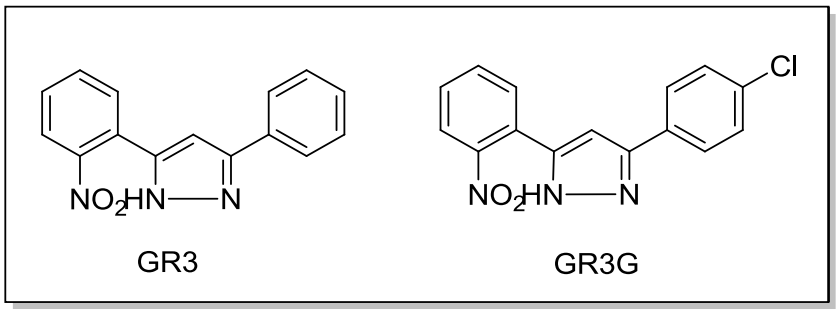

Figure 6.1.4: Structure of synthesized 5-(2-nitrophenyl)-3-aryl-1H-pyrazoles

6.1.4 Synthesis of 2-(3-aryl-1*H*-pyrazol-5-yl) aniline.

Next reduction of the pyrazoles was carried out using various reducing agents such as Fe, $FeSO_4/NH_4$, ammonium formate/ Pd/C and $NABH_4$. Unfortunately we were unsuccessful to obtain the desired reduced products. Fortunately the reduction was successful when carried out with $SnCl_2.2H_2O$ in methanol under reflux [scheme 6.1.5] (Bellamy & Ou, 1984).

The ease of reduction of the aromatic nitro group depends on the nature of the other substituents on the ring and on the reducing potential of the environment.

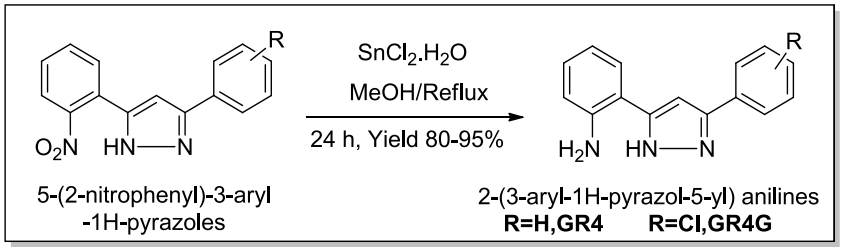

Scheme 6.1.5: Synthesis of 2-(3-aryl-1H-pyrazol-5-yl) anilines

The MPs of all the compounds (Figure 6.1.5) were found to be in range of 166-186 °C. IR spectra confirmed the product formation due to appearance of a sharp characteristic absorption frequency of primary amine (NH_2) at 3350-3380 cm^{-1} and secondary amine (NH) at 3250-3270 cm^{-1} and 1613 cm^{-1} for C=C.

^{1}H NMR spectra showed a characteristic singlet peak at 13.23 ppm for proton of NH. This was due to the fact that nitrogen causes downfield shifting because of de-shielding of protons, 7.00 ppm for proton of NH_2, aromatic protons occupied peaks between 7.00 - 8.00 ppm.

^{13}C NMR showed three most characteristic peaks at 152.59, 145.55 and 142.24 ppm for de-shielded carbon attached to NH_2, NH and N respectively. Peak corresponding to 99.5 ppm was due to pyrazole carbon. 115.59 and 115.18 ppm value represents aromatic carbon attached next to the carbon of NH_2 on either side. 129.23, 128.67, 127.81, 127.66 and 125.16 ppm are the normal aromatic carbon peak.

Mass spectra showed the molecular ion peaks at $[M+1]^+$ that is 236.1 in case of **GR4** and 270.1 for **GR4G** compounds.

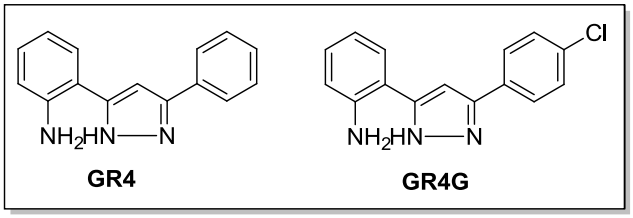

Figure 6.1.5: Structures of synthesized 2-(3-aryl-1H-pyrazol-5-yl) anilines

6.1.5 Synthesis of 2-aryl-5, 6-dihydropyrazolo [1,5-*c*]quinazoline

2-(3-aryl-1H-pyrazol-5-yl) anilines were allowed to react with a variety of aldehydes to afford quinazolines (Scheme 6.1.6). The reaction was carried out in methanol under reflux. Crude precipitates so obtained were purified through crystallization from methanol to afford the pure products (Colotta et al., 1996).

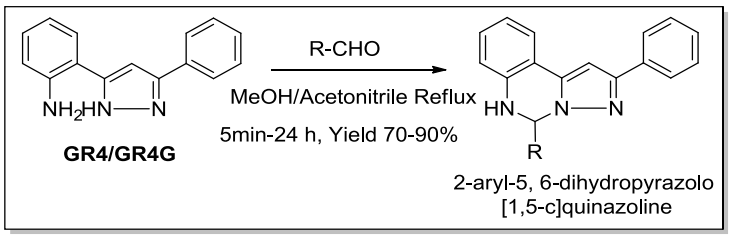

Scheme 6.1.6: Synthesis of 2-aryl-5,6-dihydropyrazolo[1,5-c]quinazolines

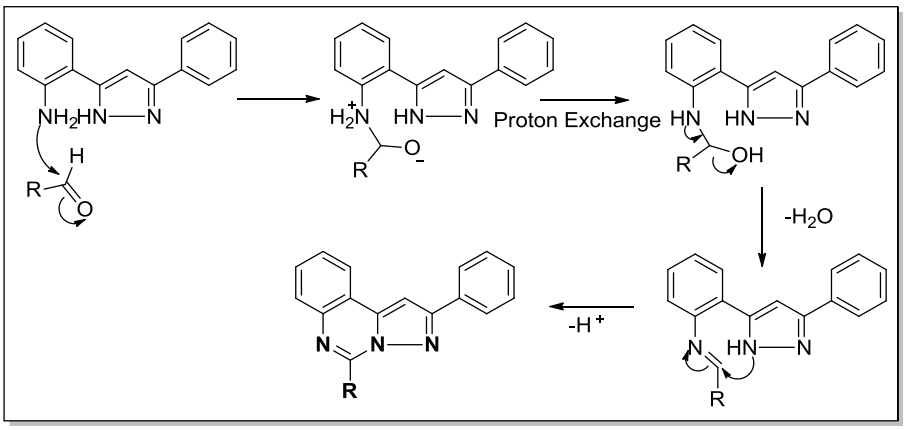

Figure 6.1.6: Mechanism of formation of 2-aryl-5,6-dihydropyrazolo[1,5-c]quinazolines

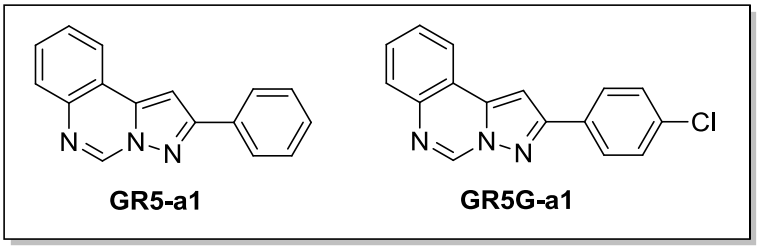

Figure 6.1.7: Structures of 2-arylpyrazolo [1,5-c]quinazolines synthesized

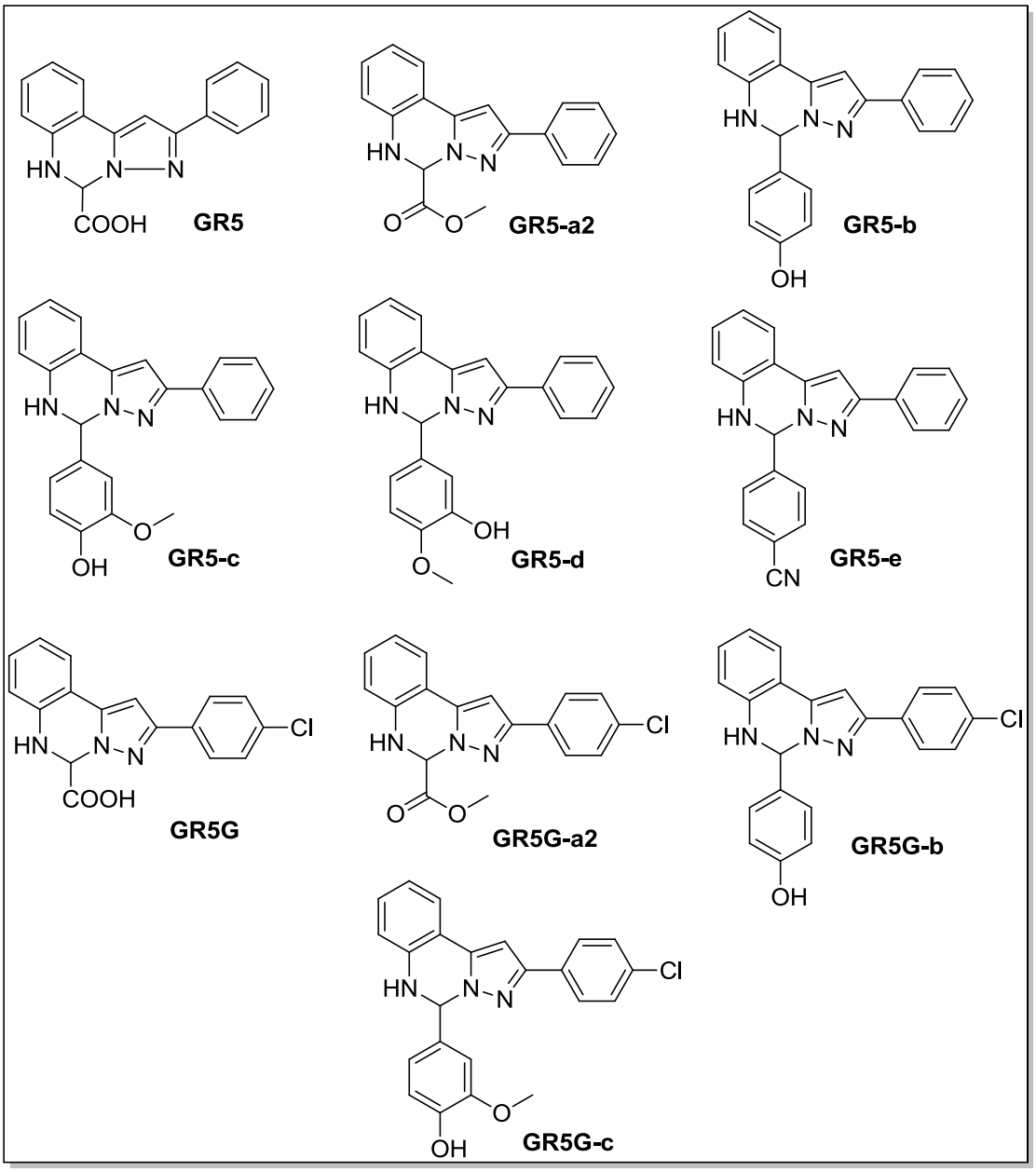

Figure 6.1.8: Structures of synthesized dihydropyrazolo [1,5-c]quinazolines

The MPs of all the compounds (Figure 6.1.8) were found to be in the range of 115-235 °C. The IR spectroscopy showed the most characteristic absorption frequencies in the range of 2900-3100 cm^{-1} for amine of quinazoline, other characteristic absorptions were obtained at 2229 cm^{-1} (C≡N), 1600-1700 cm^{-1} (C=N), 1210-1220 cm^{-1} (C-N) and 770-780 cm^{-1} (C-Cl).

^{1}H NMR spectra highlighted the characteristic sharp singlet of NH in the range of 8-14 ppm this was due to the downfield shifting of proton by nitrogen. Peaks for aromatic protons were found in the region above 7-8 ppm. Singlet at 6-7 ppm is the characteristic peak of proton attached to tertiary carbon confirming the formation of cyclised product.

^{13}C NMR confirmed the pyrazole carbon in the range between 95-100 ppm, quinazoline carbon attached with phenyl showed peak in between 70-75 ppm, carbon attached with oxygen at 145-150 ppm the reason being oxygen is more electronegative causes de-shielding.

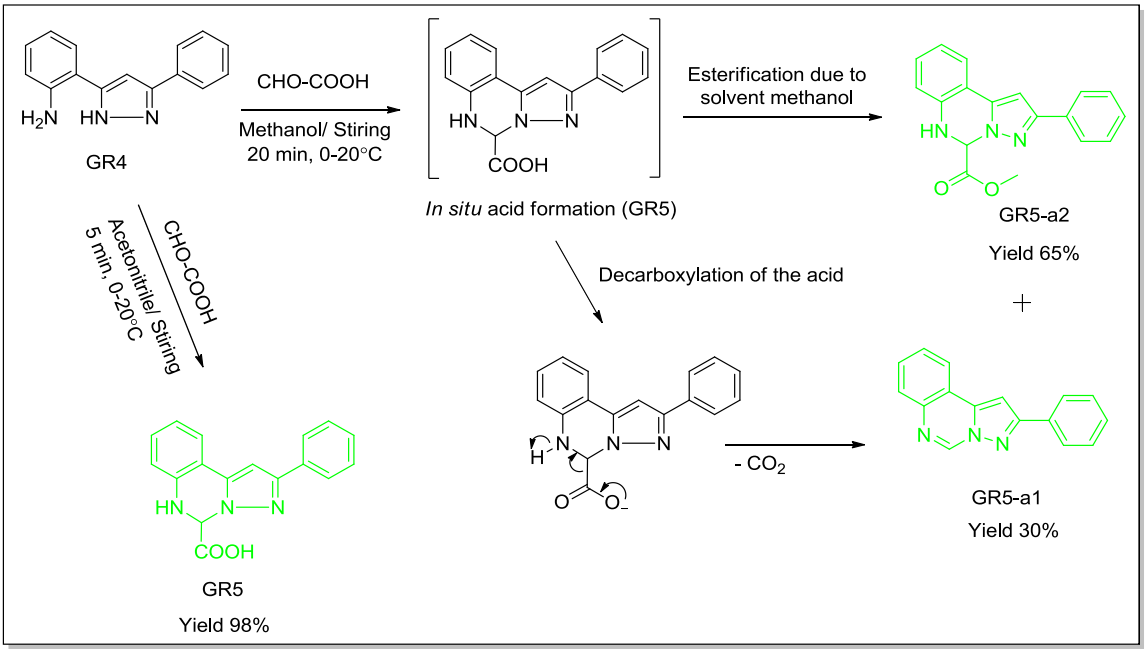

Figure 6.1.9: Synthetic strategy of dihydropyrazolo[1,5-c]quinazolines

Compounds **GR5a1** and **GR5a2** were obtained as mixtures which were separated by column chromatography. As the reaction of **GR4** with glyoxylic

acid was performed in presence of methanol, the major product (65%) **GR5a2** formed was ester instead of expected acid (Figure 6.1.9). This was due to esterification of in situ formed acid by methanol which was used as solvent. Sharp singlet of 3H at 3-4 ppm confirmed the formation of methyl ester. A singlet at 6.11 ppm confirmed the cyclisation of two amino groups. All other aromatic protons fall in the range of 7-8 ppm. ^{13}C NMR also revealed methyl carbon at 52.13 ppm confirming esterification of acid. Carbonyl carbon of ester appeared at 168.40 ppm. The HN=C-N appeared at 68.08 ppm. Carbon of pyrazole moiety falling at 96.17, 151.56 and 138.43 ppm are also the characteristic features confirming product (**GR5-a2**) formation. Two carbons of pyrazole appeared desheilded due to adjacent electronegative nitrogen, whereas one in middle at 96.17 ppm appeared shielded. All other aromatic carbons appeared in the range of 123-138 ppm.

GR5a1 obtained in small amount (30%) may be formed due to decarboxylation of the in situ formed acid **GR5** (Figure 6.1.9). Singlet peak at 9-10 ppm of N=C-N is the characteristic peak of **GR5-a1**. It appears downfield due to electron withdrawing effect of attached nitrogen. A sharp singlet at 7.24 confirmed proton of pyrazole. All other aromatic protons appeared in the range of 7-8 ppm. ^{13}C peak at 155 ppm confirms N=C-N, appearing downfield due to two adjacent electron withdrawing nitrogens. Again two carbons of pyrazole adjacent to nitrogen appear downfield at 140.09 and 139.72 and one appeared at 95 ppm.

When the same reaction of **GR4** with glyoxylic acid was performed in presence of acetonitrile as solvent instead methanol for 5 min stirring, **GR5** was obtained. It was confirmed by singlet of COOH at 11-12 ppm. This proton appears downfield due to electron withdrawing carboxyl group attached to it. All other peaks resemble the ester product **GR5-a2** except disappearance of the single peak of methyl at 3.5 ppm, further confirmed acid formation. Same pattern was followed by compounds **GR5G-a2**, **GR5G-a1** and **GR5G** which are having chloro substitution. The ^{13}C of acid appeared at 168-170 ppm. The rest of the

peaks resemble ester product **GR5-a2** except disappearance of methyl carbon at 53 ppm.

Mass spectra showed the molecular ion peak at $[M+1]^+$ and most common fragment peak at 236.1 in case of **GR4** series compounds and 270.1 for **GR4G** series. Molecular ion peak $[M+1]^+$ at 306 and $[M]^+$ at 245 confirmed the formation of **GR5-a2 and GR5-a1,** respectively.

6.2 Biological Studies

6.2.1 Evaluation of cytotoxic potential of the Compounds:

In order to examine the anticancer potential of the synthesized novel compounds, some of the representative compounds **GR5G-b, GR5G-c, GR5-b, GR5-c, GR5-d, GR5-e, GR4** and **GR4G** were screened through MTT assay which was executed with rat glial C-6 cell line. Approximately 8,000-10,000 cells were seeded per well of 96 well plate, overnight and treatments were given as stated in the experimental design. All the treatments were given in triplicates and repeated at least two to three independent experiments. MTT assay was carried out with C-6 cell line showed cytotoxic activity, thus, affirming the sensitivity and responsiveness of the compounds against brain cancer cells.

The C-6 cells were seeded in a 96 well plate and treated with the compounds at various (1-50 µM) concentrations. They were then kept for overnight incubation at 37°C in serum free media under growth conditions. The absorbance was taken spectrophotometrically at 570 nm after 24 h, 48 h and 72 h. The results of MTT assay are given below:

Antiproliferative activity against C-6 cells: It was observed that with increase in treatment time of the C-6 cells with APE1 inhibitors there was an increase in cytotoxic nature of the treated compounds from 24 h to 72 h. As evident from figure 6.2.1, 6.2.2 and 6.2.3 and table 6.2.1, 6.2.3 and 6.2.3 the compound **GR5G-c** is the only compound which showed more than 50% inhibition in cell survival at a low concentration of 5 µM after 48 h of treatment. It was observed that the at a low concentration of 15 µM **GR5G-b** has shown 62% inhibition after

24 h of treatment and inhibition in cell survival increased to 75% and 88% after 48 h and 72 h respectively. While **GR5-c** and **GR5-b** also showed more than 50% inhibition in cell survival at 15 µM after 48 h treatment. At concentration 30 µM all the compounds except **GR5-e**, **GR4G** and **GR4** showed more than 50% inhibition in cell survival rate after 24 h, more than 75% inhibition after 48 h and 90% inhibition in cell survival after 72 h. At concentration 50 µM **GR5-b** showed maximum inhibition of 90% after 24 h treatment followed by **GR5G-c**, **GR5-d** and **GR5G-b** with more than 70% inhibition in cell survival. After 48 h at 50 µM compound **GR5-b** showed maximum inhibition in cell survival 93% followed by**,** **GR5G-c**, **GR5-d** and **GR5-c** which showed 89% inhibition in cell survival. **GR5G-b** exhibited more than 80% inhibition in cell survival at 30 µM after 48 h treatment. Subsequently after 72 h treatment at 50 µM **GR5-b** showed maximum inhibition in cell survival of 95% followed by **GR5G-c**, **GR5-d** and **GR5-c** by more than 90% inhibition in cell survival, **GR5G-b** 89%, and **GR4** and **GR4G** more than 80% inhibition in cell survival. **GR5-e** displayed a poor antiproliferative activity with only 26% inhibition in cell survival even after 72 h of treatment.

Overall it seems that compounds **GR5G-b** and **GR5G-c** exhibited highest anti-proliferative effect on rat glial C-6 cells at various concentrations followed by **GR5-c, GR5-b** and **GR5-d**. IC_{50} values were determined by fitting the concentration-response (in terms of %inhibition) data in equation 1 (Copeland, 2013). Calculated IC_{50} values of some of the best compounds are listed in table 6.2.4. These compounds showed decrease in IC_{50} values with increase in treatment time. **GR5G-b** and **GR5G-c** emerged as best compounds with lowest IC_{50} values as compared to the other compounds.

$$\% \text{ Inhibition} = 100/\ 1+(\mathbf{IC_{50}}/[I]) \qquad \text{Equation 1}$$

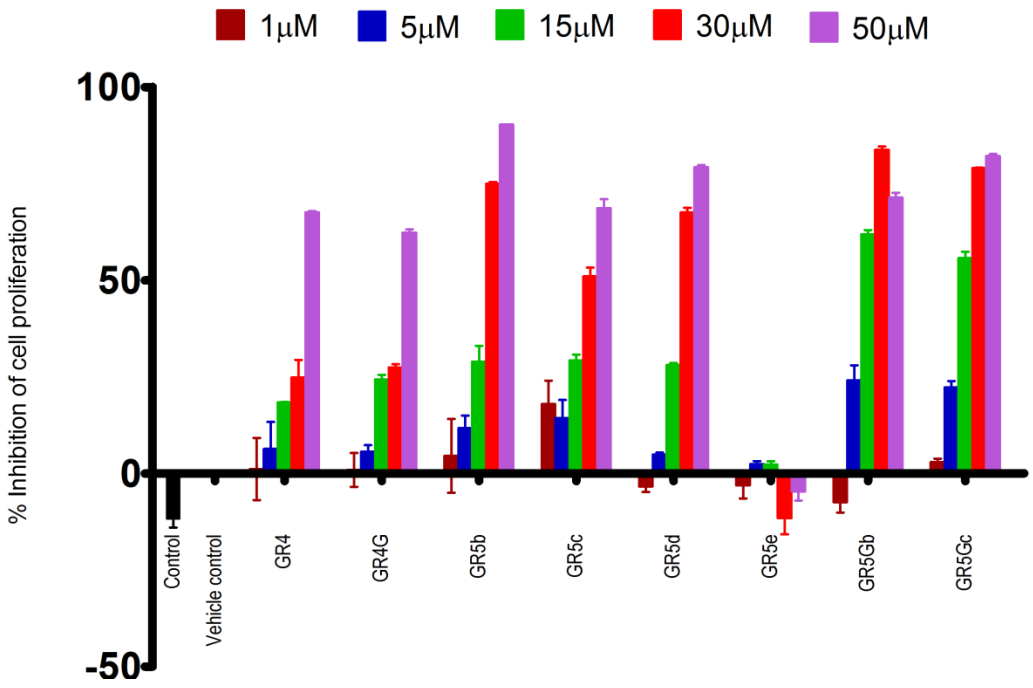

Figure 6.2.1: Percent inhibition of rat C-6 glial cells in response to treatment with synthesized compounds at concentrations of 1 µM, 5 µM, 15 µM, 30 µM and 50 µM for time duration of **24 h.**

Table 6.2.1: Percent inhibition in cell survival by synthesized compounds at 24h

Compound	**% Inhibition of cell proliferation [a] 24 h of treatment**				
	1µM	**5µM**	**15µM**	**30 µM**	**50µM**
GR4	1	6	18	25	68
GR4G	1	6	24	27	62
GR5-b	5	12	29	75	90
GR5-c	18	14	29	51	69
GR5-d	-3	5	28	67	79
GR5-e	-3	2	2	-12	-5
GR5G-b	-7	24	62	84	71
GR5G-c	3	22	57	79	82

[a] All readings are triplicates, repeated 2-3 times and expressed as mean ±S.D.

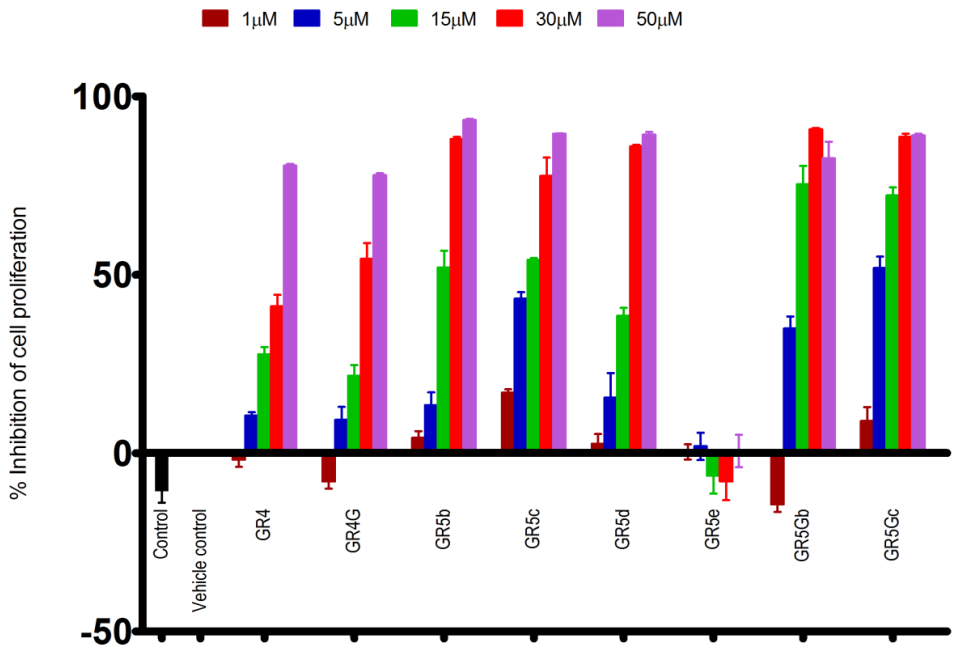

Figure 6.2.2: Percent inhibition of C-6 rat glial cells in response to treatment with synthesized compounds at concentrations of 1 µM, 5 µM, 15 µM and 50 µM for time duration of 48 h.

Table 6.2.2: Percent inhibition in cell survival by synthesized compounds at 48h

Compound	**% Inhibition of cel proliferation [a] 48 h of treatment**				
	1µM	**5µM**	**15µM**	**30 µM**	**50µM**
GR4	-2	11	28	41	81
GR4G	-8	9	22	54	78
GR5-b	4	13	52	88	93
GR5-c	16	43	54	78	89
GR5-d	2	16	39	86	89
GR5-e	0.3	2	-6	-8	1
GR5G-b	-14.	35	75	91	83
GR5G-c	9	52	72	89	89

[a] All readings are triplicates, repeated 2-3 times and expressed as mean ±S.D.

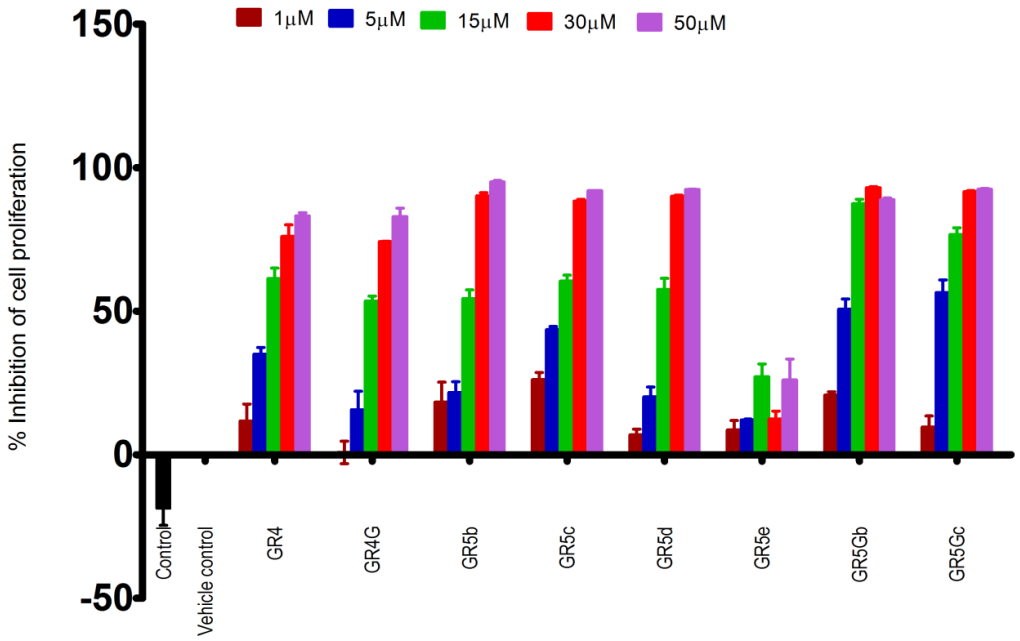

Figure 6.2.3: Percent inhibition of rat C-6 glial cells in response to treatment with synthesized compounds at concentrations of 1 µM, 5 µM, 15 µM, 30 µM and 50 µM for time duration of 72 h

Table 6.2.3: Percent inhibition in cell survival by synthesized compounds at 72h

Compound	**% Inhibition of cell proliferation [a] 72 h of treatment**				
	1µM	**5µM**	**15µM**	**30 µM**	**50µM**
GR4	12	35	61	76	83
GR4G	1	16	54	74	83
GR5-b	18	22	54	90	95
GR5-c	26	44	61	88	92
GR5-d	7	20	58	90	92
GR5-e	9	12	27	12	26
GR5G-b	21	51	88	93	89
GR5G-c	10	57	77	92	93

[a] All readings are triplicates, repeated 2-3 times and expressed as mean ±S.D.

Table: 6.2.4 IC_{50} of the compounds showing antiproliferative activity in C-6 cell line.

Sr. No.	Compounds	IC_{50} µM		
		24 h	**48 h**	**72 h**
1	**GR5G-b**	13	3.86	3.80
2	**GR5G-c**	16	6.58	4.72
3	**GR5-c**	22	7.84	5.44
4	**GR5-b**	21.5	15.83	7.78
5	**GR5-d**	39.19	21.79	8.11

6.2.2 Structure Activity Relationship (SAR) of Compounds for Antiproliferative activity:

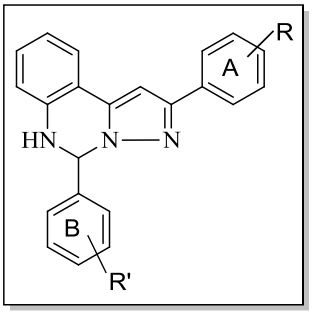

Figure 6.2.4: General structure of the tested compounds

Substitution at A ring:

The compounds with p-chloro substitution of ring A results in increased activity in comparison to compounds without any substitution at ring A. **GR5G** series showed more percentage inhibition of cell growth in C-6 cells as compared to **GR5** series. (Figure 6.2.5a and 6.2.5b).

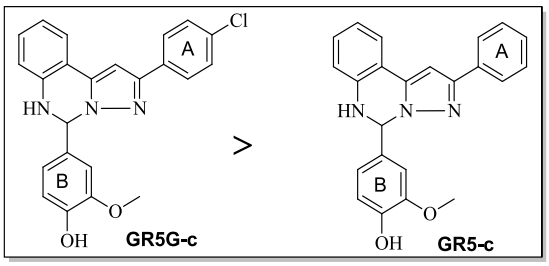

Figure 6.2.5a: Comparison of antiproliferative activity of compounds with ring A substitution

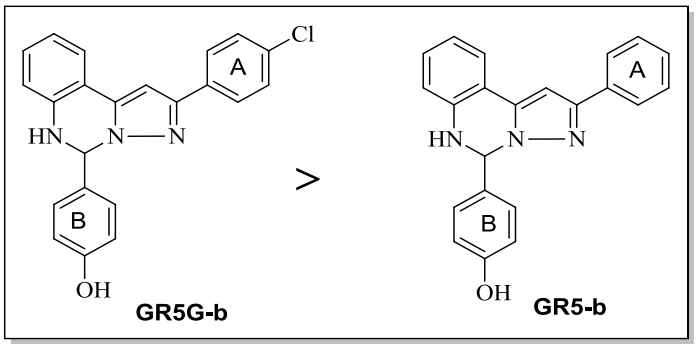

Figure 6.2.5b: Comparison of antiproliferative activity of compounds with ring A substitution

As we have observed from molecular modeling studies NH of pyrazoloquinazolo ring of **GR5G-b** is involved hydrogen bonding interactions with basic amino acid ARG 177 and ASN 229. Electron withdrawing group Cl makes the ring more electron deficient and renders the proton more acidic to form extra Hydrogen bonding interactions with guanidine moiety of basic ARG 177.

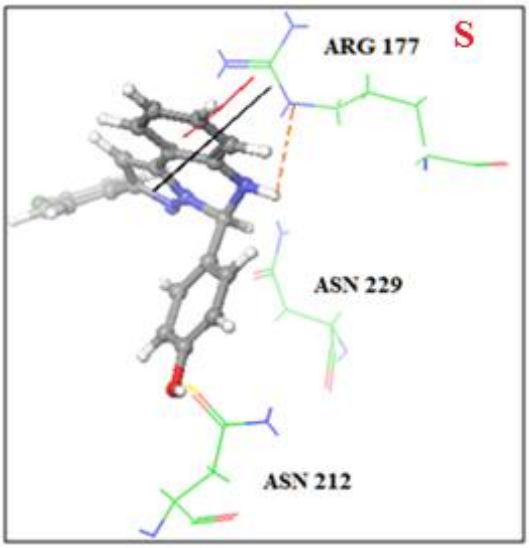

Figure 6.2.5 c: 3D docked pose of **GR5G-b** in repair active site of APE1 showing H-Bonding interaction of NH with ARG 177

Substitution at B ring:

Substitution of OH group: The substitution at ring B with OH group at para position results in increase in anti-proliferative activity as compared to substitution at meta position of B ring.

Substitution of methoxy group: Substitution of methoxy group at meta position of B ring results in increase in anti-proliferative activity as compared to substitution at para position as shown in figure 6.2.6.

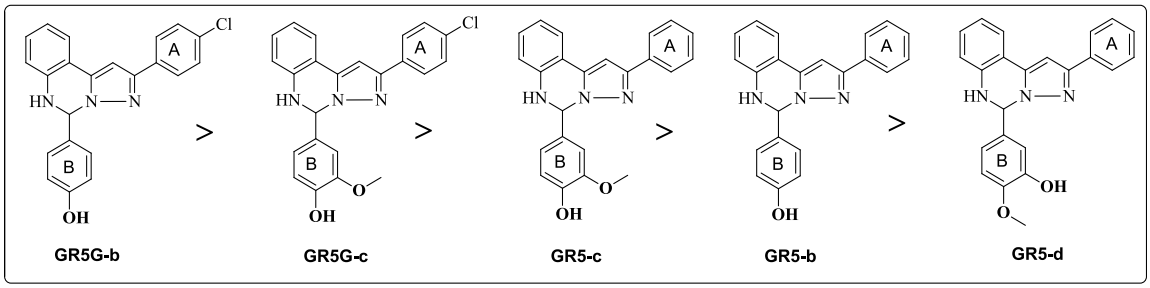

Figure 6.2.6: Comparison of antiproliferative activity of compounds with ring B substitution

Substitution of CN group:
The Substitution of CN group at para position at B ring leads to poor antiproliferative activity of the compound.

A common trend followed by the compounds showed that negatively ionisable group at para position of B ring leads to more active compounds and electronegative group at para position of A ring leads to increase in anti-proliferative activity. This almost fulfils our proposed rationale of linkage of one or more negatively ionisable groups at ends of the compounds.

6.3 Intracellular ROS measurement by DCFDA Assay

Rat C-6 glial cells were treated with the synthesized compounds **GR4, GR4G, GR5-b, GR5-c, GR5-d, GR5-e** and **GR5G-c** for the determination of ROS generated upon treatment of C-6 cells at different concentrations and time points by DCFDA assay. Fluorescence readings were read at the excitation wavelength of 478 nm and emission wavelength of 518 nm using BioTek Microplate Reader after 24 h, 48 h and 72 h(Dhiman & Garg, 2011). Vehicle

control reading was taken as 100% of ROS level and % increase in ROS production of the test compounds was compared with respect to it.

It is observed that at low concentration (1µM) all the test compounds showed increase in ROS production with increase in treatment time from 24 h to 72 h upto 300% as compared to vehicle control. The same trend was also observed with 5 µM concentration of test compounds. But some compounds as **GR5-b** and **GR5-c** showed only 50% increase in ROS production after 72 h of treatment as compared to vehicle control. At concentration 15 µM all compounds showed decrease in ROS production; **GR5-b** showed 10% ROS levels after 72 h whereas **GR5G-c** also showed 4% of ROS levels after 72 h. Other compounds also showed decrease in their ROS levels upto 40% after 72 h. At higher concentrations 30µM and 50 µM it was observed that compounds **GR5-b**, **GR5G-c**, **GR5-c** and **GR5-d** showed very low ROS levels. Overall it may be concluded that all the compounds showed significant antioxidant activity at 15 µM and above with marked decrease in ROS levels.

Further from the antiproliferative assay MTT we have observed that both these compounds **GR5G-c** and **GR5-b** emerged as potent anticancer compounds with remarked percentage inhibition of glial C-6 cell lines. From these results we may conclude that in one way our compounds are inhibiting cancer cell growth by exhibiting their antioxidant activity. By another way we know that ROS and other environmental insults regulates expression of APE1 gene (Hsieh et al., 2001; Pines et al., 2005; Ramana et al., 1998; Tell et al., 2009; Zaky et al., 2008). Increase in ROS generation upregulates APE1 to repair the damaged DNA by acting on AP-sites. Our compounds are exhibiting antioxidant property and cause decrease in ROS level which further leads to decreased expression of APE1 thus checking the cancer cell survival. AP-sites created by adjuvant DNA damaging chemotherapy are then not repaired by APE1 and this leads to cell death. Thus we may conclude that synthesized compounds are exhibiting anticancer activity via APE1 inhibition. Further studies are required to support this hypothesis.

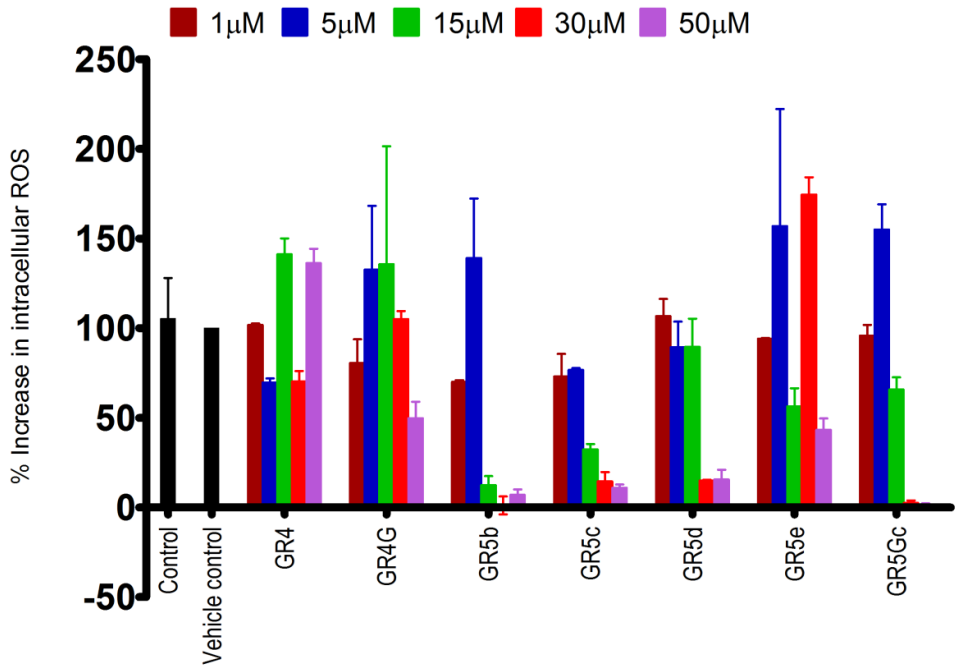

Figure 6.2.7: Percent increase in intracellular ROS levels in rat C-6 glial cells in response to treatment with synthesized compounds at various concentrations (1 µM, 5 µM, 15 µM, 30 µM and 50 µM) for a time period of **24 h**

Table 6.2.5: Percentage increase in intracellular ROS by synthesized compounds at 24 h

Compound	**% increase in ROS levels after 24 h treatment [a]**				
	1µM	**5µM**	**15µM**	**30 µM**	**50µM**
GR4	101	70	141	70	136
GR4G	81	133	136	105	50
GR5-b	70	139	12	1	7
GR5-c	73	77	32	14	11
GR5-d	107	89	90	15	16
GR5-e	94	157	56	174	43
GR5G-c	96	155.	66	2	2

[a] Values are means of two readings ±S.D.

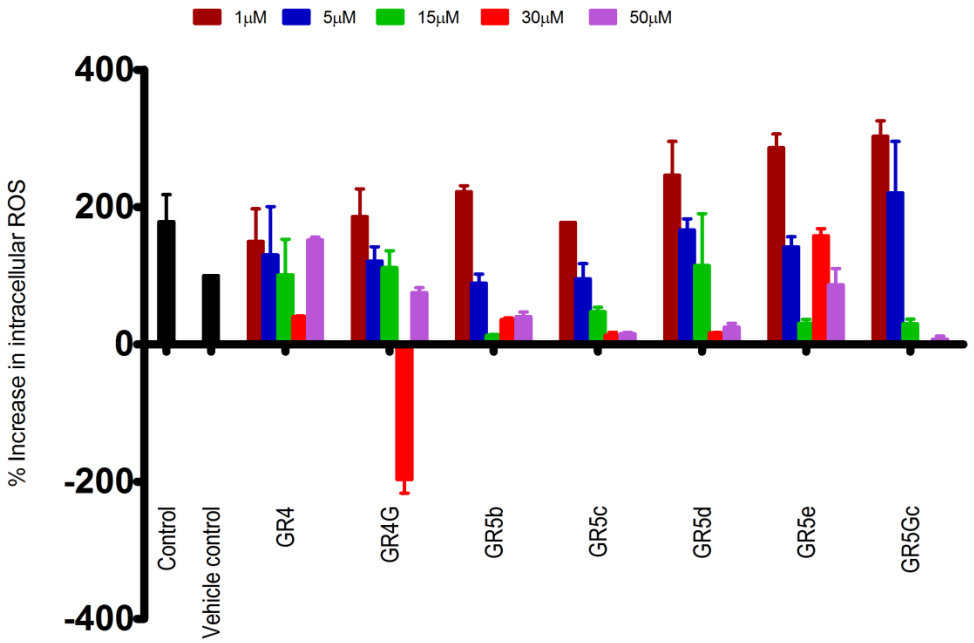

Figure 6.2.8: Percent increase in intracellular ROS levels in rat C-6 glial cells in response to treatment with synthesized compounds at various concentrations (1 µM, 5 µM, 15 µM, 30 µM and 50 µM) for a time period of **48 h**

Table 6.2.6: Percentage increase in ROS by synthesized compounds at 48 h

Compound	**% increase in ROS level after 48 h treatment[a]**				
	1µM	**5µM**	**15µM**	**30 µM**	**50µM**
GR4	150	130	101	40	152
GR4G	186	121	112	-197	75
GR5-b	223	89	13	36	41
GR5-c	177	95	48	13	15
GR5-d	246	166	115	17	25
GR5-e	286	142	31	158	87
GR5G-c	303	220	30	1	8

[a] Values are means of two readings ±S.D.

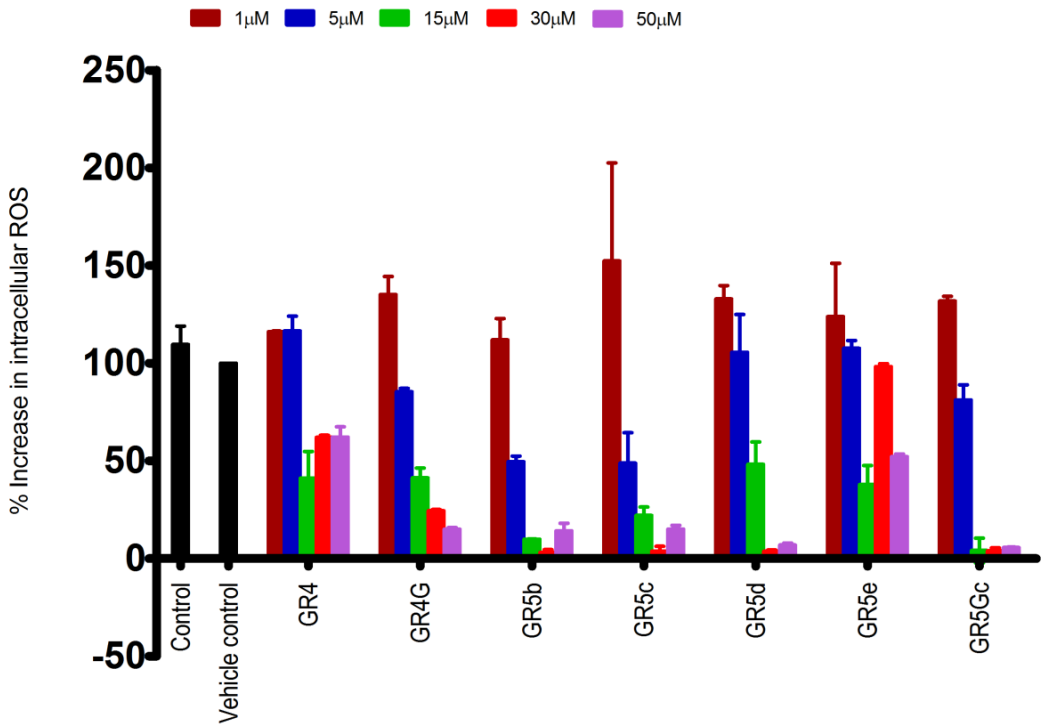

Figure 6.2.9: Percent increase in intracellular ROS levels in rat C-6 glial cells in response to treatment with synthesized compounds at various concentrations (1 µM, 5 µM, 15 µM, 30 µM and 50 µM) a time period of **72 h**.

Table 6.2.7: Percent increase in ROS by synthesized compounds at 72 h.

Compound	**% increase in ROS level after 72 h [a]**				
	1µM	**5µM**	**15µM**	**30 µM**	**50µM**
GR4	116	116	41	62	62
GR4G	135	85	41	24	15
GR5-b	112	49	10	3	14
GR5-c	152	48	23	4	15
GR5-d	133	106	48	3	7
GR5-e	124	108	38	98	52
GR5G-c	132	81	4	4	6

[a] Values are means of two readings ±S.D.

CHAPTER 7

CONCLUSIONS

7 Conclusions

Success in chemotherapy has not been attained completely yet and has remained a worried issue from years. Various reasons drive this failure, but the much talked about and hot topic is failure due to emergence of resistance to chemotherapeutic drugs due to various affecting reasons. One of the major reason here we have targeted is the resistance developed against DNA damaging chemotherapy due to over activation of DNA repair pathways which are part of normal physiology. APE1 is the key enzyme participating in the repair process of BER-pathway which is the major repair pathway responsible for 95% of the total DNA damage repair. Design and synthesis of APE1 inhibitors using rational approach has been carried out in this research work fulfilling the pharmacophoric requirements of APE1 inhibitor. Molecular modelling studies revealed that designed compounds fit well into the repair active site of APE1. A total number of fourteen compounds have been designed and synthesized having pyrazolo-quinazolines as the core structure. The purity of all the compounds was determined by melting point, IR, NMR and Mass spectrometry. The anticancer potential of the 8 representative compounds was evaluated against rat C-6 glial cell line for different concentrations and time periods. The information on inhibitory potential of the compounds against cell line proliferation obtained from MTT assay helped us to formulate the structure activity relationship studies. **GR5G-c, GR5-c and GR5G-b** were found to be potent anticancer agents, others also exhibited significant anticancer activity. Further, intracellular ROS measurement was also carried out using florescence based DCFDA assay. Compounds showing good MTT results were also found to be potential antioxidants. From both of these results it is concluded that our compounds exhibit potential anticancer activity via APE1 inhibition. Molecular docking studies of **GR5G-b** into APE1 active site highlighted favourable binding interactions and poses of the inhibitors with APE1 recommending their possible mechanism of action. The active compounds may be taken further for lead optimisation and mechanistic interventions for their in vitro binding studies on APE1 in future.

REFERENCES

Abbotts, R., & Madhusudan, S. (2010). Human AP endonuclease 1 (APE1): From mechanistic insights to druggable target in cancer. *Cancer Treat. Rev., 36*(5), 425-435.

Abbotts, R. M., Perry, C., & Madhusudan, S. (2011). Human Apurinic/Apyrimidinic Endonuclease is a Novel Drug Target in Cancer. In S. Vengrova (Ed.), *DNA repair and human health.* (pp. 495-520). warwick, U.K: Rijeka: InTech.

Alarcon, E., Romero, N., & Aguilar. (2013). *Green synthesis of chalcones derivates of acetophenone*. Paper presented at the 10th Green Chemistry Conference-an international event, Barcelona - Spain, 2013.

Almeida, K. H., & Sobol, R. W. (2007). A unified view of base excision repair: Lesion-dependent protein complexes regulated by post-translational modification. *DNA repair, 6*(6), 695-711.

Ando, K., Hirao, S., Kabe, Y., & Ogura. (2008). A new APE1/Ref-1-dependent pathway leading to reduction of NF-κB and AP-1, and activation of their DNA-binding activity. *Nucleic acids Res., 36*(13), 4327-4336.

Bapat, A., Fishel, M. L., & Kelley, M. R. (2009). Going ape as an approach to cancer therapeutics. *Antioxid. Redox Signaling, 11*(3), 651-667.

Barzilay, G., Mol, C. D., Robson, C. N., Walker, L. J., & Cunningham. (1995). Identification of critical active-site residues in the multifunctional human DNA repair enzyme HAP1. *Nat. Struct. Mol. Biol., 2*(7), 561-568.

Beernink, P. T., Segelke, B. W., Hadi, M. Z., Erzberger, J. P., Wilson, D. M., & Rupp, B. (2001). Two divalent metal ions in the active site of a new crystal form of human apurinic/apyrimidinic endonuclease, Ape1: implications for the catalytic mechanism. *J. Mol. Biol., 307*(4), 1023-1034.

Bellamy, F., & Ou, K. (1984). Selective reduction of aromatic nitro compounds with stannous chloride in non acidic and non aqueous medium. *Tetrahedron Lett., 25*(8), 839-842.

Bernstein, C., Prasad, A. R., Nfonsam, V., & Bernstein, H. (2013). DNA Damage *DNA Repair and Cancer*.

Bhakat, K. K., Mantha, A. K., & Mitra, S. (2009). Transcriptional regulatory functions of mammalian AP-endonuclease (APE1/Ref-1), an essential multifunctional protein. *Antioxid. Redox Signaling, 11*(3), 621-637.

Caldecott, K. W. (2007). Mammalian single-strand break repair: mechanisms and links with chromatin. *DNA Repair, 6*(4), 443-453.

Cao, X., Kambe, F., Ohmori, S., & Seo, H. (2002). Oxidoreductive modification of two cysteine residues in paired domain by Ref-1 regulates DNA-binding activity of Pax-8. *Biochem. Biophys. Res. Commun., 297*(2), 288-293.

Chattopadhyay, R., Bhattacharyya, A., & Crowe, S. E. (2010). Dual regulation by apurinic/apyrimidinic endonuclease-1 inhibits gastric epithelial cell apoptosis during Helicobacter pylori infection. *Cancer Res., 70*(7), 2799-2808.

Chu, Y.-C., Tsai, L.-H., Lee, M.-C., & Chen, C.-Y. (2012). Cytoplasmic Ape1 Expression Elevated by p53 aberration may predict survival and relapse in resected non-small cell lung cancer. *Ann. Surg. Oncol., 20*(3), 1-12.

Colotta, V., Catarzi, D., Varano, F., Filacchioni, G., Cecchi, L., Galli, A., & Costagli, C. (1996). Synthesis and binding activity of some pyrazolo [1, 5-c] quinazolines as tools to verify an optional binding site of a benzodiazepine receptor ligand. *J. Med. Chem., 39*(15), 2915-2921.

Copeland, R. A. (2013). Lead Optimization and Structure Activity Relationships for Reversible Inhibitor *Evaluation of enzyme inhibitors in drug discovery a guide for medicinal chemists and pharmacologists* (2 ed., Vol. 46, pp. 111-140). Hoboken, New Jersey.: John Wiley & Sons.

Crowe, S. E., Alvarez, L., Dytoc, M., Hunt, R. H., Muller, M., Sherman, P., Ernst, P. B. (1995). Expression of interleukin 8 and CD54 by human gastric epithelium after *Helicobacter Pylori* infection in vitro. *Gastroenterology, 108*(1), 65-74.

Demple, B., Herman, T., & Chen, D. S. (1991). Cloning and expression of APE, the cDNA encoding the major human apurinic endonuclease: definition of a family of DNA repair enzymes. *Proc. Natl. Acad. Sci. USA, 88*(24), 11450-11454.

Dhiman, M., & Garg, N. J. (2011). NADPH oxidase inhibition ameliorates Trypanosoma cruzi-induced myocarditis during Chagas disease. *J. Pathol., 225*(4), 583-596.

Dianov, G. L., & Parsons, J. L. (2007). Co-ordination of DNA single strand break repair. *DNA repair, 6*(4), 454-460.

Dorjsuren, D., Kim, D., Vyjayanti, V. N., Maloney, D. J., Jadhav, A., Wilson, D. M., 3rd, & Simeonov, A. (2012). Diverse small molecule inhibitors of human apurinic/apyrimidinic endonuclease APE1 identified from a screen of a large public collection. *PloS one, 7*(10), 47974.

Duguid, J. R., Eble, J. N., Wilson, T. M., & Kelley, M. R. (1995). Differential cellular and subcellular expression of the human multifunctional apurinic/apyrimidinic endonuclease (APE/ref-1) DNA repair enzyme. *Cancer Res., 55*(24), 6097-6102.

El-Mouatassim, S., Bilotto, S., Russo, G. L., Tosti, E., & Menezo, Y. (2007). APEX/Ref-1 (apurinic/apyrimidic endonuclease DNA-repair gene) expression in human and ascidian (Ciona intestinalis) gametes and embryos. *Mol. Hum. Reprod., 13*(8), 549-556.

Erzberger, J. P., & Wilson III, D. M. (1999). The role of Mg^{2+} and specific amino acid residues in the catalytic reaction of the major human abasic endonuclease: New insights from EDTA-resistant incision of acyclic abasic site analogs and site-directed mutagenesis. *J. Mol. Biol., 290*(2), 447-457.

Evans, A. R., Limp-Foster, M., & Kelley, M. R. (2000). Going APE over ref-1. *Mutat. Res., 461*(2), 83-108.

Fantini, D., Vascotto, C., Marasco, D., D'Ambrosio, C., Romanello, M., Vitagliano, L., Quadrifoglio, F. (2010). Critical lysine residues within the overlooked N-terminal domain of human APE1 regulate its biological functions. *Nucleic Acids Res., 38*(22), 8239-8256.

Fishel, M. L., He, Y., Smith, M. L., & Kelley, M. R. (2007). Manipulation of base excision repair to sensitize ovarian cancer cells to alkylating agent temozolomide. *Clin. Cancer Res., 13*(1), 260-267.

Fishel, M. L., Vascotto, C., & Kelley, M. R. (2013). DNA Base Excision Repair Therapeutics: Summary of Targets with a focus on APE1 *DNA Repair and Cancer: From Bench to Clinic* (pp. 233).

Friesner, R. A., Banks, J. L., Murphy, R. B., Halgren, T. A., Klicic, J. J., Mainz, D. T., Perry, J. K. (2004). Glide: a new approach for rapid, accurate docking and scoring. 1. Method and assessment of docking accuracy. *J. Med. Chem., 47*(7), 1739-1749.

Friesner, R. A., Murphy, R. B., Repasky, M. P., Frye, L. L., Greenwood, J. R., Halgren, T. A., Mainz, D. T. (2006). Extra precision glide: docking and scoring incorporating a model of hydrophobic enclosure for protein-ligand complexes. *J. Med. Chem., 49*(21), 6177-6196.

Fung, H., & Demple, B. (2011). Distinct roles of Ape1 protein in the repair of DNA damage induced by ionizing radiation or bleomycin. *J. Biol. Chem., 286*(7), 4968-4977.

Gaiddon, C., Moorthy, N., & Prives, C. (1999). Ref-1 regulates the transactivation and pro-apoptotic functions of p53 in vivo. *EMBO J., 18*(20), 5609-5621.

Georgiadis, M., Luo, M., Gaur, R., Delaplane, S., Li, X., & Kelley, M. (2008). Evolution of the redox function in mammalian apurinic/apyrimidinic endonuclease. *Mutat. Res., 643*(1-2), 54.

Gorman, M. A., Morera, S., Rothwell, D. G., de La Fortelle, E., Mol, C. D., Tainer, J. A., Freemont, P. S. (1997). The crystal structure of the human DNA repair endonuclease HAP1 suggests the recognition of extra-helical deoxyribose at DNA abasic sites. *EMBO J., 16*(21), 6548-6558.

Gredilla, R. (2010). DNA damage and base excision repair in mitochondria and their role in aging. *J. Aging Res., 2010*(2010), 1-21.

Grosch, S., Fritz, G., & Kaina, B. (1998). Apurinic endonuclease (Ref-1) is induced in mammalian cells by oxidative stress and involved in clastogenic adaptation. *Cancer Res., 58*(19), 4410-4416.

Hegde, M. L., Hazra, T. K., & Mitra, S. (2008). Early steps in the DNA base excision/single-strand interruption repair pathway in mammalian cells. *Cell Res., 18*(1), 27-47.

Hegde, M. L., Mantha, A. K., Hazra, T. K., Bhakat, K. K., Mitra, S., & Szczesny, B. (2012). Oxidative genome damage and its repair: implications in aging and neurodegenerative diseases. *Mech. Ageing Dev., 133*(4), 157-168.

Hirota, K., Matsui, M., Iwata, S., Nishiyama, A., Mori, K., & Yodoi, J. (1997). AP-1 transcriptional activity is regulated by a direct association between thioredoxin and Ref-1. *Proc. Natl. Acad. Sci. USA, 94*(8), 3633-3638.

Hitomi, K., Iwai, S., & Tainer, J. A. (2007). The intricate structural chemistry of base excision repair machinery: implications for DNA damage recognition, removal, and repair. *DNA Repair, 6*(4), 410-428.

Hsieh, M. M., Hegde, V., Kelley, M. R., & Deutsch, W. A. (2001). Activation of APE/Ref-1 redox activity is mediated by reactive oxygen species and PKC phosphorylation. *Nucleic Acids Res., 29*(14), 3116-3122.

HUANG, R.-P., & ADAMSON, E. D. (1993). Characterization of the DNA-binding properties of the early growth response-1 (Egr-1) transcription factor: evidence for modulation by a redox mechanism. *DNA Cell Biol., 12*(3), 265-273.

Hung, R. J., Hall, J., Brennan, P., & Boffetta, P. (2005). Genetic polymorphisms in the base excision repair pathway and cancer risk: a HuGE review. *Am. J. Epidemiol, 162*(10), 925-942.

Izumi, T., Brown, D. B., Naidu, C., Bhakat, K. K., MacInnes, M. A., Saito, H., Mitra, S. (2005). Two essential but distinct functions of the mammalian abasic endonuclease. *Proc. Natl. Acad. Sci. USA, 102*(16), 5739-5743.

Jackson, E. B., Theriot, C. A., Chattopadhyay, R., Mitra, S., & Izumi, T. (2005). Analysis of nuclear transport signals in the human apurinic/apyrimidinic endonuclease (APE1/Ref1). *Nucleic acids Res., 33*(10), 3303-3312.

Jackson, S. (2001). Detecting, signalling and repairing DNA double-strand breaks. *Biochem. Soc. Trans., 29*(6), 655.

Jayaraman, L., Murthy, K., Zhu, C., Curran, T., Xanthoudakis, S., & Prives, C. (1997). Identification of redox/repair protein Ref-1 as a potent activator of p53. *Genes Dev., 11*(5), 558-570.

Kakolyris, S., Kaklamanis, L., Giatromanolaki, A., Koukourakis, M., Hickson, I., Barzilay, G., .Georgoulias, V. (1998). Expression and subcellular localization of human AP endonuclease 1 (HAP1/Ref-1) protein: a basis for its role in human disease. *Histopathology, 33*(6), 561-569.

Kelley, M. R., & Fishel, M. L. (2008). DNA repair proteins as molecular targets for cancer therapeutics. *Anti-Cancer Agents Med. Chem., 8*(4), 417.

Kelley, M. R., Georgiadis, M. M., & Fishel, M. L. (2012). APE1/Ref-1 Role in Redox Signaling: Translational Applications of Targeting the Redox Function of the DNA Repair/Redox Protein APE1/Ref-1. *Curr. Mol. pharmacol., 5*(1), 36.

Khaliullin, I., Shapovalova, D. N. I., & Svedas, V. (2012). Construction of a Full-Atomic Mechanistic Model of Human Apurinic/Apyrimidinic Endonuclease APE1 for Virtual Screening of Novel Inhibitors. *Acta Naturae, 4*(2), 80.

Khan, S., Lopez-Dee, Z., Kumar, R., & Ling, J. (2013). Activation of NFkB is a novel mechanism of pro-survival activity of glucocorticoids in breast cancer cells. *Cancer Lett., 337*(1), 90-95.

Klungland, A., & Lindahl, T. (1997). Second pathway for completion of human DNA base excision-repair: reconstitution with purified proteins and requirement for DNase IV (FEN1). *EMBO J., 16*(11), 3341-3348.

Konieczny, M. T., Konieczny, W., Sabisz, M., Skladanowski, A., Wakiec, R., Augustynowicz-Kopeć, E., & Zwolska, Z. (2007). Acid-catalyzed synthesis of oxathiolone fused chalcones. Comparison of their activity toward various microorganisms and human cancer cells line. *EJMC, 42*(5), 729-733.

Krokan, H. E., Nilsen, H., Skorpen, F., Otterlei, M., & Slupphaug, G. (2000). Base excision repair of DNA in mammalian cells. *FEBS lett., 476*(1), 73-77.

Kubota, Y., Nash, R. A., Klungland, A., Schär, P., Barnes, D., & Lindahl, T. (1996). Reconstitution of DNA base excision-repair with purified human proteins: interaction between DNA polymerase beta and the XRCC1 protein. *EMBO J., 15*(23), 6662.

Kumar, D., & Kumar, R. (2014). Microwave-assisted synthesis of pyrazolo[1,5-c]quinazolines and their derivatives. *Tetrahedron Lett., 55*(16), 2679-2683.

Lando, D., Pongratz, I., Poellinger, L., & Whitelaw, M. L. (2000). A redox mechanism controls differential DNA binding activities of hypoxia-inducible factor (HIF) 1α and the HIF-like factor. *J. Biol. Chem., 275*(7), 4618-4627.

Levai, A. (2005). Synthesis of chlorinated 3, 5-diaryl-2-pyrazolines by the reaction of chlorochalcones with hydrazines. *Arkivoc, 9*, 344-352.

Li, Z., Bao, S., Wu, Q., Wang, H., Eyler, C., Sathornsumetee, S., Rich, J. N. (2009). Hypoxia-inducible factors regulate tumorigenic capacity of glioma stem cells. *Cancer Cell, 15*(6), 501-513.

Lindahl, T. (1993). Instability and decay of the primary structure of DNA. *Nature, 362*(6422), 709-715.

Liu, L., & Gerson, S. (2004). Therapeutic impact of methoxyamine: blocking repair of abasic sites in the base excision repair pathway. *Curr. Opin. Investig. Drugs, 5*(6), 623.

Liuzzi, M., & Talpaert-Borle, M. (1985). A new approach to the study of the base-excision repair pathway using methoxyamine. *J. Biol. Chem., 260*(9), 5252-5258.

Lokhande, P., Waghamare, B., & Sakate, S. (2005). Regioselective one-pot synthesis of 3, 5-diaryl-pyrazoles. *Indian J. Chem., 44*(11), 2338.

Luo, M., Delaplane, S., Jiang, A., Reed, A., He, Y., Fishel, M., Georgiadis, M. M. (2008). Role of the multifunctional DNA repair and redox signaling protein Ape1/Ref-1 in cancer and endothelial cells: small-molecule inhibition of the redox function of Ape1. *Antioxid. Redox Signaling, 10*(11), 1853-1867.

Luo, M., He, H., Kelley, M. R., & Georgiadis, M. M. (2010). Redox regulation of DNA repair: implications for human health and cancer therapeutic development. *Antioxid. Redox Signaling, 12*(11), 1247-1269.

Luo, M., Zhang, J., He, H., Su, D., Chen, Q., Gross, M. L., Georgiadis, M. M. (2012). Characterization of the Redox Activity and Disulfide Bond Formation in Apurinic/Apyrimidinic Endonuclease. *Biochemistry, 51*(2), 695-705.

Madhusudan, S., Smart, F., Shrimpton, P., Parsons, J. L., Gardiner, L., Houlbrook, S., Sternberg, M. J. (2005). Isolation of a small molecule inhibitor of DNA base excision repair. *Nucleic Acids Res., 33*(15), 4711-4724.

Mantha, A. K., Dhiman, M., Taglialatela, G., Perez-Polo, R. J., & Mitra, S. (2012). Proteomic study of amyloid beta (25-35) peptide exposure to neuronal cells: Impact on APE1/Ref-1's protein-protein interaction. *J. Neurosci. Res., 90*(6), 1230-1239.

Mantha, A. K., Oezguen, N., Bhakat, K. K., Izumi, T., Braun, W., & Mitra, S. (2008). Unusual role of a cysteine residue in substrate binding and activity of human AP-endonuclease 1. *J. Mol. Biol., 379*(1), 28-37.

Mantha, A. K., Sarkar, B., & Tell, G. (2013). A short review on the implications of base excision repair pathway for neurons: Relevance to neurodegenerative diseases. *Mitochondrion*. doi: 10.1016/j.mito.2013.10.007

Manvilla, B. A., Wauchope, O., Seley-Radtke, K. L., & Drohat, A. C. (2011). NMR studies reveal an unexpected binding site for a redox inhibitor of AP endonuclease 1. *Biochemistry, 50*(48), 10540-10549.

Messina, M., Kucuk, O., & Lampe, J. W. (2006). An overview of the health effects of isoflavones with an emphasis on prostate cancer risk and prostate-specific antigen levels. *J. AOAC Int., 89*(4), 1121-1134.

Milicevic, Z., Bajic, V., Zivkovic, L., Kasapovic, J., Andjelkovic, U., & Spremo-Potparevic, B. (2014). Identification of p53 and Its Isoforms in Human Breast Carcinoma Cells. *Sci. World J., 2014*(2014), 1-10. doi: 10.1155/2014/618698

Mirzayans, R., Andrais, B., Scott, A., Tessier, A., Murray, D. (2007). A sensitive assay for the evaluation of cytotoxicity and its pharmacologic modulation in human solid tumor-derived cell lines exposed to cancer-therapeutic agents. *J. Pharma. Sci., 10:*, 298-311.

Mitra, S., Izumi, T., Boldogh, I., Bhakat, K. K., Chattopadhyay, R., & Szczesny, B. (2007). Intracellular trafficking and regulation of mammalian AP-endonuclease 1 (APE1), an essential DNA repair protein. *DNA Repair, 6*(4), 461-469.

Mohammed, M., Vyjayanti, V., Laughton, C., Dekker, L., Fischer, P., Wilson, D., Hickson, I. (2011). Development and evaluation of human AP endonuclease inhibitors in melanoma and glioma cell lines. *Brit.. J. Cancer, 104*(4), 653-663.

Mohan, V., & Madhusudan, S. (2013). DNA Base Excision Repair: Evolving Biomarkers for Personalized Therapies in Cancer *New Research Directions in DNA Repair*.

Mol, C. D., Izumi, T., Mitra, S., & Tainer, J. A. (2000). DNA-bound structures and mutants reveal abasic DNA binding by APE1 DNA repair and coordination. *Nature, 403*(6768), 451-456.

Mosmann, T. (1983). Rapid colorimetric assay for cellular growth and survival: application to proliferation and cytotoxicity assays. *J. Immunol. Methods, 65*(1), 55-63.

Murai, K., Morishita, M., Nakatani, R., Fujioka, H., & Kita, Y. (2008). Oxidative decarboxylative synthesis of 2-H-imidazolines from glyoxylic acid and 1, 2-diamines. *Chem. Commun.*(37), 4498-4500.

Naidu, M. D., Agarwal, R., Pena, L. A., Cunha, L., Mezei, M., Shen, M., Chaudhary, P. (2011). Lucanthone and its derivative hycanthone inhibit apurinic endonuclease-1 (APE1) by direct protein binding. *PloS one, 6*(9), e23679.

Nishi, T., Shimizu, N., Hiramoto, M., Sato, I., Yamaguchi, Y., Hasegawa, M., Watanabe, H. (2002). Spatial redox regulation of a critical cysteine residue of NF-κB in vivo. *J. Biol. Chem., 277*(46), 44548-44556.

Nyland, R. L., Luo, M., Kelley, M. R., & Borch, R. F. (2010). Design and synthesis of novel quinone inhibitors targeted to the redox function of apurinic/apyrimidinic endonuclease 1/redox enhancing factor-1 (Ape1/ref-1). *J. Med. Chem., 53*(3), 1200-1210.

Oezguen, N., Mantha, A. K., Izumi, T., Schein, C. H., Mitra, S., & Braun, W. (2011). MD simulation and experimental evidence for Mg(2)+ binding at the B site in human AP endonuclease 1. *Bioinformation, 7*(4), 184-198.

Ono, Y., Matsumoto, K., Furuta, T., Ohmoto, T., Akiyama, K., & Seki, S. (1995). Relationship between expression of a major apurinic/apyrimidinic endonuclease (APEX nuclease) and susceptibility to genotoxic agents in human glioma cell lines. *J. Neurooncol., 25*(3), 183-192.

Ordway, J. M., Eberhart, D., & Curran, T. (2003). Cysteine 64 of Ref-1 is not essential for redox regulation of AP-1 DNA binding. *Mol. Cell. Biol., 23*(12), 4257-4266.

Pines, A., Perrone, L., Bivi, N., Romanello, M., Damante, G., Gulisano, M., Tell, G. (2005). Activation of APE1/Ref-1 is dependent on reactive oxygen species generated after purinergic receptor stimulation by ATP. *Nucleic Acids Res., 33*(14), 4379-4394.

Qin, J., Clore, G. M., Kennedy, W. P., Kuszewski, J., & Gronenborn, A. M. (1996). The solution structure of human thioredoxin complexed with its target from Ref-1 reveals peptide chain reversal. *Structure, 4*(5), 613-620.

Raffoul, J. J., Banerjee, S., Singh-Gupta, V., Knoll, Z. E., Fite, A., Zhang, H., Hillman, G. G. (2007). Down-regulation of apurinic/apyrimidinic endonuclease 1/redox factor-1 expression by soy isoflavones enhances prostate cancer radiotherapy in vitro and in vivo. *Cancer Res., 67*(5), 2141-2149.

Ramana, C. V., Boldogh, I., Izumi, T., & Mitra, S. (1998). Activation of apurinic/apyrimidinic endonuclease in human cells by reactive oxygen species and its correlation with their adaptive response to genotoxicity of free radicals. *Proc. Natl. Acad. Sci. USA, 95*(9), 5061-5066.

Rivkees, S. A., & Kelley, M. R. (1994). Expression of a multifunctional DNA repair enzyme gene, apurinic/apyrimidinic endonuclease (APE; Ref-1) in the suprachiasmatic, supraoptic and paraventricular nuclei. *Brain Res., 666*(1), 137-142.

Rodrigues, A. S., Gomes, B. C., Martins, C., Gromicho, M., Oliveira, N. G., Guerreiro, P. S., & Rueff, J. (2013). DNA Repair and Resistance to Cancer Therapy *New Research Directions in DNA Repair*

Ryu, B. J., Lee, H., Kim, S. H., Heo, J. N., Choi, S. W., Yeon, J. T., Lee, S. Y. (2014). PF-3758309, p21-activated kinase 4 inhibitor, suppresses migration and invasion of A549 human lung cancer cells via regulation of CREB, NF-kappaB, and beta-catenin signalings. *Mol. Cell. Biochem., 389*(1-2), 69-77.

Sancar, A., Lindsey-Boltz, L. A., Ünsal-Kaçmaz, K., & Linn, S. (2004). Molecular mechanisms of mammalian DNA repair and the DNA damage checkpoints. *Annu. Rev. Biochem., 73*(1), 39-85.

Sanderson, B. J., Chang, C. N., Grollman, A. P., & Henner, W. D. (1989). Mechanism of DNA cleavage and substrate recognition by a bovine apurinic endonuclease. *Biochemistry, 28*(9), 3894-3901.

Saraswathy, M., & Gong, S. (2013). Different strategies to overcome multidrug resistance in cancer. *Biotechnol. Adv., 31*(8), 1397-1407.

Seeberg, E., Eide, L., & Bjørås, M. (1995). The base excision repair pathway. *TIBS, 20*(10), 391-397.

Seiple, L. A., Cardellina, J. H., Akee, R., & Stivers, J. T. (2008). Potent inhibition of human apurinic/apyrimidinic endonuclease 1 by arylstibonic acids. *Mol. Pharmacol., 73*(3), 669-677.

Shen, Q., Uray, I. P., Li, Y., Krisko, T. I., Strecker, T. E., Kim, H. T., & Brown, P. H. (2008). The AP-1 transcription factor regulates breast cancer cell growth via cyclins and E2F factors. *Oncogene, 27*(3), 366-377.

Simeonov, A., Kulkarni, A., Dorjsuren, D., Jadhav, A., Shen, M., McNeill, D. R., Wilson III, D. M. (2009). Identification and characterization of inhibitors of human apurinic/apyrimidinic endonuclease APE1. *PloS one, 4*(6), e5740.

Sultana, R., McNeill, D. R., Abbotts, R., Mohammed, M. Z., Zdzienicka, M. Z., Qutob, H., Patel, P. M. (2012). Synthetic lethal targeting of DNA double-strand break repair deficient cells by human apurinic/apyrimidinic endonuclease inhibitors. *Int. J. Cancer, 131*(10), 2433-2444.

Taverna, P., Liu, L., Hwang, H.-S., Hanson, A. J., Kinsella, T. J., & Gerson, S. L. (2001). Methoxyamine potentiates DNA single strand breaks and double strand breaks induced by temozolomide in colon cancer cells. *Mutat. Res., 485*(4), 269-281.

Tell, G., Damante, G., Caldwell, D., & Kelley, M. R. (2005). The intracellular localization of APE1/Ref-1: more than a passive phenomenon? *Antioxid. Redox Signaling, 7*(3-4), 367-384.

Tell, G., Fantini, D., & Quadrifoglio, F. (2010). Understanding different functions of mammalian AP endonuclease (APE1) as a promising tool for cancer treatment. *Cell Growth Differ., 67*(21), 3589-3608.

Tell, G., Pellizzari, L., Cimarosti, D., Pucillo, C., & Damante, G. (1998). Ref-1 controls pax-8 DNA-binding activity. *Biochem. Biophys. Res. Commun., 252*(1), 178-183.

Tell, G., Quadrifoglio, F., Tiribelli, C., & Kelley, M. R. (2009). The many functions of APE1/Ref-1: not only a DNA repair enzyme. *Antioxid. Redox Signaling, 11*(3), 601-619.

Tell, G., Zecca, A., Pellizzari, L., Spessotto, P., Colombatti, A., Kelley, M. R., Pucillo, C. (2000). An 'environment to nucleus' signaling system operates in B lymphocytes: redox status modulates BSAP/Pax-5 activation through Ref-1 nuclear translocation. *Nucleic Acids Res., 28*(5), 1099-1105.

Tomida, A., & Tsuruo, T. (2002). Drug Resistance Pathways as Targets *Anticancer Drug Develop.* (pp. 77-90).

Vascotto, C., Bisetto, E., Li, M., Zeef, L. A., D'Ambrosio, C., Domenis, R., Altieri, F. (2011). Knock-in reconstitution studies reveal an unexpected role of Cys-65 in regulating APE1/Ref-1 subcellular trafficking and function. *Mol. Biol. Cell, 22*(20), 3887-3901.

Vascotto, C., Melissa, L., & Fishel. (2012). Blockade of Base Excision Repair: Inhibition of Small Lesions Results in Big Consequences to Cancer Cells, *DNA Repair in Cancer Therapy*.

Walker, L., Robson, C., Black, E., Gillespie, D., & Hickson, I. (1993). Identification of residues in the human DNA repair enzyme HAP1 (Ref-1) that are essential for redox regulation of Jun DNA binding. *Mol. Cell. Biol., 13*(9), 5370-5376.

Wilson, D. M., & Simeonov, A. (2010). Small molecule inhibitors of DNA repair nuclease activities of APE1. *Cell. Mol. Life Sci., 67*(21), 3621-3631.

Wilson, D. M., & Thompson, L. H. (1997). Life without DNA repair. *Proc. Natl. Acad. Sci. USA, 94*(24), 12754-12757.

Wilson III, D. M., & Bohr, V. A. (2007). The mechanics of base excision repair, and its relationship to aging and disease. *DNA Repair, 6*(4), 544-559.

Xanthoudakis, S., & Curran, T. (1992). Identification and characterization of Ref-1, a nuclear protein that facilitates AP-1 DNA-binding activity. *EMBO J., 11*(2), 653.

Xanthoudakis, S., Smeyne, R. J., Wallace, J. D., & Curran, T. (1996). The redox/DNA repair protein, Ref-1, is essential for early embryonic development in mice. *Proc. Natl. Acad. Sci. USA, 93*(17), 8919-8923.

Yang, S., Irani, K., Heffron, S. E., Jurnak, F., & Meyskens, F. L. (2005). Alterations in the expression of the apurinic/apyrimidinic endonuclease-1/redox factor-1 (APE/Ref-1) in human melanoma and identification of the therapeutic potential of resveratrol as an APE/Ref-1 inhibitor. *Mol. Cancer Ther., 4*(12), 1923-1935.

Zaky, A., Busso, C., Izumi, T., Chattopadhyay, R., Bassiouny, A., Mitra, S., & Bhakat, K. K. (2008). Regulation of the human AP-endonuclease (APE1/Ref-1) expression by the tumor suppressor p53 in response to DNA damage. *Nucleic acids Res., 36*(5), 1555-1566.

Zawahir, Z., Dayam, R., Deng, J., Pereira, C., & Neamati, N. (2008). Pharmacophore guided discovery of small-molecule human apurinic/apyrimidinic endonuclease 1 inhibitors. *J. Med. Chem., 52*(1), 20-32.

Zhang, J., Luo, M., Marasco, D., & Logsdon. (2013). Inhibition of apurinic/apyrimidinic endonuclease I's redox activity revisited. *Biochemistry, 52*(17), 2955-2966.

Zhao, J., Gao, F., Zhang, Y., Wei, K., Liu, Y., & Deng, X. (2008). Bcl2 inhibits abasic site repair by down-regulating APE1 endonuclease activity. *Sci. Signal., 283*(15), 9925.

APPENDIX

A: Spectral Data of representative compounds.

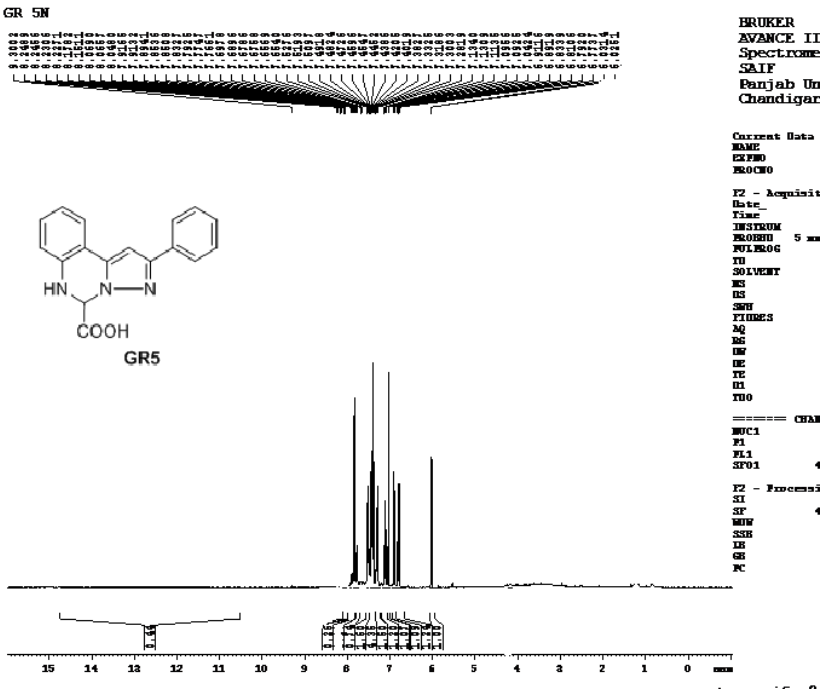

Figure 1: ^{1}H NMR spectra of **GR5**

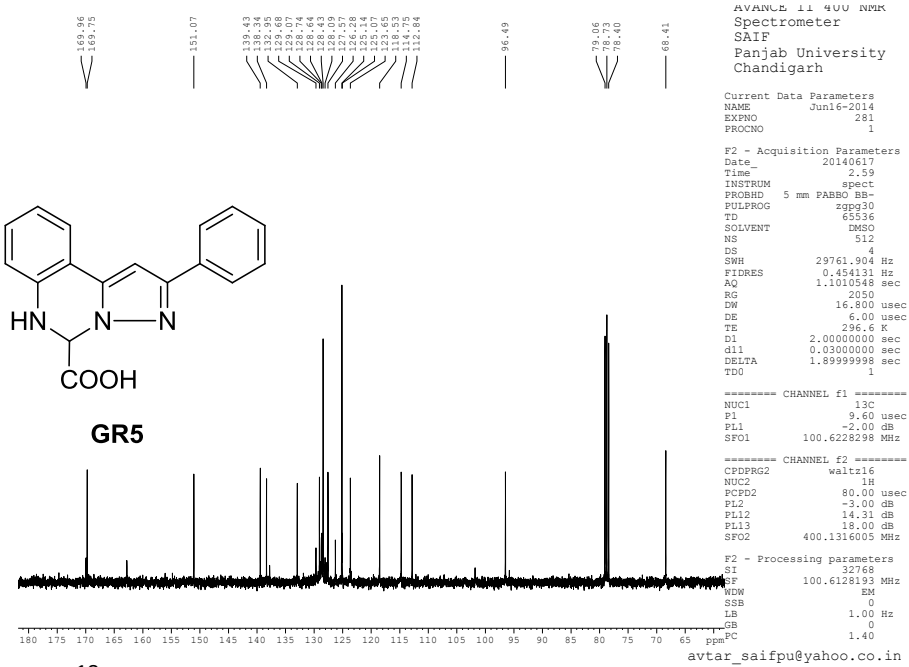

Figure 2: ^{13}C NMR spectra of **GR5**

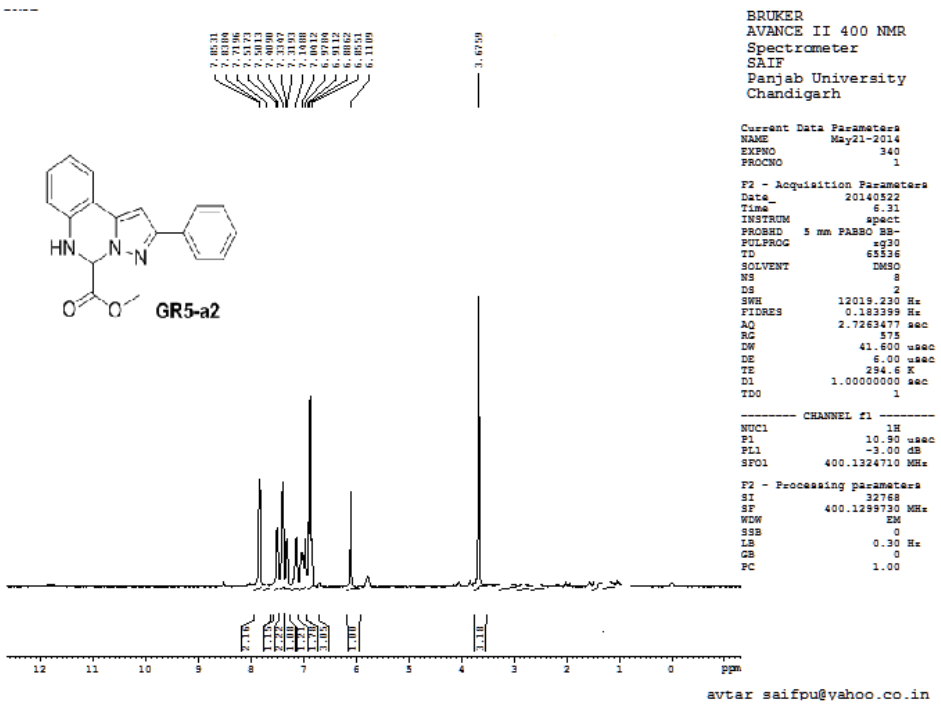

Figure 3: ^{1}H NMR spectra of **GR5-a2**

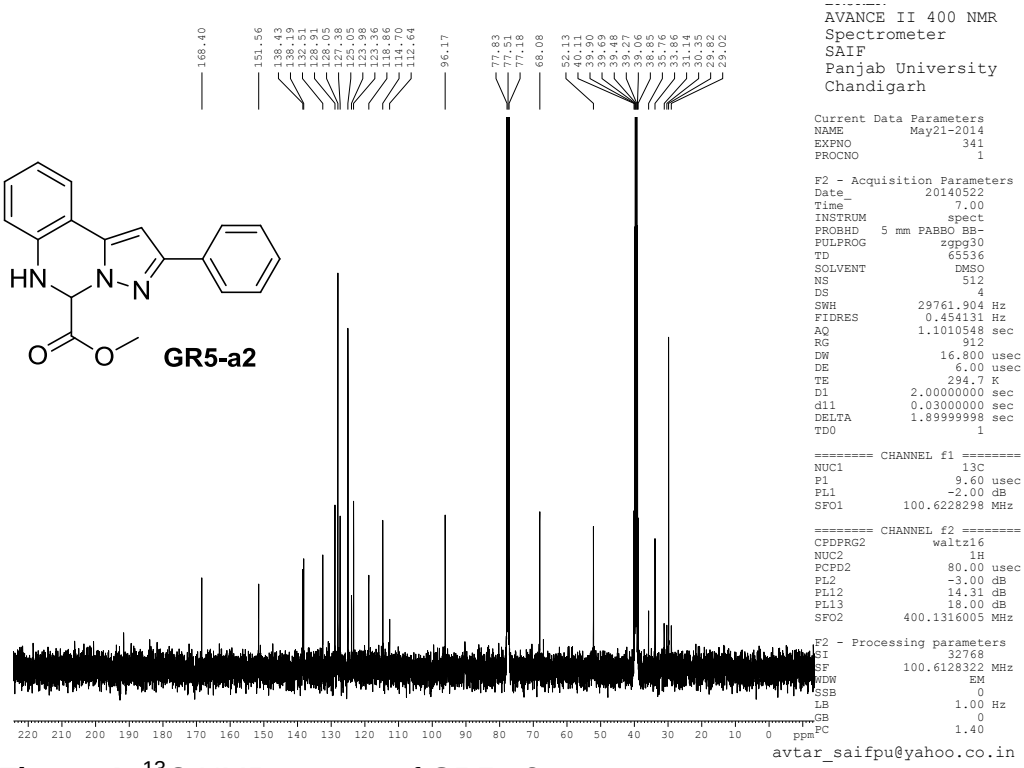

Figure 4: ^{13}C NMR spectra of **GR5-a2**

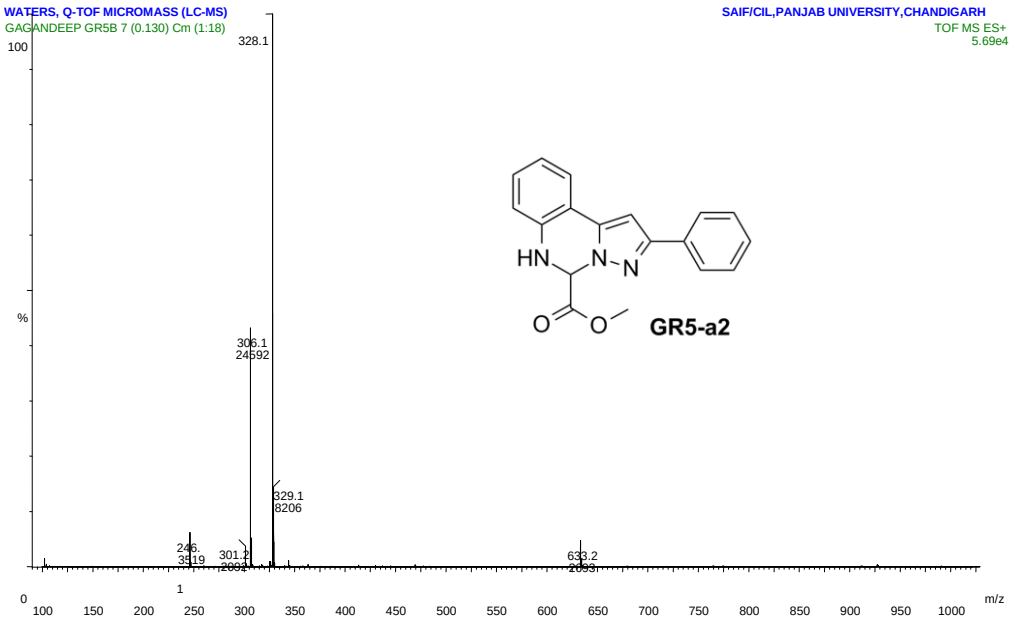

Figure 5: Mass spectra of **GR5-a2**

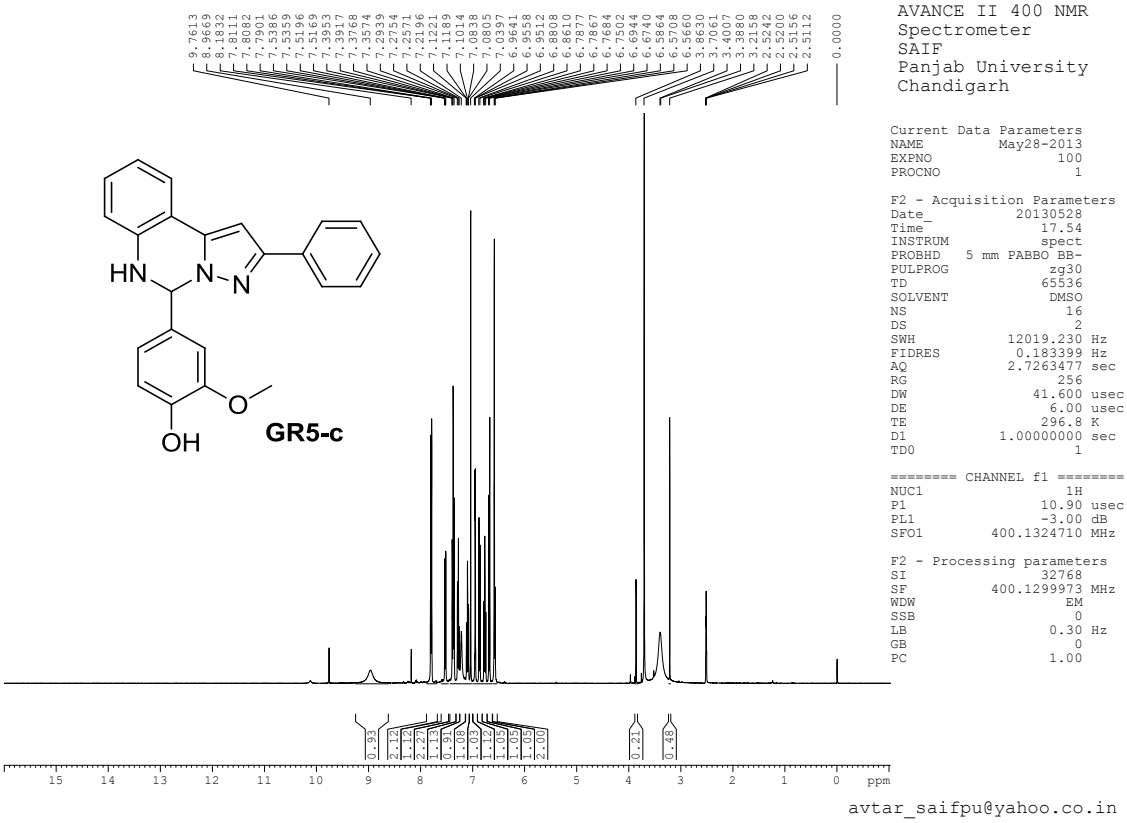

Figure 6: ^{1}H NMR spectra of **GR5-c**

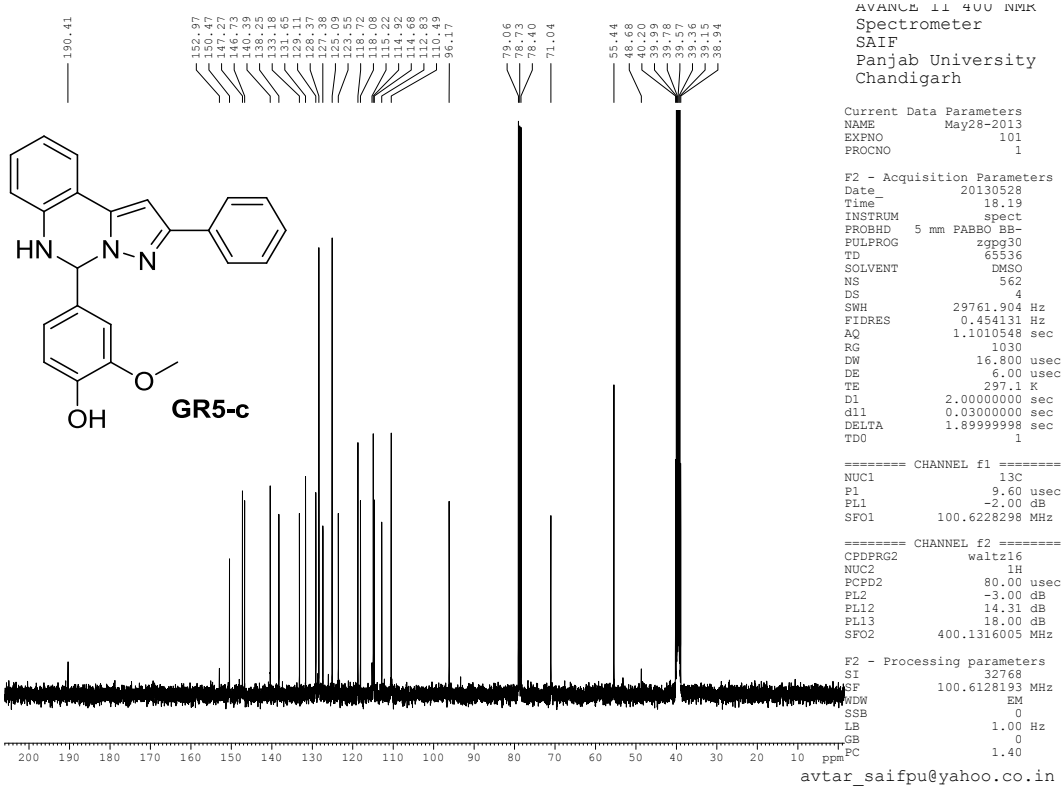

Figure 7: ^{13}C spectra of **GR5-c**

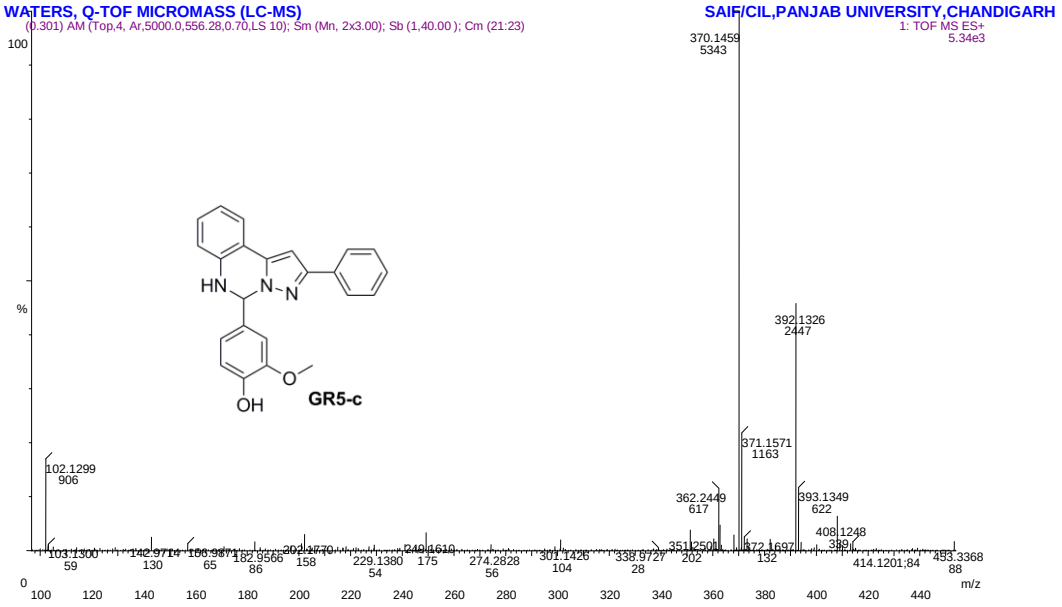

Figure 8: Mass spectrum of **GR5-c**

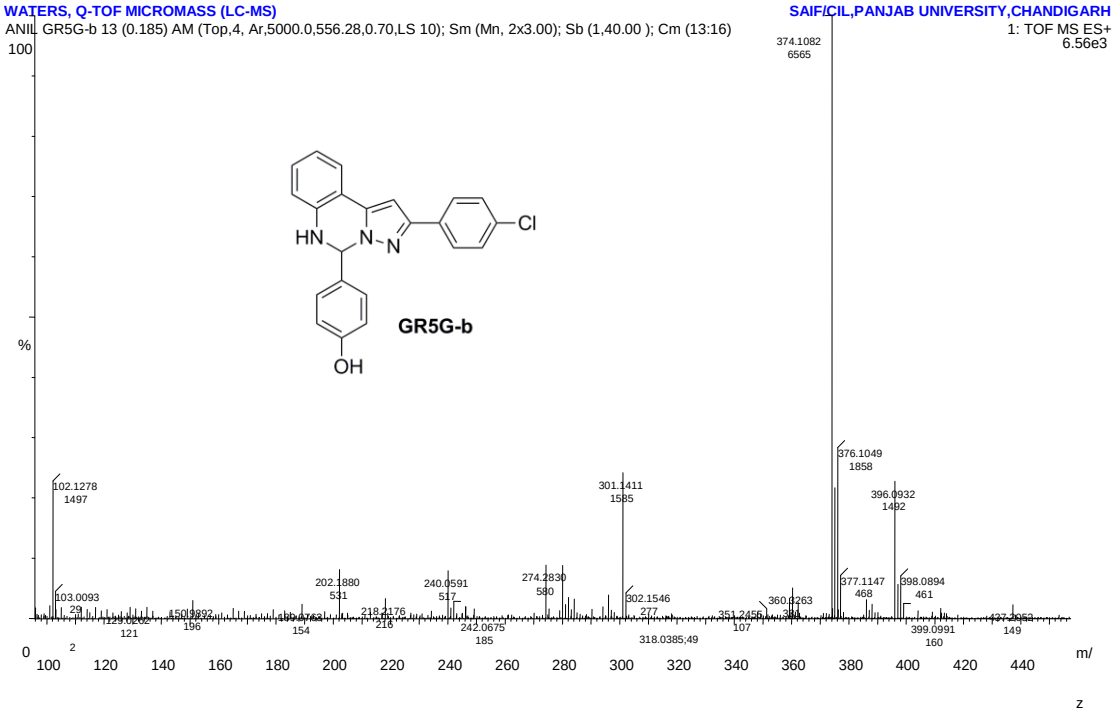

Figure 9: Mass spectrum of **GR5G-b**

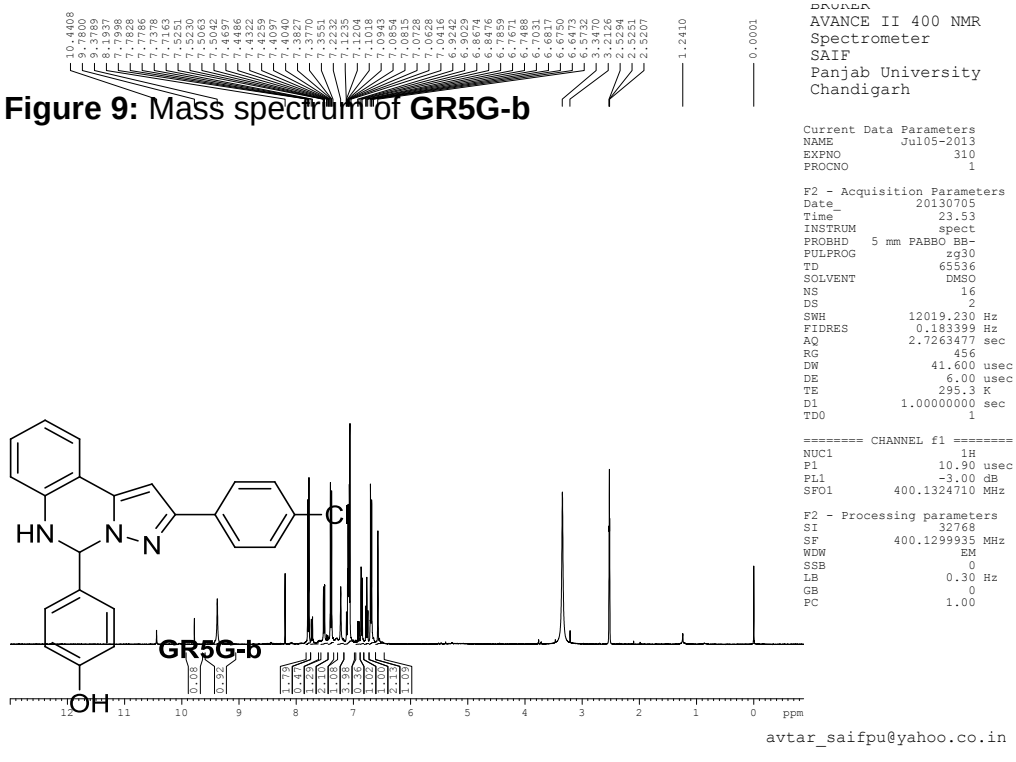

Figure 10: ^{1}H NMR spectra of **GR5G-**

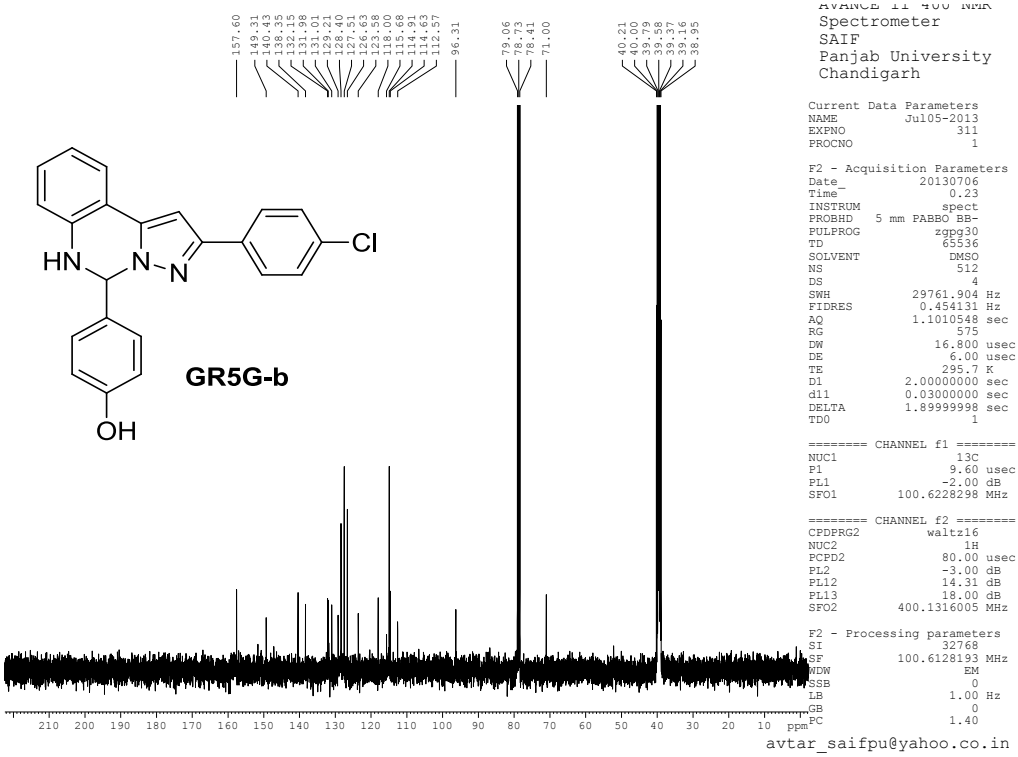

Figure 11: ^{13}C spectra of **GR5G-b**